Treatment planning optimization strategies for the relative biological effectiveness and oxygen enhancement ratio in proton therapy

Helge Henjum

Thesis for the degree of Philosophiae Doctor (PhD)
University of Bergen, Norway
2022

UNIVERSITY OF BERGEN

Treatment planning optimization strategies for the relative biological effectiveness and oxygen enhancement ratio in proton therapy

Helge Henjum

Thesis for the degree of Philosophiae Doctor (PhD)
at the University of Bergen

Date of defense: 23.09.2022

Year: 2022

Title: Treatment planning optimization strategies for the relative biological effectiveness and oxygen enhancement ratio in proton therapy

Name: Helge Henjum

Print: Skipnes Kommunikasjon / University of Bergen

Scientific environment

This study has been a part of the project "3D microdosimetry and studies of the Relative Biological Effectiveness (RBE) in proton and carbon ion therapy", funded by the Trond Mohn foundation, the Norwegian Research Council, and the University of Bergen. The project was organized by Associate Professor Kristian Smeland Ytre-Hauge within the subatomic physics group at the University of Bergen.

Most of the work has been conducted at the University of Bergen but also in collaboration with physicists and dose planners at Haukeland University Hospital. The hospital has an active research community, where a new proton therapy center is being built and will be ready for treatment in a few years. The work has also been aided by physicists at the Heidelberg Ion-Beam Therapy Center and the Norwegian University of Science and Technology.

Acknowledgements

I am grateful for the opportunity to work on my PhD, which was made possible by the financial support from the Trond Mohn Foundation. Working together with the medical physics group at the University of Bergen has been an honor, and this journey is something I feel lucky to have been a part of.

Firstly, I would like to thank my supervisor, Kristian Smeland Ytre-Hauge, for helping and guiding me throughout my PhD. Your patience and persistence have been invaluable, as help has always been available, no matter what. Your ability to always be positive has meant a lot to me, and I am very thankful for it. I would also like to thank my co-supervisor, Sara Pilskog, for always being available when clinical insight was needed. Your guidance and perspectives have really been valuable throughout this project.

Further, I would like to thank everyone in the medical physics group at the University of Bergen for providing me with insightful conversations and help, including Eivind, Andreas, Erlend, and Johannes. I want to especially thank Tordis and Lars Fredrik for always contributing helpful knowledge and feedback throughout my work, as well as for reading through my thesis. I would also like to thank Camilla Stokkevåg for guidance in my projects, as well as for always being available for clinical patient-related questions.

I would like to thank all my co-authors for collaborating with me and giving me helpful feedback, and being part of my projects. Thanks to the Medical Physics group at Haukeland University Hospital for helping me with treatment planning. Thanks to the medical physics group at NTNU, Guillermo and Kathrine, for helpful feedback and discussions regarding hypoxia. Thank you, professor Heikki Minn, for your help with the PET images.

I also wish to thank all my colleagues and friends at the institute for all the lively discussions during coffee breaks and lunches during these years. You have really made life at IFT a joy.

I would also like to thank my family for always encouraging me throughout my PhD. Knowing that you always supported and believed in me has meant a lot.

And this work could not have been possible without the loving support from my fiancée, Malin. Your patience and unconditional love and support during these years have been invaluable, and I can never thank you enough. I can't wait to become your husband.

Abstract

As cancer treatment with protons produces a higher biological effect compared to photons, a relative biological effectiveness (RBE) is used to account for the difference. In clinical proton therapy today, a constant RBE of 1.1 is used, although it is widely known that it varies, depending on fractionation dose, the linear energy transfer (LET), and the radiosensitivity of the tissue $(\alpha/\beta)_x$. This has given rise to multiple variable RBE models, which aim to model the RBE from *in vitro* cell experiments. The RBE models have found the RBE to be increasing with increasing LET and decreasing $(\alpha/\beta)_x$, and will therefore be higher in the distal part of the beam. A decreasing RBE with an increasing dose is also observed. In recent years, clinical evidence of a variable RBE for protons has arisen, showing the need for optimization strategies in proton therapy that account for the variable RBE. Furthermore, the biological effectiveness of radiotherapy has also been shown to depend on the level of oxygenation, quantified by the oxygen enhancement ratio (OER), which ideally should be accounted for in treatment planning.

In the first part of the thesis, treatment plans were optimized with respect to variable RBE using a treatment plan optimization algorithm based on the FLUKA Monte Carlo (MC) software. Different strategies were explored, including a differential approach, which maintained an RBE of 1.1 in the target and reduced the variable RBE in the organs at risk (OAR). The results showed a large case dependency, as the $(\alpha/\beta)_x$ values varied between the target volumes, where the prostate case provided the highest modification of the physical dose due to the low $(\alpha/\beta)_x$ values and thus high RBE estimated in the tumor. We also saw how LET-weighted dose models could provide a steppingstone towards using variable RBE in clinics as it is independent of the tissue type parameter that is still fraught with uncertainties.

A method for optimizing treatment plans with respect to RBE and OER weighted dose (ROWD) was developed and applied *in silico*. PET images were used to calculate the oxygen levels in patients, and treatment plans were optimized using the FLUKA MC

software-based treatment planning system. The results showed that the physical dose was the main factor that changed in the ROWD optimization, and large differences were found in the physical dose between the hypoxic and normoxic regions, although a large modification of the LET was found in the water phantom case. Further, five different ROWD models were explored by comparing the outcome of varying oxygen levels and radiosensitivity, the models from Strigari (STR), Tinganelli (TIN), Dahle (DAH), Wenzl and Wilkens (WEN), and Mein (MEI). The models were compared in a simulated water phantom case and a clinical patient case. A grouping between the models was found, as the STR and TIN model estimated a higher OER compared to the other models, possibly due to their differences in how the OER is included in the ROWD calculation. Still, a large increase in the OER in the most hypoxic areas was found for all models, suggesting that an increase in dose is needed for hypoxic cases.

In the final part of this thesis, the effect of increasing LET in the central part of the tumor using pruning techniques in proton arc therapy (PAT) was explored. By removing the highest energies of each beam in the arc, the LET levels can be increased within the target while simultaneously decreasing the LET in the surrounding normal tissue. This technique was demonstrated in a germinoma case, where PAT plans with varying degrees of pruning were created and optimized for an RBE of 1.1. A higher degree of pruning resulted in higher LET values in the target volume. This also led to an increase in RBE weighted dose to the target, and a decrease in the surrounding normal tissue. This technique could therefore contribute to OAR sparing and could be an alternative to improve the treatment of hypoxic and radioresistant tumors.

Overall, this thesis presents developments and exploration of RBE- and hypoxia-based optimization strategies for proton therapy. The thesis shows how clinical treatment planning can be improved by including more than the physical dose used in current treatment planning, such as variable RBE, LET, and hypoxia-related parameters.

Sammendrag

Sidan kreftbehandling med proton gir ein høgare biologisk effekt enn foton, blir ein relativ biologisk effekt (RBE) brukt for å ta omsyn til forskjellen. I klinisk protonterapi i dag blir ein konstant RBE på 1.1 nytta, sjølv om det er kjent at RBE varierer og avheng av fraksjonsdose, den lineære energioverføringa (LET) og radiosensitiviteten til vevet $(\alpha/\beta)_x$. Dette har gitt opphav til fleire variable RBE modellar som har som mål å modellere RBE utifrå *in vitro* celle-eksperiment. Modellane har vist at RBE aukar med minkande LET og aukande $(\alpha/\beta)_x$, og vil derfor vere høgare i den distale delen av strålen. Ein minkande RBE med aukande dose er også observert. I dei seinare år har klinisk bevis for variabel RBE blitt påvist, noko som har ført med seg eit behov for optimaliserings-strategiar i protonterapi som tar omsyn til variabel RBE. Dessutan, har den biologiske verknaden av strålebehandling vist seg å vere avhengig av nivået av oksygenering, kvantifisert av oksygenforsterkingsforholdet (OER), som ideelt sett også burde blitt tatt omsyn til i behandlingsplanlegginga.

I den første delen av oppgåva blei behandlingsplanar optimalisert med omsyn til variabel RBE ved å nytte ein behandlingsplan-optimaliseringsalgoritme basert på FLUKA Monte Carlo (MC) programvara. Ulike strategiar blei utforska, inkludert ein differensial tilnærming som oppretthaldt ein RBE på 1.1 i målvolumet, samt reduserte RBE-verdiane i risikoorgana (OAR). Resultata viste ein stor pasient-avhengigheit, sidan $(\alpha/\beta)_x$ varierte veldig mellom målvoluma, der prostatapasienten gav den høgaste modifisering av fysisk dose grunna dei lave $(\alpha/\beta)_x$ verdiane og derav høg RBE i målvolumet. Me såg og korleis LET-vekta dosemodellar kan vere eit springbrett mot å nytte variabel RBE klinisk, sidan den er uavhengig av radiosensitivitets-parameteren som framleis er full av usikkerheit.

Ein metode for å optimalisere behandlingsplanar med omsyn til RBE og OER-vekta dose blei utvikla og nytta *in silico*. PET-bilete blei nytta for å berekne oksygennivået hos pasientar, og behandlingsplanar blei optimalisert ved hjelp av det FLUKA MC

programvarebaserte behandlingsplanlegging-systemet. Resultata viste at den fysiske dosen var hovudparameteren som endra seg i ROWD optimaliseringa. Det ble funnet store forskjellar i fysisk dose mellom hypoksiske og normoksiske regionar , samt store endringa i LET i vannfantom-planen. Videre blei fem ROWD modellar utforska ved å samanlikne utfallet av varierande oksygen-nivåer, i modellane frå Strigari (STR), Tinganelli (TIN), Dahle (DAH), Wenzl og Wilkens (WEN) og Mein (MEI). Modellane blei samanlikna i eit simulert vannfantom og eit klinisk pasienttilfelle. Ei gruppering mellom modellane blei funnet, da STR og TIN modellane estimerte ein høgare OER samanlikna med dei andre modellane, moglegvis på grunn av forskjellen deira i korleis OER er inkludert i ROWD-berekningane. Likevel blei det funnet ein stor auke i OER i dei mest hypoksiske område for alle modellane, noko som tyder på at ein auke i dose er nødvendig for hypoksiske tilfelle.

I den siste delen av denne oppgåva blei effekten av å auke LET i den sentrale delen av svulsten undersøkt ved bruk av beskjæringsteknikkar i strålebogeterapi (PAT) utforska. Ved å fjerne dei høgaste energiane frå kvar stråle i bogen, kan LET-verdiane aukast innanfor målvolumet, samstundes som LET-verdiane i det friske vevet kan bli redusert. Denne teknikken blei demonstrert på eit germinom pasienttilfelle, der PAT-planar med ulik grad av beskjæring blei oppretta og optimalisert for ein RBE på 1.1. Ein høgare grad av beskjæring førte til høgare LET-verdiar til målvolumet. Det førte også til ein auke i den RBE-vekta dose til målvolumet, og ein reduksjon i det omkringliggande friske vevet. Denne teknikken kan derfor bidra til å spare risikoorgan og kan vere eit alternativ for å forbetre behandlinga av hypoksiske og radioresistente svulstar.

Samla sett viser denne oppgåva utvikling og utforsking av RBE- og hypoksibaserte optimaliseringsstrategiar for protonterapi. Oppgåva viser korleis klinisk behandlingsplanlegging kan forbetrast ved å inkludera meir enn berre den fysiske dosen som blir nytta i behandlingsplanlegging i dag, slik som variabel RBE, LET og hypoksiarelaterte parameter.

List of Publications

Papers included in this thesis:

Paper I   **Henjum H**, Dahle TJ, Fjæra LF, Rørvik E, Pilskog S, Stokkevåg CH, Mairani A, Ytre-Hauge KS (2021). *The organ sparing potential of different biological optimization strategies in proton therapy*. Adv Radiat Oncol 6(6), 100776

https://doi.org/10.1016/j.adro.2021.100776

Paper II

H Henjum, Dahle TJ, Mairani A, Pilskog S, Stokkevåg CH, Boer CG, Redalen KR, Minn H, Malinen E, Ytre-Hauge KS. *Accounting for hypoxia in proton therapy planning with a FLUKA Monte Carlo based tool.* (Submitted to Medical Physics).

Paper III   Garrido-Hernandez G, **Henjum H**, Høiskar MK, Dahle TJ, Redalen KR, Ytre-Hauge KS. *Hypoxia adapted relative biological effectiveness models for proton therapy: a simulation study.* (Submitted to Physics in Medicine & Biology).

Paper IV   **Henjum H**, Tjelta J, Fjæra LF, Pilskog S, Stokkevåg CH, Lyngholm E, Handeland AH, Ytre-Hauge KS. *Influence of LET and RBE from including pruning techniques in proton arc therapy.* (Submitted to Physics in Medicine & Biology)

Conference contributions

- **Henjum H**, Dahle TJ, Fjæra LF, Rørvik E, Pilskog S, Stokkevåg CH, Mairani A, Ytre-Hauge KS. *Implementation and exploration of biological optimization in proton therapy.* BiGART 2019, May 2019, Aarhus, Denmark. (Poster presentation)

- **Henjum H**, Dahle TJ, Fjæra LF, Rørvik E, Pilskog S, Stokkevåg CH, Mairani A, Ytre-Hauge KS. *The organ sparing potential of different biological optimization strategies in proton therapy.* NACP21, April 2021, Online conference. (Poster and presentation)

- **Henjum H**, Dahle TJ, Mairani A, Pilskog S, Stokkevåg CH, Boer CG, Redalen KR, Minn H, Malinen E, Ytre-Hauge KS. *Biological optimization in proton therapy accounting for hypoxia and variable RBE.* ESTRO21, August 2021. Online conference (Poster)

- **Henjum H**, Pilskog S, Stokkevåg CH, Tjelta J, Ytre-Hauge KS. *Exploration of RBE optimization in proton arc therapy.* ESTRO22, May 2022, Copenhagen, Denmark. (Poster)

- **Henjum H**, Tjelta J, Fjæra LF, Pilskog S, Stokkevåg CH, Ytre-Hauge KS. *Exploring LET and RBE effects from pruning techniques in proton arc therapy.* PTCOG22, June/July 2022, Miami, USA. (Accepted for oral presentation)

Publication Contributions

- Dahle TJ, Rusten E, Stokkevåg CH, Silvoniemi A, Mairani A, Fjæra LF, Rørvik E, **Henjum H**, Wright P, Boer CG, Forsback S, Minn H, Malinen E, Ytre-Hauge KS. *The FLUKA Monte Carlo code coupled with a hypoxia model for biological dose calculations in proton therapy.* Physica Medica, 76, 166-72. https://doi.org/10.1016/j.ejmp.2020.07.003

Abbreviations

[¹⁸F]-EF5	2-(2-nitro-^{1}H-imidazol-1-yl)-N-(2,2,3,3,3-pentafluoropropyl)-acetamide labeled with ^{18}F
CNAO	National Center for Oncological hadrontherapy, Italy
CT	Computed Tomography
CTV	Clinical Target Volume
DICOM	Digital Imaging and Communications in Medicine
DSB	Double Strand Break
DVH	Dose Volume Histogram
FLAIR	FLUKA Advanced Interface
FLUKA	Fluktuierende Kaskade
GTV	Gross Tumor Volume
HNC	Head and Neck Cancer
ICRP	International Commission on Radiological Protection
ICRU	International Commission on Radiation Units & Measurements
IMPT	Intensity Modulated Proton Therapy
IMRT	Intensity Modulated RadioTherapy
LEM	Local effect model
LET	Linear Energy Transfer
LQ	Linear Quadratic
MC	Monte Carlo
MCN	Model by McNamara
MKM	Microdosimetric kinetic model
MRI	Magnetic Resonance Imaging
OAR	Organ At Risk
OER	Oxygen Enhancement Ratio
PB	Pencil Beam
PBS	Pencil Beam Scanning
PET	Positron emission tomography
PHYS	Plan optimized with respect to physical dose
PTV	Planned Target Volume
RBE	Relative Biological Effectiveness

RBE$_{1.1}$	Biological dose calculated with RBE of 1.1
ROI	Region Of Interest
ROR	Rørvik model
ROWD	RBE and OER- Weighted Dose
SFO	Single Field Optimization
SOBP	Spread Out Bragg Peak
SSB	Single Strand Break
TPS	Treatment Planning System

Contents

1.   Introduction

Cancer is a term for mutated cells that rapidly grow in the body, invading other regions and organs. In 2020, there were approximately 19.3 million new cancer cases worldwide and it was one of the leading causes of death with around 10 million casualties (Sung *et al.* 2021). Radiation therapy is one of the primary modalities for treating cancer, alongside surgery and chemotherapy. The principle is to deliver ionizing radiation to the malignant cancer cells, destroying their ability to proliferate while still sparing the surrounding healthy tissue.

The primary radiation used for radiation therapy is high energetic X-rays. X-rays were first discovered by Wilhelm Rontgen (Röntgen 1896) in 1896, using a Crookes tube. Soon after, E. H. Grubbe got the idea of using it therapeutically after suffering from X-ray dermatitis due to exposure to radiation (Lederman 1981). Today, external radiotherapy (with the ionization source outside of the body) use linear accelerators to create high energetic photons. Due to technological advances, such as volumetric modulated arc therapy (VMAT), radiotherapy is a big part of the continuous improving prognosis for multiple cancer types. However, photons do not have a finite range, and parts of a photon beam will therefore pass through the tumor and deposit dose both proximal and distal to the target.

External radiotherapy with protons is a relatively new cancer treatment modality, which uses the energy deposition properties of charged particles to spare even more healthy tissue than photons. It was first proposed by Robert R. Wilson in 1946, but the first hospital based treatment centers did not open until 1990 (Coutrakon *et al.* 1994). Today, over 100 particle therapy centers are in use, and more are planned, including two proton therapy centers in Norway (PTCOG 2022).

The physical properties of protons lead to an increased biological effect compared to photons. This difference is quantified through the relative biological effectiveness (RBE), where the proton RBE is the ratio between the dose from photons and the proton dose needed to produce the same biological effect. Based on *in vivo* experiments done

in the 1970s, the value was set to a constant of 1.1, assuming that protons are 10% more effective in killing cells compared to photons (Paganetti *et al.* 2019). This value is used clinically at proton centers today. However, this value was set conservatively to ensure tumor control, and the RBE could be higher. The RBE is also known to vary and depends on several different parameters, such as tissue type, dose fractionation and the linear energy transfer (LET). To account for these parameters, several different variable RBE models have been developed based on *in vitro* cell survival data. The models all show an increasing RBE with increasing LET, decreasing fractionation dose and decreasing tissue sensitivity. An increasing amount of data from clinical studies from proton therapy patients also indicates an increase in biological effects at the end of the proton beam where the LET is high (Paganetti 2022). This suggests that effects from variable RBE should be considered for the proton treatment plan.

The variations in biological effects could also be considered more in treatment planning of radioresistant tumors. When the oxygen-level of a tumor is low, known as hypoxia, it is more resistant to radiation (Vaupel and Mayer 2007). The levels of oxygen within in a tumor is highly heterogenous, meaning some areas may be hypoxic and other normoxic (Bader, Dewhirst, and Hammond 2020). It is therefore important to both quantify the level of hypoxia in the tumor, as well as accounting for this in the clinical treatment plan. The biological and physical properties of the protons offer a potential to precisely deposit higher dose to circumvent the radio resistance.

Today, proton therapy is generally delivered through intensity modulated proton therapy (IMPT) where different inhomogeneous treatment fields are optimized simultaneously using multi field optimization. As for VMAT using photons, proton arc therapy is considered as a new option to increase the quality and robustness of the treatment further. By rotating the proton beam around the patient, additional degree of freedom is achieved. Although it provides a low dose bath to the healthy tissue, the integral dose has been shown to be lower than for IMPT (Ding *et al.* 2016), and it could also provide a better RBE and LET distribution (Mein *et al.* 2021).

This thesis aimed to explore how treatment plans can be created with respect to biological effects and show how treatment outcome can be improved by including LET effects and hypoxia as part of the treatment planning both with conventional field arrangements and new delivery techniques such as proton arc therapy. Using Monte Carlo (MC) code, different methods were created to account for variable RBE and hypoxia in the treatment planning and then compared. This would add knowledge to how different strategies to handle RBE effects can be used in clinical proton therapy.

2. Physics of proton therapy

Protons that travel through tissue lose energy primarily through ionization of the atoms. The energy loss rate increases with depth as the proton energy is decreased and the maximum energy deposition occurs at the end of their range. This physical property makes protons superior to photons for radiation therapy as dose beyond its range is negligible, thereby providing sparing of healthy tissue distal to the tumor.

2.1 Interactions of protons with matter

Protons have several different ways of interacting with matter, and with varying mechanisms of energy depositions, as illustrated in Figure 2.1.
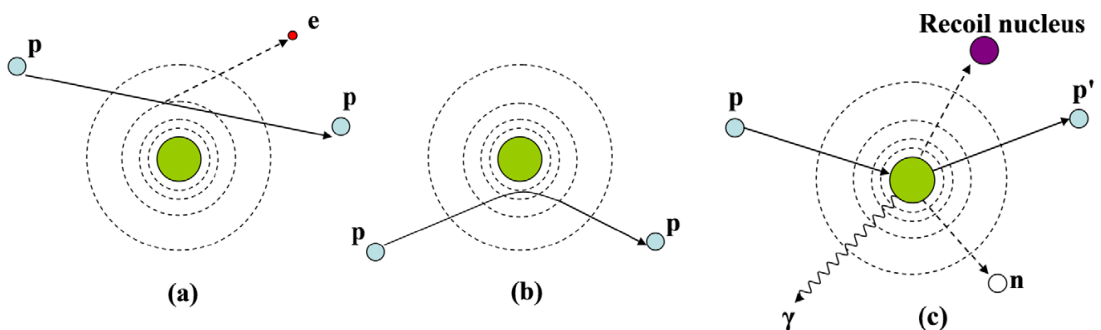
Figure 2.1 Illustration of the three main interactions between a proton and an atom: (a) the inelastic interactions with the atomic electron, (b) Coulomb-scattering of the atomic nuclei and (c) nuclear interactions. Adapted from (Newhauser and Zhang 2015).

Interaction through inelastic Coulomb scattering to the atomic electron is accountable for slowing down the charged particle and is the main cause of dose deposition from protons (Newhauser and Zhang 2015). The charged particle will free the atomic electron from the atom, losing a small fraction of its energy in the process, and continue in a near straight path as the mass of the proton is significantly larger than the electron (Figure 2.1a). The rate of energy loss, from a particle with charge z, traveling through

a medium with atomic number A and charge Z, is often referred to as the stopping power, described by the Bethe-Bloch equation (Bethe 1930; Bloch 1933):

$$-\frac{dE}{dx} = 2\pi N_a r_e^2 m_e c^2 \rho \frac{Z}{A} \frac{z^2}{\beta^2} \left[\ln \left(\frac{2m_e \gamma^2 v^2 W_{max}}{I^2} \right) - 2\beta^2 - \delta - 2\frac{C}{Z} \right] \quad (2.1)$$

where E is the energy lost over a distance x, N_a is Avogrado's number, r_e is the classical electron radius, m_e is the electron mass, c is the speed of light in vacuum, ρ is the density of the absorbing material, β is the relativistic velocity given as v/c with v being the speed of the incident particle, γ is the Lorentz-factor defined as $\sqrt{1 - \beta^2}$, W_{max} is the maximum energy transfer from a single collision, I is the mean excitation potential, δ is the density correction and C is the shell correction factor. The stopping power of the proton is illustrated in Figure 2.2a.

The most influential factor in the Bethe-Bloch equation is the term z^2/β^2, which shows that the energy loss is inversely proportional to the relativistic velocity and that the energy loss rate increases with the square of the incident particle's charge. This means that the stopping power will be highest when the particles has almost stopped, leading to a sharp peak, called the Bragg Peak (Figure 2.2b).

The Bethe-Bloch formula also suggests that all protons with a specific energy would end up in a sharp peak at the stopping point, which can be found by integration. However, due to statistical fluctuations in the slowing down process, the Bragg Peak would be broadened for beams with a high amount of particles (Schardt, Elsässer, and Schulz–Ertner 2010). These fluctuations can be described mathematically by the Vavilov distribution, which becomes Gaussian for many collisions. It has a $1/\sqrt{m}$ dependency, where the m is the particle mass. Thus heavier ions are less susceptible for range straggling compared to protons.
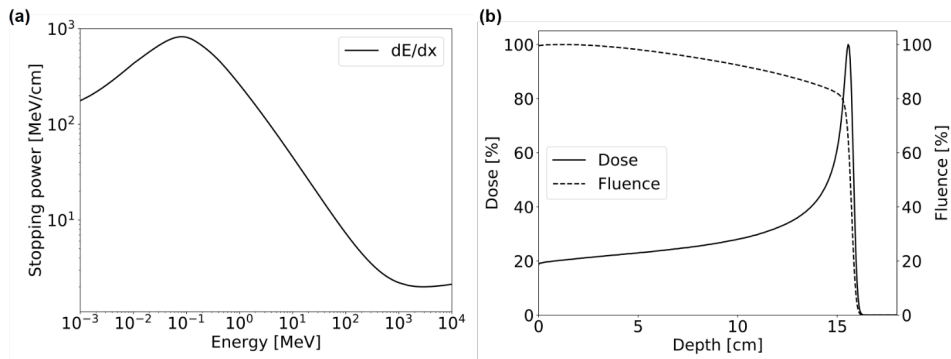
Figure 2.2 (a) The stopping power in water as a function of the kinetic energy of the proton. (b) Dose deposition of a 150 MeV proton beam in water (solid line) resulting in a Bragg peak, and the corresponding fluence (Fjæra 2021).

Elastic Coulomb scattering between the proton and the atomic nuclei (Figure 2.1b) results in an angular deflection of the proton. Such collisions lead to a broadening of a proton beam with depth. A single elastic interaction will have a small effect on the trajectory of the charged particle, however, the sum of all the deflections for a beam can lead to a high lateral spreading of protons (Mohan and Grosshans 2017). This is called multiple Coulomb scattering, and similar to the range straggling, the magnitude of the spread is mass dependent. This gives heavier ions an advantage compared to protons as the lateral scattering from the heavier ions will be lower. The Coulomb scattering is therefore necessary to include in dose calculations in treatment planning systems (Newhauser and Zhang 2015).

Protons can also undergo nuclear interactions with the atomic nuclei if the energy is high enough to overcome the Coulomb barrier of the nucleus (Figure 2.1c). This interaction is non-elastic, meaning the nucleus is irreversibly transformed. As the proton is removed from the treatment field, a small decrease in dose from the primary proton will occur, however, this is compensated for in the creation of secondary particles (Newhauser and Zhang 2015).

2.2 Dosimetry

Ionizing radiation is defined as radiation with energies high enough to remove electrons from an atom or molecule. The energy deposited in the medium from ionizing radiation is termed absorbed dose and is defined by the international commission of radiation protection (ICRP) as the mean energy ΔE imparted to matter with mass Δm (ICRP 103, 107), and can be written as:

$$D = \frac{\Delta E}{\Delta m} \tag{2.2}$$

The unit for absorbed dose, or physical dose, is Gray (Gy), where 1 Gy is 1 J/kg. Absorbed dose is the standard for reporting dose in photon radiotherapy.

2.2.1 Spread-Out Bragg Peak

The dose deposition from a single monoenergetic proton beam will increase significantly at the end of its range resulting in a peak, called the Bragg Peak. A single beam is not capable of producing homogenous dose to a certain region, so a spread-out Bragg peak (SOBP) is created. The SOBP consists of multiple beams with different energies so that uniform dose is achieved. Both the Bragg peak and the SOBP is illustrated in Figure 2.3 alongside the lateral dose.
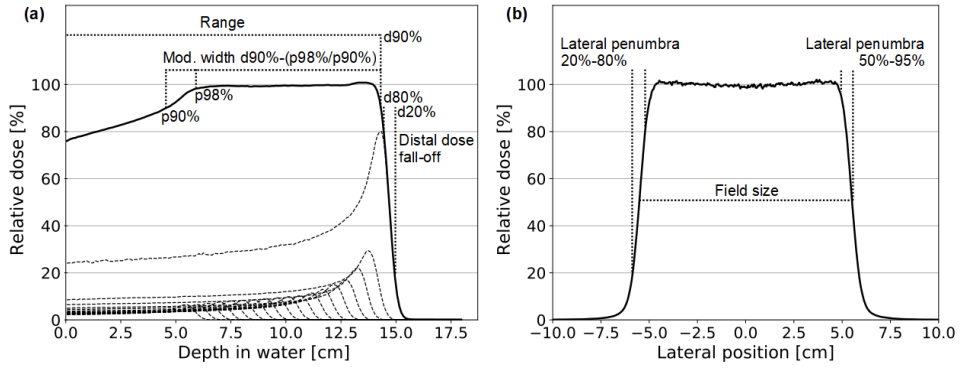
Figure 2.3 a) A SOBP (solid lines) consisting of several Bragg peaks (dashed lines). The belonging metrics as range, modulation width and distal dose fall-off are also given. b) The belonging lateral dose for the SOBP with the different lateral penumbra definitions (Fjæra 2021).

2.3 The linear energy transfer

An important parameter in proton therapy is the linear energy transfer (LET), which is defined by the ICRU as the energy dE transferred from a charged particle per unit length dl (Thomas 2012):

$$LET = \frac{dE}{dl} \tag{2.3}$$

The LET describes the radiation quality and is an important biological parameter as high LET is associated with increased biological effect (Barendsen 1964).

We can further divide this definition into restricted and unrestricted LET, depending on what particles are included in the calculation. If the energies of the incident protons are high enough, secondary delta-ray electrons can be produced, potentially depositing their energy far from the proton trajectory. We therefore define the restricted LET as the energy lost by the primary charged particle, omitting secondary delta-ray electrons with a higher energy than a certain threshold:

$$LET_\Delta = S_{el} - \frac{dE_{ke,\Delta}}{dl} \qquad (2.4)$$

Here, S_{el} is the linear electronic stopping power, and $dE_{ke,\Delta}$ is the mean sum of energies above a threshold Δ. If no such threshold has been applied (i. e, $\Delta = 0$) it will result in an unrestricted LET which is the value most often used in proton therapy.

At a single point along the proton beam, the protons and secondary particles will have a specter of energies, leading to a specter of LET values. To simplify the LET value, it is common to use an average value in each point. There are two main ways to average the LET; dose averaged, which is most commonly used in proton therapy, and track averaged (Figure 2.4). Dose averaged LET (LET_d) is defined as the sum of the LET contributions to a location z, weighted by the dose:

$$LET_d(z) = \frac{\int_0^\infty S_{el}(E)D(E,z)dE}{\int_0^\infty D(E,z)dE} \qquad (2.5)$$

where the $D(E,z)$ is the dose, S_{el} is the electronic stopping power and E is the kinetic energy of the proton. The dose can also be estimated with the fluence (Φ) and electronic stopping power, with the continuous slowing down approximation (CSDA), and will be given as:

$$D(E,z) = \frac{S_{el}(E)\Phi(E,z)}{\rho(z)} \qquad (2.6)$$

where ρ is the mass density of the medium. Substituting (2.6) in (2.5) we can write the dose-averaged LET as:

$$LET_d(z) = \frac{\int_0^\infty S_{el}^2(E)\Phi(E,z)dE}{\int_0^\infty S_{el}\Phi(E,z)dE} \qquad (2.7)$$

The track averaged LET (LET_t) is given as:

$$LET_t(z) = \frac{\int_0^\infty S_{el}(E)\Phi(E,z)dE}{\int_0^\infty \Phi(E,z)dE} \qquad (2.8)$$

For protons, the dose and track averaged LET are similar, except for low protons energies, as the dose averaged LET will be higher at the end of the beam (Grzanka, Ardenfors, and Bassler 2018).
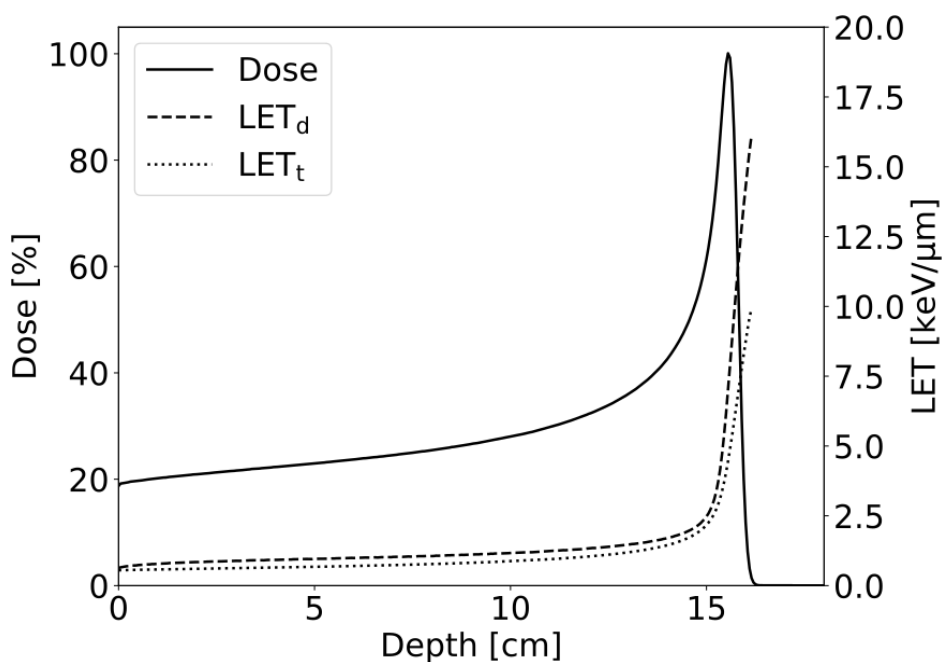

Figure 2.4 The dose from a 150 MeV proton in water with the corresponding dose averaged LET (dashed line), and the track averaged LET (dotted line). The LET values are cut off at 1% dose levels (Fjæra 2021).

3. Radiobiology

When any biological system gets irradiated with ionizing radiation, a series of complex processes occur, with significantly different timescales. In the physical phase, a proton will typically eject an electron from the atom, which will traverse the DNA and, with sufficient energy, start a cascading event of ionization. This leads to a chemical reaction where the ionization and excitation can either cause damage to the biological tissue through direct action or create broken molecules known as free radicals, causing damage through indirect damage (Joiner and Van der Kogel 2009).

The damage can lead to either single strand break (SSB) or double strand break (DSB) of the DNA. In the biological phase, the majority of the radiation damage from the SSB is fully repaired from the radiation damage, while the DSB lead to cell death and mutations. Cell death for proliferating cells, such as stem cells, is when they lose their ability to reproduce, which is a common end point in *in vitro* experiments (Hall 2012). Late effects from radiation includes mainly toxicities, but can also include secondary tumors, however this time-scale extends up to several years (Joiner and Van der Kogel 2009).

3.1 The linear quadratic model

The relationship between the absorbed dose and the fraction of surviving cells is most commonly described by the linear quadratic model, where the cell survival S after a dose D is given as:

$$-\ln(S) = \alpha D + \beta D^2$$

(3.1)

Here, α and β are often referred to as radiosensitivity parameters and are found through the fitting of experimental *in vitro* data or clinical radiotherapy (van Leeuwen *et al.* 2018). The α parameter represent single hit events, and is independent of the fractionation dose, while the β parameter represent multiple-hit cell damage. The ratio

between the parameters (α/β) is used to describe the fractionation sensitivity, where a higher α/β means lower fractionation sensitivity (McMahon 2018).

Usually, tumors have an estimated α/β of 10 Gy, while in some cases, as breast and prostate tumors, the value is between 1-4.5 Gy (van Leeuwen *et al.* 2018). Healthy craniospinal tissue has a low α/β of 1-2 Gy, and will often be especially sensitive to radiation (Chang *et al.* 2014).

Since protons have an increased cell killing ability, the curve in the LQ model will naturally be steeper compared to photons. Similar, as a high LET particles causes more concentrated dose deposition, hence more damage to the DNA, high LET has a steeper curve. This is seen in Figure 3.1.

3.2 The relative biological effectiveness

As explained in chapter 2, there are differences in how photons and protons deposit their energies in tissue, and thus a difference in how efficient the two modalities are in terms of inducing biological damage. To account for this, a relative biological effectiveness (RBE) is used in proton therapy. The RBE is defined as the ratio between a reference dose (usually photons) and proton dose needed to produce the same biological effect:

$$RBE = \frac{D_{ref}}{D_{proton}} \qquad (3.2)$$

In clinical proton therapy today, a constant RBE of 1.1 is used. The value is based on *in vivo* cell experiments, and even though it is approved by the ICRU (2007) , it is also a consensus that the RBE varies, which can be seen in Figure 3.1, where the photon dose needed to have the same biological effect (when looking at 10% clonogenic cell survival), is 35% higher than for photons. The RBE-weighted dose can therefore be written as:

$$RBE\text{-}weighted\ dose = D * RBE$$

$$(3.3)$$

We separate between total physical dose, D, and dose from protons D_p, as only D_p is used in the RBE calculations.
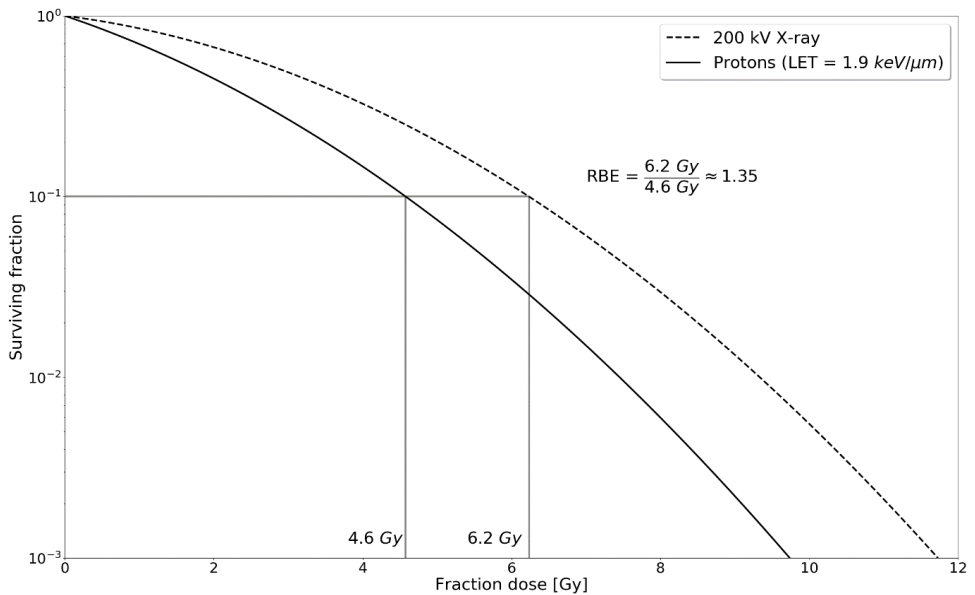
Figure 3.1 The survival fractions for two types of radiation, X-ray (solid) and 1.9 $keV/\mu m$ protons (dashed). The RBE is calculated for 10% survival fraction and is estimated to be 1.35. Data from Mara et al. (2020)

3.3 Modelling the biological effects

Several variable RBE models have been developed in recent years. The models can be divided into two subgroups, mechanistic and phenomenological RBE models. The mechanistic models are based on the mechanism of the cell death and are considered biophysical models. Two of these models are the microdosimetric kinetic model (MKM) and the local effect model (LEM), which are used clinically in carbon-ion

therapy. These models aim to use mechanistic parameters decided for photons, and predict the effects for higher LET irradiation (McMahon and Prise 2019).

The other model group is phenomenological models and is based on dose response data from *in vitro* cell experiments, where the parameters are decided by regression. The most common parameters to model after are the LET and the radiosensitivity parameters α and β.

A mathematical formulation of the RBE can be achieved through combining the definition of RBE in (3.1) with the LQ-model in (3.2):

$$RBE(D, \alpha, \alpha_x, \beta, \beta_x) = \frac{1}{2D_p}\left(\sqrt{\left(\frac{\alpha_x}{\beta_x}\right)^2 + 4D_p\frac{\alpha_x}{\beta_x}\frac{\alpha}{\alpha_x} + 4D_p^2\frac{\beta}{\beta_x}} - \frac{\alpha_x}{\beta_x}\right) \qquad (3.4)$$

where D is the physical dose from the protons, α and β are the proton radiosensitivity parameters from the LQ model, and α_x and β_x are the photon radiosensitivity parameters from the LQ model. The expression in (3.4) can be further simplified by looking at the extreme values for the physical dose:

$$\lim_{D \to 0} RBE = RBE_{max} = \frac{\alpha}{\alpha_x} \qquad (3.5)$$

$$\lim_{D \to \infty} RBE = RBE_{min} = \sqrt{\beta/\beta_x} \qquad (3.6)$$

Inserting (3.4) and (3.5) into (3.3), we achieve a new expression for the RBE:

$$RBE\left(D, \left(\frac{\alpha}{\beta}\right)_x, RBE_{max}, RBE_{min}\right) = \frac{1}{2D_p}\left(\sqrt{\left(\frac{\alpha}{\beta}\right)_x^2 + 4D_p\left(\frac{\alpha}{\beta}\right)_x RBE_{max} + 4D^2 RBE_{min}} - \left(\frac{\alpha}{\beta}\right)_x\right) \qquad (3.7)$$

All LQ-based RBE models have this equation in common, and the difference comes from the modelling of the RBE_{max} and RBE_{min} (Rørvik 2017). The shape of RBE_{max} and RBE_{max} is usually in linear form, and given as

$$RBE_{max/min} = k_1 + k_2 \frac{LET}{(\alpha/\beta)_x} \tag{3.8}$$

where k_1 and k_2 is the fitting parameters. RBE_{min} is also often set to a constant value of 1.

Several different phenomenological models have been developed (Belli, Campa, and Ermolli 1997; Wilkens and Oelfke 2004; Tilly *et al.* 2005; Chen and Ahmad 2012; Carabe *et al.* 2012; Wedenberg, Lind, and Hardemark 2013; Jones 2015; McNamara, Schuemann, and Paganetti 2015; Mairani *et al.* 2017; Rørvik *et al.* 2017), and a comparison of many of the published models was made by Rørvik *et al.* (2018) showing the similarities in terms of the LET dependency.

Another way to model RBE and LET effects is through LET-weighted dose models, where the RBE is still 1.1 but additional LET objectives are added to avoid high LET in organs at risk (OARs), and instead move these values into the target. These models are not based on cell data but rather assume a linear relationship between the LET and RBE, formulated as

$$RBE = 1 + c \times LET \tag{3.9}$$

The c is a scaling parameter varied through literature based on the reduction of RBE variability (McMahon, Paganetti, and Prise 2018), mean RBE of 1.1 to a water phantom (Unkelbach et al. 2016), and median RBE of 1.1 to the tumor volume (Fjæra *et al.* 2017).

3.4 Hypoxia

Tumor hypoxia occurs when the oxygen consumption by the tumor tissue is higher than in the surrounding vasculature system (Koch and Evans 2015). The increased radioresistance can be described by the oxygen enhancement ratio (OER). The OER

quantifies the ratio of the dose at a given oxygen pressure to that at a normal oxygen pressure (normoxic) producing the same biological effect:

$$OER = \frac{D_{hypoxic}}{D_{normoxic}} \qquad (3.10)$$

As the OER decreases with increasing LET, carbon ions are highly efficient in reducing the OER, while x-rays and protons are in general similar, except at the end of range for protons (Wenzl and Wilkens 2011).

Imaging of hypoxia is usually done with Positron Emission Tomography (PET), which utilizes radioactive tracers to acquire metabolic and biochemical information in the patient. Even though there are no ideal hypoxia tracers, some have been demonstrated as feasible, depending on the type of tumors (Fleming *et al.* 2015). The levels of hypoxia in the tumors are usually quantified through the partial oxygen levels (pO2), where mild hypoxia starts at a pO2 level of 19 mmHg, while moderate hypoxia can be found at semi quantitative pO2 levels of 3.8 mmHG (Koch and Evans 2015). The connection between oxygen levels and radioresistance is not clear, but radiation therapy relies on the formation of free radicals to induce DNA damage, which is enhanced by the presence of oxygen (Fleming *et al.* 2015). There are several methods suggested to radiosensitize the hypoxic tumors, however, no option is available clinically (Apilan and Mothersill 2021). Another option to improve hypoxic patient outcome is to modify the treatment plan, so the levels of hypoxia are considered. The technique of dose painting, where the dose to hypoxic volumes are increased, and LET painting, where the LET values are boosted in the hypoxic regions, have been suggested but not yet used clinically (Bassler *et al.* 2014; Bassler *et al.* 2010; Malinen and Sovik 2015). There has also been suggested quantifying the OER directly in the RBE calculations, giving rise to several models that quantify the RBE and OER based on oxygen levels and radiation quality (Wenzl and Wilkens 2011; Tinganelli *et al.* 2015; Strigari *et al.* 2018; Mein *et al.* 2021; Dahle *et al.* 2020). An illustration of the

LET dependency of the Dahle model, and how the varying degree of oxygen levels reduces the RBE and OER weighted dose (ROWD) in a water phantom can be seen in Figure 3.2. The models are based on *in vitro* cell experiments, where the difference in cell survival between hypoxic and normoxic tissue was calculated at 10% cell survival.
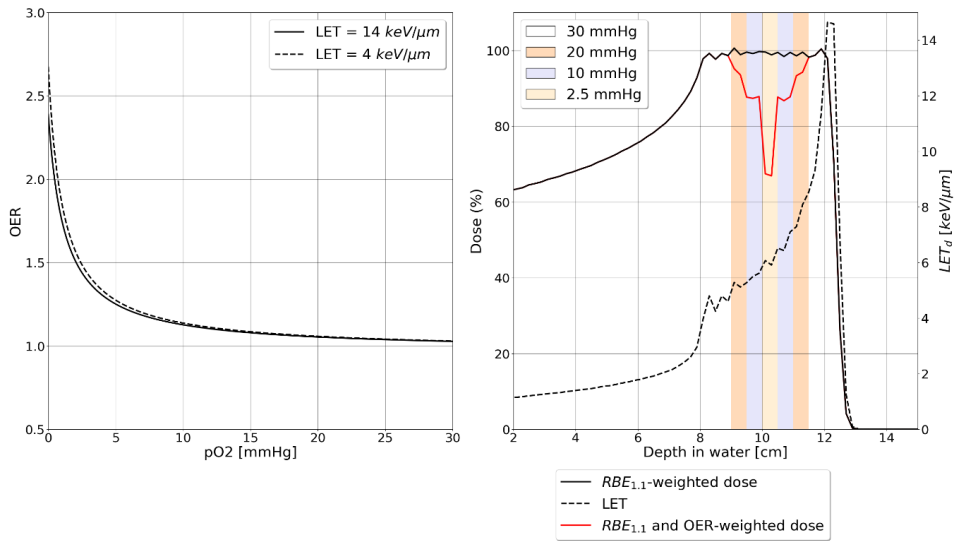

Figure 3.2 pO2 and LET dependency for the OER model from Dahle et al. (2020) (left) and the RBE and OER weighted dose in a water phantom with varying degrees of hypoxia (right).

4. Treatment planning

The first step in the treatment planning process is to acquire anatomical images of the patient, where the gold standard is computed tomography (CT). It provides information about the photon attenuation, which can be used to create a 3D image of the patient. The CT images, alongside other modalities, are used for delineation of the regions of interest in the patient and are done by a physician or dose planner. The first target region is the gross tumor volume (GTV) which consists of the visible tumor. The clinical tumor volume (CTV) includes the sub-clinical spread of the tumor, and the planning tumor volume (PTV) includes any uncertainties in beam delivery (Paganetti 2016). It has also become common to robust plan for the CTV, as the PTV concept has a limitation, e.g., where the worst-case scenario with respect to different uncertainties is planned for (Unkelbach and Paganetti 2018). The OARs are also delineated for planning purposes so that the dose can be minimized in these regions. In the treatment planning system (TPS), the CT and delineated structures are used to create a treatment plan for the patient, which includes the dose distribution and plan settings to assure delivery of this dose distribution with the selected proton beam. The dose optimization in commercial TPSs is based on inverse planning, where the TPS will iteratively try to optimize a dose distribution plan that satisfies the pre-determined objectives and the given field angles.

4.1 Dose calculation

The standard way to calculate dose in treatment planning is through analytical pencil beam (PB) algorithms. Most clinical implementations of these algorithms are based on the works of Hong *et al.* (1996) and Schaffner *et al.* (1999). Firstly, the target is covered in spots, both distally and laterally, and each spot gets assigned a pencil beam which is transported through the medium. As the pencil beam traverse through the medium, the dose to each voxel is calculated based on analytical equations. When all pencil beams

have been transported, the dose is summed up to achieve the final dose distribution (Saini *et al.* 2018).

4.1.1 Monte Carlo

Monte Carlo (MC) simulations are known to be the gold standard in terms of accurate tracking of particles through mediums. A particle is sampled from a source, and its path through matter is discretized. At every small step, the particle-matter interactions are calculated from a probability function, tracking the path of the particle through the medium (Paganetti 2016). With a large enough sample size, an accurate representation of the particle dose deposition can be made. A clear advantage of MC compared to pencil beam algorithms is the ability to score the LET, which is the basis of RBE calculation.

As high statistics are needed to provide results with certainty, and the calculations often are complex, significant computational power and storage are required. Although MC could improve treatment planning, it has not been available in the treatment planning process due to the time limit, and most of the software is CPU-based MC. However, fast GPU-based MC simulations have recently been implemented and verified in clinical TPSs, e.g., Raystation (Schreuder *et al.* 2019a, 2019b; Fracchiolla *et al.* 2021), which will be important moving forward for a more accurate description of the dose distribution.

Most MC software have flexible frameworks which are ideal for research purposes. This includes the FLUKA MC code (Bohlen *et al.* 2014; Ferrari *et al.* 2005), which is used in both Heidelberg Ion-beam Therapy Center (HIT) and CNAO as both a treatment planning tool and for research (Parodi *et al.* 2012) (Tessonnier *et al.* 2014). Our group developed a FLUKA MC based dose recalculation system, which converts clinical DICOM files to a format readable for the FLUKA software, and vice versa. Mairani *et al.* (2013) and Bohlen *et al.* (2013) developed a FLUKA based TPS that optimized clinical particle therapy plans with respect to variable RBE, which have been used in this thesis. Further, other MC toolkits such as the GEANT4 and MCNPX all

show good agreement to both FLUKA and experimental results (Kimstrand *et al.* 2008).

4.2 Optimization

In treatment planning, the goal is to achieve sufficient dose coverage to the tumor volume while still avoiding high doses to critical structures. This can be divided into objectives and constraints and is used for treatment plan optimization. The objective function represents the objective of the optimization, while the constraints impose limitations of optimization. The objectives and constraints are parameterized through a cost function, which shows the difference between the planned dose to the region of interest (ROI) and the calculated dose through a dose volume histogram (DVH). To calculate how costly a treatment plan is, the dose D_i in a voxel i can be written as the sum of all dose contributions d_{ij} from a pencil beam j with weighting x_j

$$D_i = \sum_j x_j \cdot d_{ij} \qquad (4.1)$$

The dose contributions from the pencil beams are then used in cost functions, where the most common are the quadratic objective and penalty functions, used for the target and OAR, respectively:

$$O(d) = \sum_{i \in PTV} w_{PTV} (D_i - \widehat{D}_i)^2 + \sum_{j \in OAR} w_{OAR} H (D_j - \widehat{D}_j)(D_j - \widehat{D}_j)^2 \qquad (4.2)$$

where D_i is the sum of the dose contribution to the PTV, $\widehat{D}_i$ the prescribed dose the target, D_j the dose contribution to the OAR, $\widehat{D}_j$ the maximum dose limit to the OAR, H the Heaviside step function and w the respective weighting of each contribution. The Heaviside step function, H, is 1 when the dose in the voxel is above the dose limit, and 0 if not. Equation (4.2) only represent an example of a cost function as multiple

modifications can be made. We want to minimize this function, and thus achieve an optimization problem

$$\min_{x_j}\{O(d)\}$$

(4.3)

Meaning that we want to minimize the optimization problem based on the beam weighting parameter x_j.

This can be done by several different algorithms, such as the plain gradient algorithm and the Broyden–Fletcher–Goldfarb–Shanno (BFGS) algorithm, which are implemented in the Eclipse TPS.

4.2.1 **LET and RBE -optimization**

With intensity-modulated proton therapy (IMPT) many different field setups and energies can be used, which will give the clinician multiple alternatives to deliver an optimal plan, also with respect to RBE and LET, without compromising the RBE of 1.1. Even though this is not directly RBE and LET optimization, it could be a steppingstone towards it. This has been explored by Fjæra *et al.* (2017) and Mein *et al.* (2022), and similar techniques are also in clinical use (Indelicato *et al.* 2014). Fager *et al.* (2015) divided the target into subvolumes which were assigned individual IMPT fields which showed an increased LET in the target without sacrificing tumor coverage.

There are also studies showing how treatment planning could include LET in the optimization. This is demonstrated by several studies by either implementing LET directly (Giantsoudi *et al.* 2013; Cao *et al.* 2017; Inaniwa *et al.* 2017) as an objective in the treatment planning process, or using a dose-weighted LET model (Unkelbach *et al.* 2016) to optimize the plan with respect to LET weighted dose, as mentioned in 3.3. This approach could also be used to treat hypoxic tumors by elevating the LET values in regions with low oxygen to increase the cell killing in so-called LET painting.

However, it has been shown that LET painting is more efficient for heavier ions than protons due to the limited range of LET values for protons (Malinen and Sovik 2015).

Another approach to RBE optimization is to include phenomenological models in the dose calculation, as mentioned in 3.3, and plan according to the RBE-weighted dose (Wan Chan Tseung *et al.* 2016; Guan *et al.* 2018). Other optimization techniques include distal edge tracking, as proposed by Bai *et al.* (Bai *et al.* 2020), where the PB spots with non-optimal LET distribution were penalized, which provided comparable results to LET optimization.

Reviews of the clinical RBE in proton therapy suggested that the opportunity to calculate RBE and LET clinically should be implemented at most PT centers for this reason (Paganetti *et al.* 2019), and now several different PT centers in Europe have local procedures for calculating the RBE clinically (Hahn *et al.* 2021) mostly based on MC (Sorensen *et al.* 2021). However, there is still no consensus for future RBE and LET strategies between different centers, but LET and RBE calculations are becoming available in clinical TPSs, and optimization is expected to be introduced soon.

4.3 Beam Delivery

There are two main methods for delivering proton dose, passive scattering, and active scanning. Passive scattering uses different components to shape and conform the proton beam such that the target receives a homogenous dose. For active scanning, or Pencil Beam Scanning (PBS), dipole magnets are used to steer the beam so the prescribed dose is delivered to predetermined spots in the target.

Single field optimization (SFO) consists of simple linear addition of multiple fields. In SFO, the fluence of each field is optimized so that the dose will be as homogenous as possible. The weighting of each field can also be different and is done to reduce the contribution from either field with low homogeneity, or if it ends in a critical organ (Lomax 2016).

The proton beam can also be sculpted by multiple fields using multi-field optimization (MFO), meaning the fields are optimized in unison. Unlike SFO, the different fields in the plan are aware of each other, and the combined dose distribution is only guided by the optimization goals (Langen and Zhu 2018).

4.3.1 Intensity-Modulated Proton Therapy (IMPT)

MFO opens up for IMPT, which exploits PBS flexibility to allow each proton field to assume an arbitrary dose distribution as long as the sum of fields provides desired distribution (Kooy and Grassberger 2015). The degree of freedom achieved through IMPT compared to SFO is significant, as the weighting of each pencil beam is now individual and only related to the overall objective. This also leads to an increased computational time and complexity in the treatment planning process. However, a physician or treatment planner will have considerable more choices to improve the treatment plan (Kooy and Grassberger 2015).

4.4 Proton Arc Therapy (PAT)

A new emerging treatment planning technique for protons is Proton Arc Therapy (PAT) which consists of rotating the gantry around the patient in an arc, delivering a continuous dose similar to the photon therapy technique Volumetric Arc Therapy (VMAT). This concept was first suggested in 1997 (Sandison *et al.* 1997), but it was not until recently that Ding *et al.* (2016) used the potential of IMPT to create the first PAT plans. This has led to several treatment planning studies showing the potential of PAT in different clinical scenarios (Blanco Kiely and White 2016; Rah *et al.* 2016; Li *et al.* 2018; Ding *et al.* 2019; Liu *et al.* 2020b; Chang *et al.* 2020; Liu *et al.* 2021b). Although not yet clinically available, beam delivery testing has been performed (Li *et al.* 2019), as well as studies aiming to optimize beam delivery time (Gu *et al.* 2020) (Liu *et al.* 2020b) (Nesteruk *et al.* 2021). Different delivery techniques such as stereotactic treatment have also been improved with arcing techniques (Liu *et al.* 2021a; Liu *et al.* 2021b).

The additional degree of freedom achieved with PAT gives rise to new planning methods such as mono-energetic beams (Sanchez-Parcerisa *et al.* 2016; Bertolet and Carabe 2020; Carabe-Fernandez *et al.* 2020), which can give a LET distribution in the target and reduce it in healthy tissue while also decrease the treatment time.

5. Thesis objective

The overall objective of this thesis was to provide knowledge of and explore how different optimization strategies could be used in proton therapy planning to account for variable RBE and OER. By introducing optimization strategies which accounts for biology in proton therapy clinics, treatment outcome could be improved. The specific objectives of each paper are described in the following

Paper I:

- Optimize proton therapy plans with respect to LET and variable RBE models
- Investigate the effect of different RBE and LET based proton optimization strategies on dose distributions in OARs and target volumes

Paper II:

- Develop a proton optimization tool for voxel-by-voxel based hypoxia treatment using clinical PET and CT images
- Include hypoxia modelling in variable RBE models to optimize ROWD

Paper III:

- Review different ROWD models in terms of pO_2 and LET dependency
- Compare how the OER from the different models varies within different scenarios

Paper IV:

- Investigate the effect of beam pruning in PAT plans on RBE and LET distributions

6. Materials and methods

6.1 FLUKA MC recalculation tool

In this thesis, treatment plans for the clinical patient cases and water phantoms were originally made in Eclipse TPS (Varian Medical Systems, Palo Alto, California, US). Dose verification and recalculation from these plans were done by the FLUKA MC code, which also has been used as the primary tool for re-optimization of plans.

To achieve the density information about the tissue, treatment planning CT images are converted into voxels in the graphical interface for FLUKA, FLAIR. The conversions curves were calibrated previously in our group (Fjæra 2016). For complex simulations, subroutines were used in FLUKA to sample primary particles, as well as score biological parameters.

The *source.f* subroutine is used to simulate the pencil beams in the plan. In this subroutine, the property from a primary particle is randomly sampled from the pencil beam distribution. These properties include energy spot position and beam focus, while we define the pencil beam by energy and position.

The *fluscw.f* subroutine is used to score dose to water from all particles, as well as the LET and the dose from protons and deuterium. These values are needed to calculate the RBE-weighted dose as described in section 3.3. As described in section 2.3, we use the fluence of a particle to calculate dose described in equation (2.6), and the fluence can be estimated as the infinitesimal length dl_i of the trajectory of a particle i, divided by the infinitesimal volume dV (Papiez and Battista 1994):

$$\theta_i = \frac{dl_i}{dV} \tag{6.1}$$

The fluence θ_i can further be weighted by a factor W_i defined in the subroutine to modify the spatial scoring. The scored quantity will then be:

$$scoring = \sum_i W_i \times \theta_i \tag{6.2}$$

Applying this, we can achieve the dose scored to water by summing over all dose contributions i in a voxel, multiply by the LET contribution from particle i in water (LET_i^w) and divide by the density of water ρ^w:

$$D^w = \sum_i \frac{1}{\rho^w} LET_i^w \times \theta_i \tag{6.3}$$

The LET value from water is obtained through the built-in function in FLUKA called GETLET, which outputs LET based on particle type, energy, and type of material.

In our study, we calculate the dose from all particles, along with the dose from only protons, which are needed for RBE calculations.

For the LET, the dose to water was multiplied by the LET

$$LET^w D^w = \sum_i \frac{1}{\rho^w} (LET_i^w)^2 \times \theta_i \tag{6.4}$$

To achieve the LET_d, dose division was done offline in a separate python script (Fjæra *et al.* 2017).

For our studies, the *fluscw.f* subroutine was modified again, so the α and β for every respective model were calculated online, as this is required for the FLUKA MC based optimizer.

6.2 Methods for optimization of proton therapy treatment plans

6.2.1 The optimizer

A FLUKA MC based optimization tool developed by Mairani *et al.* (2013) and Bohlen *et al.* (2013) was used in this thesis. The tool was modified to fit our in-house recalculation system described in chapter 6.1.

The optimizer uses information from the FLUKA simulation to create new treatment plans. More specifically, the inputs for the optimizer are the physical dose and biological variables, α and β, information about the initial weightings of each pencil beam, and voxel location for the region of interest (ROI). The α and β are LET dependent, and an OER and pO$_2$ dependency were introduced in Paper II and III. The optimizer uses this information to create an optimal plan based on given dose objectives and outputs a file with the new pencil beam weightings.

There are two algorithms implemented in the optimizer, the dose-difference algorithm, and a plain gradient algorithm. Both algorithms allowed for optimization based on variable RBE and showed similar results.

6.2.2 Patient material

A simulated water phantom case was used to explore different optimization strategies. The phantom consisted of a 4 x 4 x 4 cm^3 SOBP, starting at 8 cm depth and with a prescribed dose of 2 Gy(RBE$_{1.1}$). The phantom was used to investigate the effects of RBE optimization (Paper I), and further, the oxygen levels in the phantom were varied to explore the effect of hypoxia in ROWD optimization (Paper II) and model variation (Paper III). The oxygen levels varied from fully normoxic to fully hypoxic in the middle of the target (Figure 6.1). Two plans were created for the water phantom in Paper II, a single field SOBP case and an SOBP with two opposing fields.
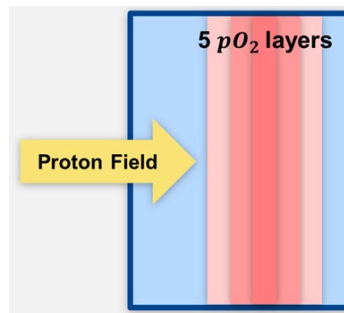

Figure 6.1 Illustration of the water phantom with varying oxygen levels where the amount of redness represents lower pO$_2$ levels.

In Paper I, three different patient cases were used to demonstrate how RBE based optimization strategies would work for different clinical scenarios. A prostate tumor case, a pituitary adenoma (brain tumor) case, and a rhabdomyosarcoma (head and neck cancer, HNC) case were planned using the Eclipse TPS and multi field optimization. The $(\alpha/\beta)_x$ values used for the different cases were found in the literature and are listed in the table below.

Table 6-1 Plan properties for the different patient cases used in Paper I.

	Brain tumor	**Prostate**	**Head and neck**
Number of fields and field angles	GA 257°, PSA 0° GA 291°, PSA 60°	2 opposing fields	GA 55°, PSA 0° GA 85°, PSA 0° GA 135°, PSA 0°
Prescribed dose to PTV [Gy(RBE)]	54	67.5	50.4
OARs included in the optimization	Brainstem Left optic nerve	Rectum Bladder	Left pterygoid Right parotid gland
$(\alpha/\beta)_x$ **PTV [Gy]**	10.6 (Pedicini *et al.* 2015)	1.5 (Brenner and Hall 1999)	2.8 (Mendonca and Timmerman 2002)
$(\alpha/\beta)_x$ **OAR [Gy]**	2.1 (Meeks *et al.* 2000)	3.5 (Terry and Denekamp 1984)	2.8 (Mendonca and Timmerman 2002)
GA – Gantry Angle PSA – Patient Support Angle			

For Paper II and III, HNC cases were explored with prescribed doses of 70 Gy(RBE) divided into 35 fractions, where the pO_2 values were estimated from [^{18}F]-EF5 PET images. The conversion from PET-uptake to pO_2 has been previously published by our group (Dahle *et al.* 2020). The HNC cases differed in the levels of hypoxia, as one case was significantly more hypoxic than the other. We evaluated the PTV coverage as well as the dose to the parotid glands. Only the estimated pO_2 values in the PTV were used,

while the OARs were assumed to be normoxic. The $(\alpha/\beta)_x$ for the tumor was 10 Gy (van Leeuwen *et al.* 2018), while for the OAR, an $(\alpha/\beta)_x$ of 3 Gy was used (Emami *et al.* 1991). The PET images were acquired at Turku University Hospital in Finland using a GE D690 PET/CT scanner (General Electric Medical Systems, Milwaukee, WI, USA).

In Paper IV, we demonstrated a method of pruning the energy layers in PAT-beams to increase the LET and RBE in the target. The pruning technique was demonstrated on a germinoma case, with a prescribed dose of 54 Gy(RBE) divided into 30 fractions. For a plan to be valid, the optimization criteria were 95% of the prescribed dose to 100% of the PTV and 107% of the prescribed dose to 0% of the PTV ([V95%, V107%]).

6.2.3 Model selection

Several different RBE models have been developed in recent years, and three RBE models were included in this study based on their difference in origin. Both the Rorvik (ROR) (Paper I-IV) and McNamara (MCN) model (Paper I) is based on *in vitro* data, but the MCN model assumes a linear relationship with LET, whereas the ROR model assumes a non-linear fit to the LET-spectrum. Both models also depend on the radiosensitivity parameter $(\alpha/\beta)_x$.

The RBE_{max} and RBE_{min} parameters for the MCN model are given as:

$$RBE_{max}(MCN) = 0.99064 + \frac{0.35605\ Gy}{\left(\frac{\alpha}{\beta}\right)} LET_d \qquad (6.5)$$

$$RBE_{min}(MCN) = 1.1012 - 0.0038703 Gy^{-\frac{1}{2}}(keV\ \mu m)^{-1}\sqrt{\left(\frac{\alpha}{\beta}\right)_x} LET_d \qquad (6.6)$$

while the RBE_{max} and RBE_{min} for the ROR model are given as:

$$RBE_{max}(d(L)) = \int_0^\infty r_{max}(L)d(L)dL$$

$$r_{max}(L) = 1 + \frac{\text{Gy}}{(\alpha/\beta)_x}\left(0.578\left(\tfrac{\text{keV}}{\mu\text{m}}\right)^{-1}L - 0.0808\left(\tfrac{\text{keV}}{\mu\text{m}}\right)^{-2}L^2 + 0.00564\left(\tfrac{\text{keV}}{\mu\text{m}}\right)^{-3}L^3\right.$$

$$\left. - 9.92 \times 10^{-5}\left(\tfrac{\text{keV}}{\mu\text{m}}\right)^{-4}L^4\right), \qquad L < 37.0\,\frac{\text{keV}}{\mu\text{m}} \tag{6.7}$$

$$r_{max}(L) = 1 + 10.5\,\frac{Gy}{(\alpha/\beta)_x}, \qquad L \geq 37.0\,\frac{\text{keV}}{\mu\text{m}}$$

$$RBE_{min} = 1$$

where L is the LET, $d(L)$ is the LET spectrum, and $r_{\max}$ is the biological weighting function.

The LET-weighted dose (LWD) model (Paper I and IV) is independent of cell data and is instead fitted to a linear relationship with the LET as described in section 3.3. The c parameter was varied for the different studies. In Paper I, it was normalized to a median RBE of 1.1 in the target, and in Paper IV the c parameter was set to $0.055\ \mu m/keV$, as described by McMahon *et al* (2018) to reduce the biological variability between RBE models.

6.2.4 Optimization strategies

Two different RBE optimization strategies were used in Paper I, full RBE optimization (FO) and differential optimization (DO). In full RBE optimization, both the PTV and OARs were optimized with respect to variable RBE. These plans were denoted FO_{ROR} FO_{MCN} and FO_{LWD} for the full MCN, ROR, and LWD strategy, respectively. RBE optimization strategy used an RBE of 1.1 in the target and variable RBE to the OARs. Similar to the full strategies, the differential optimization strategies are denoted DO_{ROR} DO_{MCN} and DO_{LWD} for the variable RBE models. In Paper II, only full optimization was deployed on the target and OAR.

6.3 Optimization of treatment plans for hypoxic tumors

To compare how OER is accounted for in treatment planning, as well as optimize plans with respect to hypoxia, OER models were studied. The different published models to account for OER and RBE in proton therapy were compared in a simulated water phantom and a clinical patient case (Paper III).

6.3.1 RBE and OER calculations and optimization

We defined an RBE and OER Weighted Dose (ROWD), which combined the OER and RBE calculation as:

$$D_{\text{OER,RBE}} = \frac{D}{D_p} \left(\sqrt{\left(\frac{\alpha_x}{2\beta_x}\right)^2 + \frac{\alpha_h D_p + \beta_h D_p^2}{\beta_x}} - \frac{\alpha_x}{2\beta_x} \right) \tag{6.8}$$

where α_x and β_x are the aerobic tissue radiosensitivity parameters and α_h and β_h are the pO_2-dependent proton radiosensitivity parameters. The pO_2-dependent proton radiosensitivity parameters are found by combining α and β values from RBE models, with the definition of OER found in equation (3.10):

$$\alpha_h = \alpha_{RBE}/\text{OER}(L, p_h) \tag{6.9}$$

$$\beta_h = \beta_{RBE}/\text{OER}^2(L, p_h) \tag{6.10}$$

where α_{RBE} and β_{RBE} are the biological parameters for the variable RBE models.

6.3.2 OER models

Several models for calculating the OER based on pO_2 have been proposed, generally based on *in vitro* data from different cell lines under normoxic and hypoxic conditions. The models are then fitted to a reverse-sigmoid-shaped curve, which describes the relationship between the pO_2 and OER through the Alper-Howard-Flanders formalism. We left out models from this study which would either result in heavy, time-consuming

calculations or earlier versions of models. The models we studied were from Wenzl and Wilkens (WEN) (Wenzl and Wilkens 2011), Tinganelli (TIN) (Tinganelli *et al.* 2015), Strigari (STR) (Strigari *et al.* 2018), Dahle (DAH) (Dahle *et al.* 2020) and Mein (Mein *et al.* 2021), and the different properties were compared in Paper III.

6.3.3 Calculation of hypoxia

In papers II and III, the OER as a function of LET and hypoxia was calculated in the *fluscw.f* subroutine as:

$$\text{OER}(L, p_h) = \frac{\sqrt{\alpha^2(L, p_h) - 4\beta(p_h) \cdot \ln(0.1)} - \alpha(L, p_h)}{\sqrt{\alpha^2(L, p_a) - 4\beta(p_a) \cdot \ln(0.1)} - \alpha(L, p_a)} \cdot \frac{\beta(p_a)}{\beta(p_h)} \tag{6.11}$$

where the L is the dose-averaged LET, p_h and is the partial pressure of oxygen (pO_2) in a given voxel in the patient, while p_a is the partial pressure of oxygen in normoxic tissue. The radiosensitivity parameters $\alpha(L, p)$ and $\beta(L, p)$ for hypoxic and normoxic tissue are given by:

$$\alpha(L, p) = \frac{(a_1 + a_2 \cdot L) \cdot p + (a_3 + a_4 \cdot L) \cdot K}{p + K}, \tag{6.12}$$

$$\sqrt{\beta(p)} = \frac{b_1 \cdot p + b_2 \cdot K}{p + K}, \tag{6.13}$$

where p is the pO_2 for both the hypoxic and normoxic tissue, where the normoxic value was set to 60 mmHg, and K is a parameter set to 3 mmHg (Alper and Howard-Flanders 1956). The remaining model parameters were found by non-linear least square curve fit of the *in vitro* proton data, and given as: a_1 = 0.10 Gy^{-1}, a_2 = 0.0010 µm/(Gy·keV), a_3 = 0.010 Gy^{-1}, a_4 = 0.0100 µm/(Gy·keV), b_1 = 0.765 Gy^{-1} and b_2 = 0.273 Gy^{-1}.

6.4 Pruning techniques in PAT

6.4.1 Pruning the treatment plans

In Paper IV, we wanted to demonstrate different pruning techniques in PAT arc therapy. Therefore, seven different plans were created in the Eclipse TPS for this study to compare the effects of the pruning:

- A PAT plan consisting of a 240-degree arc where no beams were positioned anterior to the patient (Figure 6.2c). The beams had a 10-degree separation, and this plan was used as a reference plan.

- Six pruned PAT plans (PX-PAT, where X represents the degree of pruning) were created from the reference plan. The pruning was performed by shrinking the PTV in all dimensions corresponding to approximately one energy layer of the beam and adding margins in all directions except for the distal part. An illustration of the pruning process can be seen in Figure 6.2a and b, while the highest energies for each beam for the different PX-PAT plans can be seen in Figure 6.2d
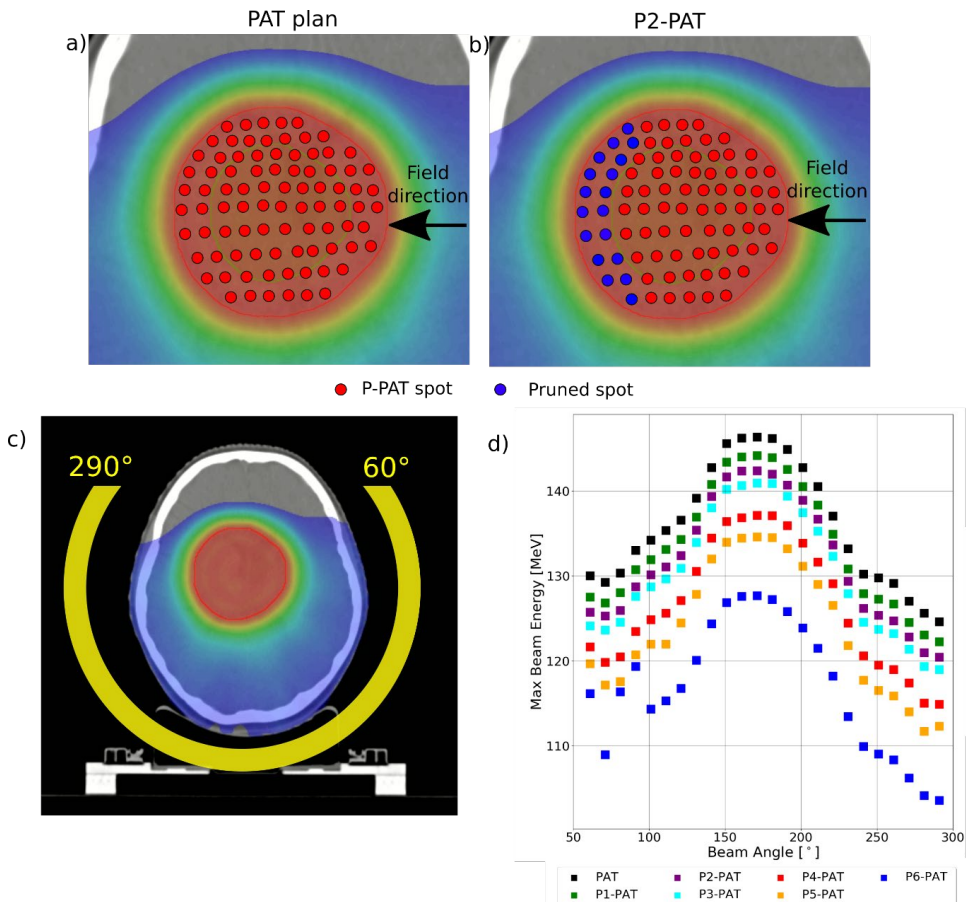
Figure 6.2 a) Illustration of a spot map for a PAT plan, b) and the P2-PAT plan where the blue color represents the pruned spots in this map. The red outline shows the PTV, and the green outline shows the shrunken PTV volume. c) shows the beam positioning for the arc around the tumor volume, and d) shows the maximum energy from each beam in the arc.

To visualize biological effects, the plans were recalculated in our in-house FLUKA MC recalculation system with respect to two variable RBE models, the ROR model and the LET-weighted dose model (LWD). The clinical OARs that were included in this study were the left hippocampi and right optic nerve, alongside a 2 cm spherical shell covering the PTV, to observe the surrounding LET effects.

6.5 Ethical considerations

The patient data applied in this study originate from Haukeland University Hospital (Paper I and III) and Turku University Hospital (Paper II and IV), and was used with permission from these facilities. The patient material was anonymized. The patients from Turku University Hospital were part of a study registered at ClinalTrials.gov under the number NCT 01774760.

7. Summary of results

7.1 Paper I: Exploring OAR sparing techniques with different RBE based optimization strategies

In Paper I, we saw how different RBE based optimization strategies would affect the LET$_d$, RBE-weighted dose, and physical dose distribution for different patient cases. A clear difference was observed in both physical dose and LET$_d$ for the different variable RBE models (Figure 7.1). For the prostate case, there was a large difference between the $(\alpha/\beta)_x$- dependent models (MCN and ROR), and the LWD model, as the mean physical dose to the target from the FO$_{MCN}$ and the FO$_{ROR}$ strategies were respectively 10% and 5 % lower than for the RBE$_{1.1}$. For both LWD strategies, there were negligible differences compared to the reference plan.
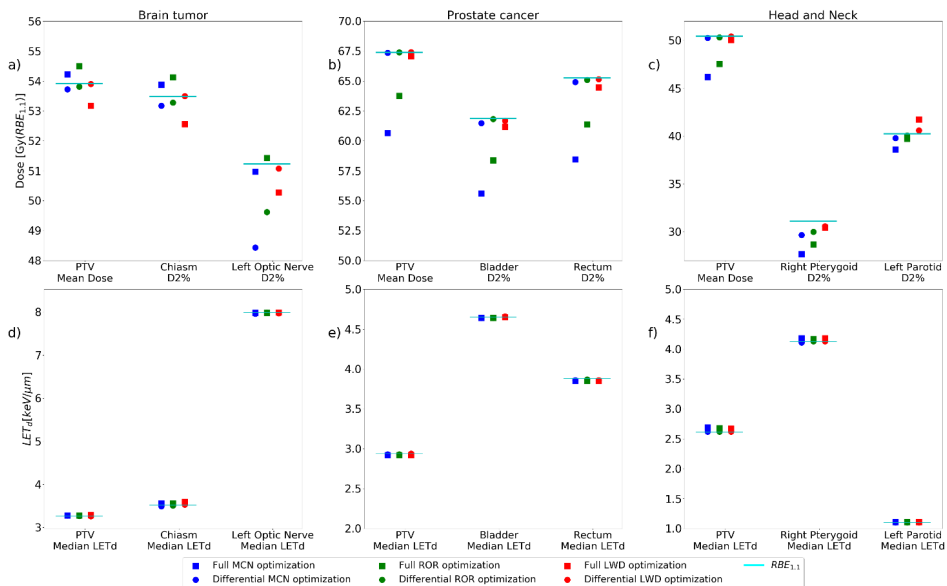

Figure 7.1 Overview of RBE$_{1.1}$-weighted dose (top row) and LET$_d$ (bottom row) resulting from the different optimization strategies. The colors indicate the respective RBE and LWD models, while the cyan line represents the reference plan (RBE$_{1.1}$ optimization). The square markers represent the full strategy, while the circle markers represent the differential strategies.

The brain tumor showed less variation in results compared to the prostate case. Here, the differential optimization strategies (variable RBE only in OARs) provided the highest OAR sparing: DO_{MCN} reduced the maximum OAR dose by 3-5%, as compared to the reference $RBE_{1.1}$ plan, while still fulfilling the prescribed $RBE_{1.1}$-dose to the target. For FO_{LWD}, the reduction varied between 2-3% for the different OARs. The physical dose in the target was also significantly reduced with this strategy (Figure 7.1b)

In the head and neck case, it was again the full strategies that provided the highest difference compared to the reference plan. The FO_{MCN} plan reduced the maximum dose to the right pterygoid by 10%, the full ROR reduced it by 7%, and the full LWD reduced it by 2% (Figure 7.1c). This study shows that for tumors with high $(\alpha/\beta)_x$, small differences are seen between the optimization strategies, while for low $(\alpha/\beta)_x$ tumors, the differences were high, illustrating how heavily it affects the biological optimization.

7.2 Paper II: Optimizing treatment plans with respect to hypoxia.

A FLUKA MC based optimization method for hypoxia was created and demonstrated on a simulated water phantom and two HNC cases.

For the water phantom case, a homogenous ROWD dose was achieved in the SOBP, verifying our method. Including pO_2 in the optimization caused an increase in the maximum physical dose of up to 30%, and an LET_d increase from approximately 5 keV/μm to 12 keV/μm was seen in the most hypoxic area. This shows how our hypoxia optimization method could account for hypoxia, and the outcome of the optimization was highly dependent on the pO_2 levels.

For the HNC cases, one case had significantly lower pO_2 levels compared to the other case, thus representing different clinical scenarios. The hypoxic case had 95% of the

PTV under 60 mmHg, while this was 50% for the normoxic case. The optimization depended heavily on these levels. Both provided comparable dose coverage to the PTV but differed in mean physical dose to the PTV. The mean physical dose to the PTV increased by 12.2 Gy for the ROR(OER) plan compared to the reference $RBE_{1.1}$ plan, and 9.3 Gy higher for the $RBE_{1.1}$(OER) plan Figure 7.2, top left panel). For the normoxic case, the increase was smaller, as the mean physical dose to the PTV increased by 3.5 Gy for the ROR(OER) plan compared to the reference $RBE_{1.1}$ plan, and 1.1 Gy higher for the $RBE_{1.1}$(OER) plan (Figure 7.2, bottom left panel).

The increased dose to the PTV led to an increased dose to the OARs, as the maximal physical dose was 10.7 Gy higher for the ROR(OER) plan compared to the reference plan. For the normoxic case, the same increase was only 3.3 Gy (Figure 7.2, right column).
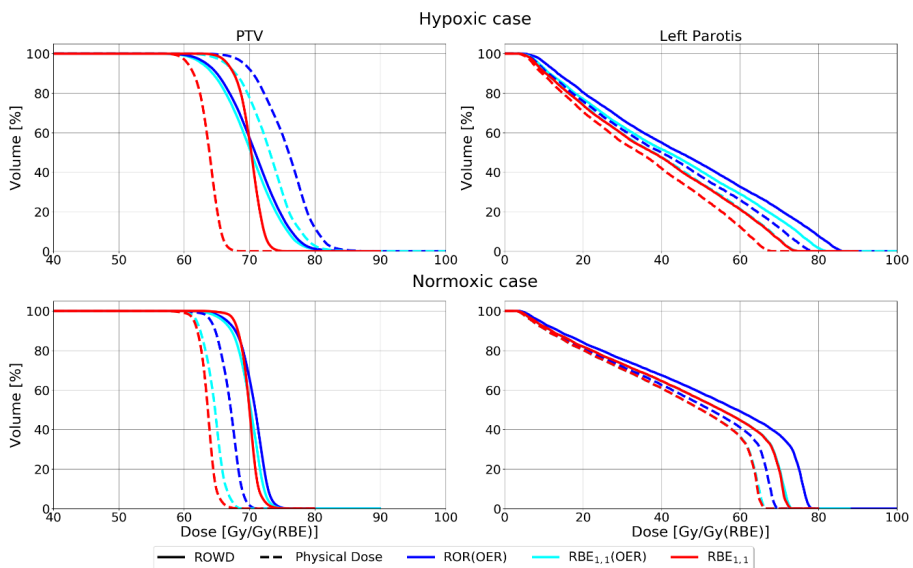

Figure 7.2 DVHs for the different plans optimized with respect to ROWD for the hypoxic case (top row) and the normoxic case (bottom row), where the solid lines represent the ROWD, while the dashed lines represent the respective physical dose.

7.3 Paper III: Exploration and comparison of OER models in proton therapy

The five ROWD models were successfully implemented in FLUKA and compared. Even though large differences were seen between some of the models, they all showed a similar shape. All models show an increase in OER as the pO_2 decreased. For the water phantom, this corresponded to a reduction between 25% and 40% when comparing the ROWD models to RBE models not accounting for the OER.

In the first hypoxic region (pO_2 = 20mmHg), the lowest ROWD is predicted by TIN, while the highest ROWD can be seen from MEI, DAH, and WEN. In the next region (pO_2 = 10mmHg), the STR, WEN, DAH, and MEI are comparable. In the most hypoxic area, the lowest ROWD is predicted by STR and the highest from DAH and MEI.

For the HNC case, all models provide a significantly lower ROWD than the $RBE_{1.1}$ reference plan. The median ROWD (ROWD to 50% of the volume) varied between 53.6 to 60.2 Gy(RBE), while the prescribed dose was 70 Gy(RBE). WEN and DAH showed similar results both in terms of $RBE_{1.1}$ and ROR adaptation. These models showed similar ROWD to MEI, which again showed higher ROWD than STR and TIN (Figure 7.3).
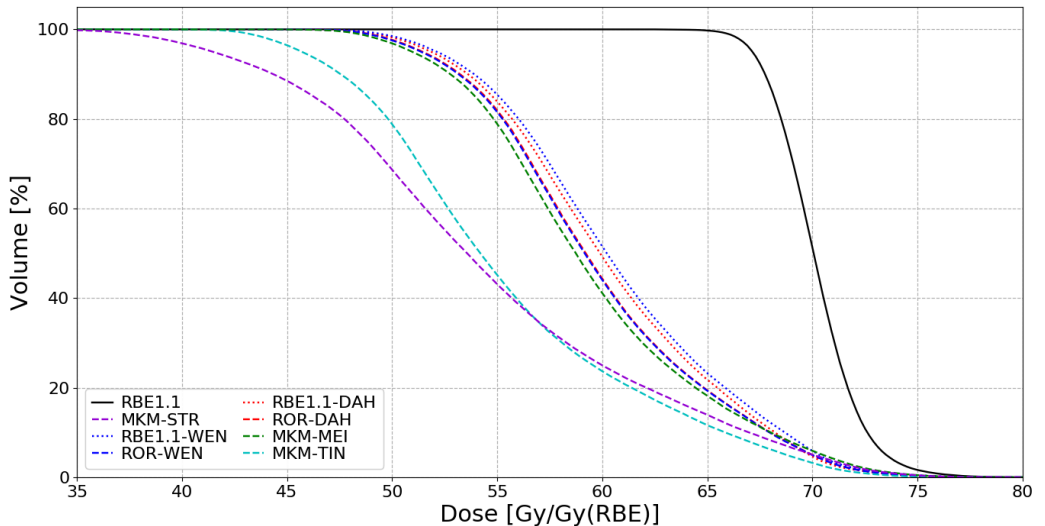
Figure 7.3 DVH for all ROWD models, including the RBE$_{1.1}$ reference plan (solid black line).

7.4 Paper IV: Exploring LET and RBE effects from pruning in proton therapy

The pruned PAT (P-PAT) plans significantly increased the LET$_d$ in the target compared to the reference P-PAT plan (Figure 7.4a), with an elevation of mean LET$_d$ of 0.4, 0.7, and 1.5 μm/keV for the P4-, P5-, and P6-PAT plan, respectively. This also lead to a corresponding decrease in the LET$_d$ in the surrounding healthy tissue and the OARs for all plans (Figure 7.4b,c, and d).

For the RBE-weighted doses, all plans were comparable in terms of PTV coverage. All P-PAT plans reduced the mean RBE-weighted dose from the variable RBE models (ROR and LWD) to the surrounding tissue, except the P6-PAT plan, which increased the RBE-weighted dose. However, this plan showed the largest increase in the RBE weighted dose to the target, so a potential decrease in overall physical dose could be applied to compensate for this.
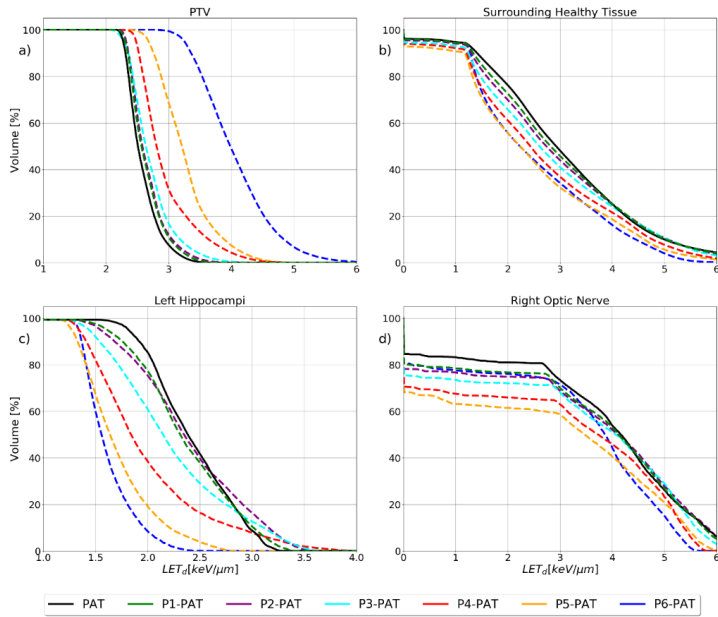
Figure 7.4 LET$_d$ volume histogram for the PTV, healthy surrounding tissue, and the OARs calculated with 2 Gy(RBE$_{1.1}$) dose cutoffs. The dashed lines represent the P-PAT plans, while the solid lines represent the PAT plan.

8. Discussion

This thesis shows how optimizing both the physical dose and LET distribution in proton therapy plans may utilize more of the potential of proton therapy. Pencil beam scanning in proton therapy gives high flexibility and allows for LET redistribution. The treatment can therefore be adapted to provide a superior biological effect compared to both photon therapy and the current clinical proton therapy treatment, where an RBE of 1.1 is used.

The strategies presented in this study may provide helpful insight into how variable RBE optimization can be implemented and exploited. This includes how a differential RBE strategy could provide an intermediate step towards full RBE or LET optimization (Paper I). The optimization strategies were further explored when applying RBE in hypoxic cases, where the hypoxia data was derived from PET images, and the belonging treatment plans were optimized on a voxel-by-voxel basis (Paper II). Several approaches to hypoxia-modelling were explored and compared, which revealed good agreement between several models, but also significant deviations between the estimates of some models (Paper III). The model differences and also the large OER values considering the change in dose prescription they suggest, reveals that more research effort is needed to find a path to clinical implementation. Further, the emerging treatment technique, PAT, was used in a novel method of PAT pruning (Paper IV). This study showed how the increased degree of freedom in PAT could provide more biologically advantageous treatment plans by shifting high RBE regions from healthy tissue into the tumor volume.

8.1 RBE based optimization strategies

Optimizing proton therapy plans with respect to RBE is motivated by recent clinical evidence of a higher RBE at the distal end of the beam (Peeler *et al.* 2016; Underwood *et al.* 2018; Engeseth *et al.* 2019; Eulitz *et al.* 2019; Bahn *et al.* 2020; Bolsi *et al.* 2020; Engeseth *et al.* 2020; Oden *et al.* 2020; Engeseth *et al.* 2021; Bertolet *et al.* 2022;

Engeseth *et al.* 2022). These are related to asymptomatic toxicity, corresponding to radiation-induced image change from either MRI or CT. In addition, a study by Wang *et al.* (2020) showed an increased risk of rib fracture due to high RBE in healthy tissue. A recent study by Harrabi *et al.* (2021) revealed a significant correlation between image change and high LET values, suggesting that LET is an important factor in terms of radiation-induced image change. The clinical evidence indicates that the treatment planning today should consider accounting for a variable RBE, and different RBE optimization strategies have thus been explored in this thesis.

In vitro experiments using proton beams have shown an increased RBE with higher values of LET, which has its maximum at the distal end of the proton beam. This increase is reflected by the phenomenological RBE models, which are based on such *in vitro* data sets (Rørvik *et al.* 2017). Even though the RBE models estimate different magnitudes of RBE values depending on the dose level, LET, and tissue type, they all project a similar shape of elevated RBE towards the distal end. A biological shift in the dose can also be observed, extending the beam range up to 1-2 mm compared to the RBE of 1.1 used clinically (Paganetti *et al.* 2002). This is also the case for mechanistic dose models, which also show an increase in RBE at the distal part of the beam (Grun *et al.* 2013; Giovannini *et al.* 2016) and a similar biological shift as the phenomenological models. New *in vivo* experiments support this, as an elevated RBE is observed at the distal end with the increased LET, even for high fraction doses (Saager *et al.* 2018). Thus, when applied for biological dose reduction in OARs in treatment planning, applying different models may give a similar result in terms of physical dose and LET to the OARs as all models will push "in the same direction." However, if the models are simultaneously used to optimize the target dose, the different levels of physical dose to the target could also affect the OAR dose significantly. This was seen in Paper I, where the optimization reduced the physical dose in the distal part of the beam for the brain tumor case and the head and neck case for most variable RBE models. In addition to the model differences, the optimization in Paper I also showed a great case dependency. The main parameter that was changed

for the different cases was the $(\alpha/\beta)_x$, which caused large differences in the RBE. The $(\alpha/\beta)_x$ is an uncertain parameter and can vary greatly between certain tumor types and endpoints (Paganetti 2022), which will therefore affect the RBE as we saw that the physical dose outcome from the different patient cases varied substantially as an effect of the diverse $(\alpha/\beta)_x$.

Additionally, the difference in anatomy and field setup will also cause differences in the LET distribution and in the potential to "move" the LET in the optimization process, as seen in Paper I, where the optimization of the prostate case did not shift any LET values. In general, the field setup is important as it could provide more freedom to adjust both the physical dose and the LET for the target. For instance, more field angles or arc treatments (as applied in photon therapy) would give the freedom to also substantially change the LET in prostate patients.

Most RBE models have a linear dependency on the LET, as well as a dependency on the $(\alpha/\beta)_x$ (Rørvik *et al.* 2018) and although the RBE models possess uncertainties from the *in vitro* data, the acquiring of better *in vitro* data, i.e. large datasets with smaller deviations and precise reporting of beam quality and other relevant parameters, will reduce these uncertainties.

A tissue independent approach to optimization with a variable RBE is to simply use a linear LET dependency on the dose, with a scaling parameter c, and the shape $RBE = 1 + c \times LET_d$. This type of RBE is often referred to as LET-weighted dose and excludes the dose dependency of RBE, which is easily observable *in vitro* and was used in Paper I and IV with different scaling parameters. The LWD approach was first introduced by Unkelbach *et al.* (2016) as a way to reoptimize an RBE$_{1.1}$ plan with respect to LET. The scaling parameter c, has been varied between studies and thus altered the estimated effect of LET$_d$ in the planning. The scaling parameter used by Unkelbach was 0.04 µm/keV, which corresponds to a mean RBE of 1.1 for an SOBP of 5 cm modulation and 10 cm range in a water phantom. The RBE will then be below 1.1 in the proximal part of the beam, while an increase towards the distal part of the

beam will be observed. Different modifications of this model have been proposed in studies from other groups. Fjæra *et al.* (2017) scaled the c value so that the median RBE in the CTV would correspond to 1.1 which was also used in the RBE optimization strategies in Paper I, where the values ranged between 0.032 µm/keV and 0.039 µm/keV. This RBE would still lead to a median value of 1.1 in the target; however, the high RBE values that usually appear at the distal part of the beams would be lower. Using a c value of 0.055 µm/keV in Paper III, resulted in a significantly higher RBE than for the ROR model in the PTV ($(\alpha/\beta)_x = 10$ Gy), while similar to the ROR model for healthy tissue with low $(\alpha/\beta)_x$. This c value was found through fitting the LWD model to the survival curve of two cell lines with vastly different $(\alpha/\beta)_x$ to reduce the biological variability (McMahon, Paganetti, and Prise 2018).

Although this LWD modification account to some degree for the biological uncertainty of the *in vitro* data by fitting the LWD directly to the cell survival data, $(\alpha/\beta)_x$ should not be ignored, although this varies for different patient cases. This is highlighted in a study by Mara *et al.* (2020) reporting new experimental *in vitro* data from four human cell lines, suggesting that most phenomenological models are underestimating the impact of $(\alpha/\beta)_x$. The *in vitro* data are also endpoint specific, meaning that different OARs could both have low and high $(\alpha/\beta)_x$, depending on the choice of endpoint.

The report by Paganetti *et al.* (2019) also suggested that clinics should consider the consequences of regions with low $(\alpha/\beta)_x$ near the tumor. Studies have also shown that the tumor volume can be underdosed when the $(\alpha/\beta)_x$ becomes higher (Jones 2014; Sethi *et al.* 2014). Similar results were found in Paper I where the target $(\alpha/\beta)_x$ varied across each case, and the RBE observed was distinctively lower for target volumes with high $(\alpha/\beta)_x$. Considering that late radiation induced side-effects in healthy tissue are generally associated with lower $(\alpha/\beta)_x$ values compared to tumors, there is an increased risk of underestimating the dose to healthy tissue when using a conservative RBE of 1.1. Paganetti *et al*. (2019) therefore recommended in an extensive rapport

that the RBE could be increased to 1.2 or 1.3 in areas with low $(\alpha/\beta)_x$ located in the end of SOBPs.

By using variable RBE in the OARs only, the risk of underdosing the target is removed, while high RBE-weighted doses caused by increased LET in the distal part of the beam can be avoided. Thus, a differential RBE optimization strategy could be a steppingstone towards implementing variable RBE models clinically, as the RBE in the tumor is 1.1, and a variable RBE is deployed in the OARs. A similar approach has been suggested by Sanchez-Parcerisa *et al.* (Sanchez-Parcerisa *et al.* 2019), where the MCN model was used to reduce the biological dose to the surrounding OARs.

However, to what degree *in vitro* based RBE estimates can be representative of normal tissue damage is very uncertain (Paganetti 2022). Still, with emerging knowledge of normal tissue RBE, both *in vivo* (Suckert *et al.* 2020) and clinically (Underwood *et al.* 2018; Peeler *et al.* 2016; Oden *et al.* 2020; Harrabi *et al.* 2021; Eulitz *et al.* 2019; Engeseth *et al.* 2020; Engeseth *et al.* 2019; Engeseth *et al.* 2022; Engeseth *et al.* 2021; Bolsi *et al.* 2020; Bertolet *et al.* 2022; Bahn *et al.* 2020) better and more endpoint specific RBE estimates could enable the use of differential optimization clinically. Additionally, an LWD approach could be a good intermediate step towards using variable RBE in clinics, as it could reduce the biological dose to some extent in the OARs while avoiding translational uncertainties between *in vitro* and *in* vivo data associated with the $(\alpha/\beta)_x$.

8.2 Hypoxia in optimization of IMPT

There have been several attempts to model the effects of low oxygenation, giving rise to multiple RBE and OER weighted dose (ROWD) models, where the main difference is how they incorporate the OER into the RBE. The ROWD model used for treatment plan creation in Paper II was based on the Dahle model. This model was developed in a previous study of ours (Dahle *et al.* 2020) and was based on *in vitro* data from protons in normoxic and hypoxic conditions. This is in contrast to all other published models,

which are based on *in vitro* data from not only protons but also heavier ions (Wenzl and Wilkens 2011; Tinganelli *et al.* 2015; Strigari *et al.* 2018; Mein *et al.* 2021). All of these models were compared, and the differences were explored in Paper III. A similarity between all models was the inclusion of the Alper-Howard-Flanders relation (Alper and Howard-Flanders 1956), which first included the oxygen level as a parameter to quantify hypoxia. The difference between the models was the range of *in vitro* data used, as well as how they implemented the OER into the LQ model. However, as seen in Paper III, the Dahle model estimated a similar OER as the Wenzl and Wilkens model, and the Mein model, while an overall higher OER was estimated from the Tinganelli model and Strigari model. This would lead to an overall higher physical dose in the hypoxic area. The physical dose would also depend on the normalization of the models, as we assumed a normoxic pO_2 value of 160 mmHg, which would give a higher OER compared to using normoxic values of 60 mmHg as in Paper II. The uncertainty of the models could be traced back to the conversion from pO_2 to OER, which is based on *in vitro* data from experiments comparing normoxic and hypoxic cell survival. With respect to the LET dependence of the models, this could be a critical point if heavier ions are included and the models are intended for protons. It is well known from RBE models that different biological effectiveness may be found for different ions for the same LET (Scholz 2003). Thus giving a general LET dependence of the OER may also be an oversimplification, and the impact of this should be investigated further.

The treatment plans optimized for hypoxia showed a significant increase in physical dose to the target, illustrating how the doses would have to be scaled according to the OER model. However, the prescribed dose to the target was high (70Gy($RBE_{1.1}$)), and it is therefore also possible that the dose is too high in the normoxic area, and not too low in the hypoxic areas. This is, therefore, a topic that needs more investigation. Mortensen *et al.* (2012) showed that 63% of the cases in their study of HNC patients included hypoxic volumes, while this was the case for 35% of the patients in a gene base study by Toustrup *et al.* (2012). The median tumor pO_2 in HNC cancers has also

been found to be low, varying between 10 and 14.6 mmHg (McKeown 2014). With improved quantification of hypoxia, it may therefore be possible with dose de-escalation in parts of the target, giving room for more normal tissue sparing.

Although there exist multiple PET-tracers which are able to detect hypoxia, they all have a varying degree of effectiveness depending on the tumor site. For instance, ^{18}F-EF5 is a recommended tracer for brain tumors as well as head and neck tumors (Fleming *et al.* 2015) and has shown an ability to quantify pO_2 values in these regions, also seen in Paper II. There is, however, uncertainty associated with the usage of ^{18}F-EF5 or other PET tracers to quantify oxygen levels, as hypoxic tumors are complex micro-environments and can change between the treatment planning and treatment delivery (Hompland, Fjeldbo, and Lyng 2021) (Powathil *et al.* 2012). This could affect the treatment planning process, as a variation in the hypoxic volume could lead to inadequate plans. However, multiple studies (Wright *et al.* 2021) (Silvoniemi *et al.* 2018) have also shown high repeatability between ^{18}F-EF5 images for head and neck cancers acquired within different time periods. This shows the robustness of the treatment planning method shown in Paper II, although repeated imaging may be warranted.

Although we saw an increase in LET_d for the water phantom case in Paper II, it was the physical dose that was increased in the hypoxic regions in the HNC case, similar to dose painting. Two methods for including hypoxia in treatment planning are dose painting and LET painting, where Malinen and Sovik (2015) found no increase in tumor control probability with LET painting as compared to only dose painting with protons. For carbon ions, however, the LET painting effect was greater. This had previously been seen by Bassler *et al.* (2010), which saw a greater reduction in OER in a boost volume for carbon ions compared to protons, illustrating a higher effect from the LET-painting with heavier ions than protons.

PAT has shown that the LET increases substantially in the target as compared to IMPT. This was demonstrated by Mein *et al.* (2021) for three different types of ions, and even

though carbon ions showed the highest effect, the high LET for protons in the target also reduced the hypoxia-effect in the regions with the lowest pO$_2$ values. And even though LET painting showed no effect for protons with IMPT (Malinen and Sovik 2015), the higher LET$_d$ values achieved with PAT, as seen in Paper IV, could improve LET painting with protons. Clinical dose painting has not yet been performed with protons; however, a clinical study by Welz *et al.* (2017) showed how photon dose escalation to known hypoxic volumes could increase the loco-regional tumor control, as compared to patients with regular treatment, without additional toxicities. Including dose painting in the target by elevating the dose in certain areas, as in Paper II, could therefore be a safe option in terms of additional toxicities.

8.3 PAT in treatment planning

Although the concept of PAT contradicts one of the main rationales behind proton therapy, where a small dose bath from photons is removed, studies show a lower integral dose to the surrounding tissue compared to IMPT (Ding *et al.* 2016) (Ding *et al.* 2018) (Liu *et al.* 2020a) (Engwall *et al.* 2022).

PAT also has an important impact on the biology of proton therapy as it distributes the LET more superior compared to IMPT (Toussaint *et al.* 2019). Combined with the increased degrees of freedom, PAT allows for techniques in terms of LET manipulation that are not feasible to the same degree using IMPT. The idea of LET re-distribution by pruning IMPT fields was presented by Fager *et al.* (2015) which demonstrated that by adding multiple IMPT fields covering only parts of the PTV, higher LET values could be re-distributed in the target volume. This technique was further developed for PAT in Paper III, where pruning the highest energies of each beam in the arc led to a substantial increase of LET in the target. As the LET distribution is vastly different for IMPT compared to PAT, Li *et al.* (2021) compared how LET optimization would affect these two modalities, and PAT was found to improve the LET distribution to both the

target and the OAR, again illustrating how the new degrees of freedom from PAT could improve treatment planning.

Other studies have also exploited the fact that each individual PAT beam does not need to cover the target as well. By using monoenergetic beams with PAT in cell experiments, Carabe *et al.* (2020) showed an increased biological effect for PAT compared to IMPT. It was also found that the monoenergetic PAT plans had a larger amount of unrepaired DSB compared to IMPT due to a denser energy deposition, as expected, with higher LET values. Further studies have explored different techniques to create monoenergetic arc plans (Blanco Kiely and White 2016) and both mono- and bi-energetic plans (Sanchez-Parcerisa *et al.* 2016), illustrating the flexibility of PAT compared to IMPT. Bertolet and Carabe (2020) also increased the LET within the target by using monoenergetic beams without any additional LET based objectives. Similarly, in Paper IV, the LET distribution was optimized in the target, as this indirect way of optimizing plans could lead to higher tumor control due to the increased biological effect. Combining RBE based optimization, as applied in Paper I, with PAT could therefore show a greater improvement in terms of OAR sparing, as LET values could more efficiently be re-distributed into the target volume. By including pruning techniques in the optimization of PAT plans, the elevated LET values in the target could help the optimizer achieve a better outcome.

8.4 RBE in the future

Even though the *in vivo* and *in vitro* data show an increased RBE in the distal part of the proton beam, clinical evidence would be a strong factor in the introduction of variable RBE in clinics.

For tumors tissues, *in vitro* studies have shown that the main DNA repair mechanism is through homologous recombination (HR) (Fontana *et al.* 2015; Grosse *et al.* 2014; Liu *et al.* 2015) and Zhou et al. (2021) demonstrated how a defection in HR occurred in the Bragg peak region of a proton beam. This implies that high LET values cause

more complex damage to DNA, rendering it harder to repair, leading to an increased biological effect. *In vivo* data, although uncertain, also supports the elevated LET at the distal end of the proton beam when irradiating normal tissue (Gueulette *et al.* 2000; Gueulette *et al.* 2001; Sorensen *et al.* 2017; Saager *et al.* 2018).

The sum of evidence of a variable RBE in proton therapy has not only led to careful recommendations of RBE inclusion in the clinics for special cases such as when the beam ends in tissue with low $(\alpha/\beta)_x$ (Paganetti *et al.* 2019), but also warranted more studies. Clinical trials to include LET in treatment planning for anal canal squamous cell cancer and pediatric ependymoma are also started, which could directly show how LET optimization could reduce the risk for toxicity (MD Anderson Cancer Center 2018b, 2018a).

There is consensus in nearly all recent RBE reports that variable RBE should be considered in clinics. However, to which degree it should be implemented is not yet agreed on. As there is a need for more clinical RBE data, Hahn *et al.* (2022) proposed that proton therapy centers in Europe should agree on a system for reporting LET$_d$, such that late effects due to LET could easier be followed up. This is supported by Kalholm *et al.* (2021) which reported a large inconsistency when reporting LET values from studies, as well as the calculation techniques. Bauer *et al.* (2021) postulated that today's treatment is not sufficient in terms of knowledge of radiosensitive areas with high RBE and therefore suggest that biological guided plan optimization should be included to achieve risk minimization in the treatment of low-grade glioma. This could include visualization of RBE effects in the clinics in terms of LET and variable RBE models. This was recently done in a study by Mein *et al.* (2022), which showed that evaluating treatment plans with varying field angles for LET and RBE could help clinical decision-making. This was also seen by Fjæra *et al.* (2017), where the lower LET values in the brainstem were observed by changing the treatment field angles for a pediatric brain tumor case. A similar approach was presented in Paper IV, where we

created seven different plans for a single case with different beam properties and evaluated the RBE effects before recommending a plan.

9. Conclusion

In this thesis, different RBE and hypoxia-based methods with the aim to show how the treatment in proton therapy can be improved were presented. This work shows how clinical treatment planning can be improved by including more than the physical dose used in current treatment planning, such as variable RBE, LET, and hypoxia related parameters.

The introduction of variable RBE optimization strategies and further investigation of their influence on treatment plans (Paper I) revealed that full optimization with RBE models shows the largest potential for OAR sparing but can lead to reduced physical dose in tumors with low $(\alpha/\beta)_x$. This decrease in tumor dose was avoided with our differential optimization strategy while also including some OAR sparing. We therefore suggest the latter as a step towards planning with variable RBE clinically. To improve control of hypoxic tumor volumes, our method with the inclusion of OER alongside RBE in treatment plan optimization (Paper II) showed how a more homogeneous biological effect across the target volume can be achieved through increasing the physical dose and LET in the hypoxic regions. It is however important to select a relevant OER model, since we found clear distinctions between the OER estimates using different models. The models based primarily on data from heavy ions resulted in higher OER estimates compared to models using more proton in vitro data (Paper III). With reliable hypoxia imaging and OER modeling, ROWD calculations could become a useful tool for treatment plan evaluation and optimization.

To further account for LET effects that recently have been correlated to the risk of toxicity, PAT through pruning energy layers can reduce LET to surrounding tissue and OARs whilst increasing LET in the target (Paper IV). This technique could be even more efficient when combined with RBE or ROWD models.

With the technological advances in treatment delivery, as well as increased quality of patient imaging, new knowledge of the RBE accompanied by biological optimization

shows great potential and should be considered for improving patient outcome moving forward.

References

Alper, T., and P. Howard-Flanders. 1956. 'Role of oxygen in modifying the radiosensitivity of E. coli B', *Nature*, 178: 978-9.

Apilan, A. G., and C. Mothersill. 2021. 'Targeted and Non-Targeted Mechanisms for Killing Hypoxic Tumour Cells-Are There New Avenues for Treatment?', *Int J Mol Sci*, 22.

Bader, S. B., M. W. Dewhirst, and E. M. Hammond. 2020. 'Cyclic Hypoxia: An Update on Its Characteristics, Methods to Measure It and Biological Implications in Cancer', *Cancers (Basel)*, 13.

Bahn, E., J. Bauer, S. Harrabi, K. Herfarth, J. Debus, and M. Alber. 2020. 'Late Contrast Enhancing Brain Lesions in Proton-Treated Patients With Low-Grade Glioma: Clinical Evidence for Increased Periventricular Sensitivity and Variable RBE', *Int J Radiat Oncol Biol Phys*.

Bai, X., G. Lim, D. Grosshans, R. Mohan, and W. Cao. 2020. 'A biological effect-guided optimization approach using beam distal-edge avoidance for intensity-modulated proton therapy', *Med Phys*, 47: 3816-25.

Barendsen, G. W. 1964. 'Impairment of the Proliferative Capacity of Human Cells in Culture by Alpha-Particles with Differing Linear-Energy Transfer', *Int J Radiat Biol Relat Stud Phys Chem Med*, 8: 453-66.

Bassler, N., O. Jakel, C. S. Sondergaard, and J. B. Petersen. 2010. 'Dose- and LET-painting with particle therapy', *Acta Oncol*, 49: 1170-6.

Bassler, N., J. Toftegaard, A. Luhr, B. S. Sorensen, E. Scifoni, M. Kramer, O. Jakel, L. S. Mortensen, J. Overgaard, and J. B. Petersen. 2014. 'LET-painting increases tumour control probability in hypoxic tumours', *Acta Oncol*, 53: 25-32.

Bauer, J., E. Bahn, S. Harrabi, K. Herfarth, J. Debus, and M. Alber. 2021. 'How can scanned proton beam treatment planning for low-grade glioma cope with increased distal RBE and locally increased radiosensitivity for late MR-detected brain lesions?', *Med Phys*, 48: 1497-507.

Belli, M., A. Campa, and I. Ermolli. 1997. 'A Semi-Empirical Approach to the Evaluation of the Relative Biological Effectiveness of Therapeutic Proton Beams: The Methodological Framework', *Radiation Research*, 148.

Bertolet, A., R. Abolfath, D. J. Carlson, R. A. Lustig, C. Hill-Kayser, M. Alonso-Basanta, and A. Carabe. 2022. 'Correlation of LET With MRI Changes in Brain and Potential Implications for Normal Tissue Complication Probability for Patients With Meningioma Treated With Pencil Beam Scanning Proton Therapy', *Int J Radiat Oncol Biol Phys*, 112: 237-46.

Bertolet, A., and A. Carabe. 2020. 'Proton monoenergetic arc therapy (PMAT) to enhance LETd within the target', *Phys Med Biol*.

Bethe, H. 1930. 'Zur Theorie des Durchgangs schneller Korpuskularstrahlen durch Materie', *Annalen der Physik*, 397: 325-400.

Blanco Kiely, J. P., and B. M. White. 2016. 'Dosimetric feasibility of single-energy proton modulated arc therapy for treatment of chordoma at the skull base', *Acta Oncol*, 55: 1243-45.

Bloch, F. 1933. 'Zur Bremsung rasch bewegter Teilchen beim Durchgang durch Materie', *Annalen der Physik*, 408: 285-320.

Bohlen, T. T., J. Bauer, M. Dosanjh, A. Ferrari, T. Haberer, K. Parodi, V. Patera, and A. Mairani. 2013. 'A Monte Carlo-based treatment-planning tool for ion beam therapy', *J Radiat Res*, 54 Suppl 1: i77-81.

Bohlen, T. T., F. Cerutti, M. P. W. Chin, A. Fosso, A. Ferrari, P. G. Ortega, A. Mairani, P. R. Sala, G. Smirnov, and V. Vlachoudisl. 2014. 'The FLUKA Code: Developments and Challenges for High Energy and Medical Applications', *Nuclear Data Sheets*, 120: 211-14.

Bolsi, A., L. Placidi, A. Pica, F. J. Ahlhelm, M. Walser, A. J. Lomax, and D. C. Weber. 2020. 'Pencil beam scanning proton therapy for the treatment of craniopharyngioma complicated with radiation-induced cerebral vasculopathies: A dosimetric and linear energy transfer (LET) evaluation', *Radiother Oncol*, 149: 197-204.

Brenner, David J., and Eric J. Hall. 1999. 'Fractionation and protraction for radiotherapy of prostate carcinoma', *International Journal of Radiation Oncology*Biology*Physics*, 43: 1095-101.

Cao, W., A. Khabazian, P. P. Yepes, G. Lim, F. Poenisch, D. R. Grosshans, and R. Mohan. 2017. 'Linear energy transfer incorporated intensity modulated proton therapy optimization', *Phys Med Biol*, 63: 015013.

Carabe-Fernandez, A., I. Karagounis, K. Huynh, A. Bertolet, N. Francois, M. M. Kim, A. Maity, E. Abel, and R. G. Dale. 2020. 'Radiobiological effectiveness difference of proton arc beams versus conventional proton and photon beams', *Phys Med Biol*.

Carabe, A., M. Moteabbed, N. Depauw, J. Schuemann, and H. Paganetti. 2012. 'Range uncertainty in proton therapy due to variable biological effectiveness', *Phys Med Biol*, 57: 1159-72.

Chang, David S., Foster D. Lasley, Indra J. Das, Marc S. Mendonca, and Joseph R. Dynlacht. 2014. *Basic Radiotherapy Physics and Biology*.

Chang, S., G. Liu, L. Zhao, J. T. Dilworth, W. Zheng, S. Jawad, D. Yan, P. Chen, C. Stevens, P. Kabolizadeh, X. Li, and X. Ding. 2020. 'Feasibility study: spot-scanning proton arc therapy (SPArc) for left-sided whole breast radiotherapy', *Radiat Oncol*, 15: 232.

Chen, Y., and S. Ahmad. 2012. 'Empirical model estimation of relative biological effectiveness for proton beam therapy', *Radiat Prot Dosimetry*, 149: 116-23.

Coutrakon, G., J. Hubbard, J. Johanning, G. Maudsley, T. Slaton, and P. Morton. 1994. 'A performance study of the Loma Linda proton medical accelerator', *Med Phys*, 21: 1691-701.

Dahle, T. J., E. Rusten, C. H. Stokkevag, A. Silvoniemi, A. Mairani, L. F. Fjæra, E. Rørvik, H. Henjum, P. Wright, C. G. Boer, S. Forsback, H. Minn, E. Malinen, and K. S. Ytre-Hauge. 2020. 'The FLUKA Monte Carlo code coupled with an

OER model for biologically weighted dose calculations in proton therapy of hypoxic tumors', *Phys Med*, 76: 166-72.

Ding, X., X. Li, A. Qin, J. Zhou, D. Yan, C. Stevens, D. Krauss, and P. Kabolizdeh. 2018. 'Have we reached proton beam therapy dosimetric limitations? - A novel robust, delivery-efficient and continuous spot-scanning proton arc (SPArc) therapy is to improve the dosimetric outcome in treating prostate cancer', *Acta Oncol*, 57: 435-37.

Ding, X., X. Li, J. M. Zhang, P. Kabolizadeh, C. Stevens, and D. Yan. 2016. 'Spot-Scanning Proton Arc (SPArc) Therapy: The First Robust and Delivery-Efficient Spot-Scanning Proton Arc Therapy', *Int J Radiat Oncol Biol Phys*, 96: 1107-16.

Ding, X., J. Zhou, X. Li, K. Blas, G. Liu, Y. Wang, A. Qin, P. Chinnaiyan, D. Yan, C. Stevens, I. Grills, and P. Kabolizadeh. 2019. 'Improving dosimetric outcome for hippocampus and cochlea sparing whole brain radiotherapy using spot-scanning proton arc therapy', *Acta Oncol*, 58: 483-90.

Emami, B., J. Lyman, A. Brown, L. Cola, M. Goitein, J. E. Munzenrider, B. Shank, L. J. Solin, and M. Wesson. 1991. 'Tolerance of normal tissue to therapeutic irradiation', *International Journal of Radiation Oncology*Biology*Physics*, 21: 109-22.

Engeseth, G. M., R. He, D. Mirkovic, P. Yepes, A. S. R. Mohamed, S. Stieb, C. D. Fuller, R. Wu, X. Zhang, L. B. Hysing, H. E. S. Pettersen, C. H. Stokkevag, R. Mohan, S. J. Frank, and G. B. Gunn. 2021. 'Mixed Effect Modeling of Dose and Linear Energy Transfer Correlations With Brain Image Changes After Intensity Modulated Proton Therapy for Skull Base Head and Neck Cancer', *Int J Radiat Oncol Biol Phys*, 111: 684-92.

Engeseth, G. M., L. B. Hysing, P. Yepes, H. E. S. Pettersen, R. Mohan, C. D. Fuller, C. H. Stokkevag, R. Wu, X. Zhang, S. J. Frank, and G. B. Gunn. 2022. 'Impact of RBE variations on risk estimates of temporal lobe necrosis in patients treated with intensity-modulated proton therapy for head and neck cancer', *Acta Oncol*, 61: 215-22.

Engeseth, G. M., A. S. Mohamed, S. Stieb, C. D. Fuller, A. S. Garden, D. I. Rosenthal, J. Phan, W. H. Morrison, J. P. Reddy, M. Brydøy, C. H. Stokkevåg, R. Y. Wu, S. J. Frank, and G. B. Gunn. 2019. 'Radiation Associated Brain Necrosis following Proton Therapy for Head and Neck Skull Base and Intracranial Tumors', *International Journal of Radiation Oncology*Biology*Physics*, 105: S5-S6.

Engeseth, G. M., S. Stieb, A. S. R. Mohamed, R. He, C. H. Stokkevag, M. Brydoy, C. D. Fuller, A. S. Garden, D. I. Rosenthal, J. Phan, W. H. Morrison, J. P. Reddy, R. Wu, X. Zhang, S. J. Frank, and G. Brandon Gunn. 2020. 'Outcomes and patterns of radiation associated brain image changes after proton therapy for head and neck skull base cancers', *Radiother Oncol*, 151: 119-25.

Engwall, E., C. Battinelli, V. Wase, O. Marthin, L. Glimelius, R. Bokrantz, B. Andersson, and A. Fredriksson. 2022. 'Fast robust optimization of proton PBS arc therapy plans using early energy layer selection and spot assignment', *Phys Med Biol*.

Eulitz, J., E. G. C. Troost, F. Raschke, E. Schulz, B. Lutz, A. Dutz, S. Lock, P. Wohlfahrt, W. Enghardt, C. Karpowitz, M. Krause, and A. Luhr. 2019. 'Predicting late magnetic resonance image changes in glioma patients after proton therapy', *Acta Oncol*, 58: 1536-39.

Fager, M., I. Toma-Dasu, M. Kirk, D. Dolney, E. S. Diffenderfer, N. Vapiwala, and A. Carabe. 2015. 'Linear energy transfer painting with proton therapy: a means of reducing radiation doses with equivalent clinical effectiveness', *Int J Radiat Oncol Biol Phys*, 91: 1057-64.

Ferrari, Alfredo, Paola R Sala, Alberto Fasso, and Johannes Ranft. 2005. "FLUKA: A multi-particle transport code (Program version 2005)." In.

Fjæra, L. F. 2021. 'Studies of the linear energy transfer and relative biological effectiveness in proton therapy of pediatric brain tumors', University of Bergen.

Fjæra, L. F., Z. Li, K. S. Ytre-Hauge, L. P. Muren, D. J. Indelicato, Y. Lassen-Ramshad, G. M. Engeseth, M. Brydoy, A. Mairani, S. Flampouri, O. Dahl, and C. H. Stokkevag. 2017. 'Linear energy transfer distributions in the brainstem depending on tumour location in intensity-modulated proton therapy of paediatric cancer', *Acta Oncol*, 56: 763-68.

Fjæra, Lars Fredrik. 2016. 'Development of a Monte Carlo Based Treatment Planning Verification Tool for Particle TherapyDevelopment', University of Bergen.

Fleming, I. N., R. Manavaki, P. J. Blower, C. West, K. J. Williams, A. L. Harris, J. Domarkas, S. Lord, C. Baldry, and F. J. Gilbert. 2015. 'Imaging tumour hypoxia with positron emission tomography', *Br J Cancer*, 112: 238-50.

Fontana, A. O., M. A. Augsburger, N. Grosse, M. Guckenberger, A. J. Lomax, A. A. Sartori, and M. N. Pruschy. 2015. 'Differential DNA repair pathway choice in cancer cells after proton- and photon-irradiation', *Radiother Oncol*, 116: 374-80.

Fracchiolla, F., E. Engwall, M. Janson, F. Tamm, S. Lorentini, F. Fellin, M. Bertolini, C. Algranati, R. Righetto, P. Farace, M. Amichetti, and M. Schwarz. 2021. 'Clinical validation of a GPU-based Monte Carlo dose engine of a commercial treatment planning system for pencil beam scanning proton therapy', *Phys Med*, 88: 226-34.

Giantsoudi, D., C. Grassberger, D. Craft, A. Niemierko, A. Trofimov, and H. Paganetti. 2013. 'Linear energy transfer-guided optimization in intensity modulated proton therapy: feasibility study and clinical potential', *Int J Radiat Oncol Biol Phys*, 87: 216-22.

Giovannini, G., T. Bohlen, G. Cabal, J. Bauer, T. Tessonnier, K. Frey, J. Debus, A. Mairani, and K. Parodi. 2016. 'Variable RBE in proton therapy: comparison of different model predictions and their influence on clinical-like scenarios', *Radiat Oncol*, 11: 68.

Grosse, N., A. O. Fontana, E. B. Hug, A. Lomax, A. Coray, M. Augsburger, H. Paganetti, A. A. Sartori, and M. Pruschy. 2014. 'Deficiency in homologous recombination renders Mammalian cells more sensitive to proton versus photon irradiation', *Int J Radiat Oncol Biol Phys*, 88: 175-81.

Grun, R., T. Friedrich, M. Kramer, K. Zink, M. Durante, R. Engenhart-Cabillic, and M. Scholz. 2013. 'Physical and biological factors determining the effective proton range', *Med Phys*, 40: 111716.

Grzanka, L., O. Ardenfors, and N. Bassler. 2018. 'Monte Carlo Simulations of Spatial Let Distributions in Clinical Proton Beams', *Radiat Prot Dosimetry*, 180: 296-99.

Gu, W., D. Ruan, Q. Lyu, W. Zou, L. Dong, and K. Sheng. 2020. 'A novel energy layer optimization framework for spot-scanning proton arc therapy', *Med Phys*, 47: 2072-84.

Guan, F., C. Geng, D. Ma, L. Bronk, M. Kerr, Y. Li, D. Gates, B. Kroger, N. Sahoo, U. Titt, D. Grosshans, and R. Mohan. 2018. 'RBE Model-Based Biological Dose Optimization for Proton Radiobiology Studies', *Int J Part Ther*, 5: 160-71.

Gueulette, John, Lothar Böhm, Jacobus P. Slabbert, Blanche M. De Coster, Gerald S. Rutherfoord, Arnout Ruifrok, Michelle Octave-Prignot, Peter J. Binns, A. Nicholaas Schreuder, Julian E. Symons, Pierre Scalliet, and Dan T. L. Jones. 2000. 'Proton relative biological effectiveness (RBE) for survival in mice after thoracic irradiation with fractionated doses', *International Journal of Radiation Oncology*Biology*Physics*, 47: 1051-58.

Gueulette, John, Jacobus P. Slabbert, Lothar Böhm, Blanche M. De Coster, Jean-François Rosier, Michelle Octave-Prignot, Arnout Ruifrok, A. Nicholaas Schreuder, André Wambersie, Pierre Scalliet, and D. T. L. Jones. 2001. 'Proton RBE for early intestinal tolerance in mice after fractionated irradiation', *Radiotherapy and Oncology*, 61: 177-84.

Hahn, C., J. Oden, A. Dasu, A. Vestergaard, M. Fuglsang Jensen, O. Sokol, C. Pardi, F. Bourhaleb, A. Leite, L. de Marzi, E. Smith, A. Aitkenhead, C. Rose, M. Merchant, K. Kirkby, L. Grzanka, J. Pawelke, and A. Luhr. 2022. 'Towards harmonizing clinical linear energy transfer (LET) reporting in proton radiotherapy: a European multi-centric study', *Acta Oncol*, 61: 206-14.

Hahn, C., J. Ödén, A. Dasu, A. Vestergaard, J. Folsted Kallehauge, C. Pardi, F. Bourhaleb, A. Leite, L. de Marzi, E. Smith, A. Aitkenhead, M. Merchant, K. Kirkby, E. G. C. Troost, and A. Lühr. 2021. 'OC-0418 European multi-centric study on variable proton RBE dose calculations for multiple anatomical sites', *Radiotherapy and Oncology*, 161: S314-S15.

Hall, Eric J. Giaccia Amato J. Ovid Technologies Inc. 2012. 'Radiobiology for the radiologist'.

Harrabi, S. B., B. von Nettelbladt, C. Gudden, S. Adeberg, K. Seidensaal, J. Bauer, E. Bahn, A. Mairani, M. Alber, T. Haberer, J. Debus, and K. Herfarth. 2021. 'Radiation induced contrast enhancement after proton beam therapy in patients with low grade glioma - How safe are protons?', *Radiother Oncol*, 167: 211-18.

Hompland, T., C. S. Fjeldbo, and H. Lyng. 2021. 'Tumor Hypoxia as a Barrier in Cancer Therapy: Why Levels Matter', *Cancers (Basel)*, 13.

Hong, L., M. Goitein, M. Bucciolini, R. Comiskey, B. Gottschalk, S. Rosenthal, C. Serago, and M. Urie. 1996. 'A pencil beam algorithm for proton dose calculations', *Phys Med Biol*, 41: 1305-30.

ICRU. 2007. 'Prescribing, Recording, and Reporting Proton-Beam Therapy', *Journal of the ICRU*, 7: 21-8.

Inaniwa, T., N. Kanematsu, K. Noda, and T. Kamada. 2017. 'Treatment planning of intensity modulated composite particle therapy with dose and linear energy transfer optimization', *Phys Med Biol*, 62: 5180-97.

Indelicato, D. J., S. Flampouri, R. L. Rotondo, J. A. Bradley, C. G. Morris, P. R. Aldana, E. Sandler, and N. P. Mendenhall. 2014. 'Incidence and dosimetric parameters of pediatric brainstem toxicity following proton therapy', *Acta Oncol*, 53: 1298-304.

Joiner, Michael, and Albert Van der Kogel. 2009. *Basic Clinical Radiobiology*.

Jones, B. 2014. 'Patterns of failure after proton therapy in medulloblastoma', *Int J Radiat Oncol Biol Phys*, 90: 25-6.

———. 2015. 'A Simpler Energy Transfer Efficiency Model to Predict Relative Biological Effect for Protons and Heavier Ions', *Front Oncol*, 5: 184.

Kalholm, F., L. Grzanka, E. Traneus, and N. Bassler. 2021. 'A systematic review on the usage of averaged LET in radiation biology for particle therapy', *Radiother Oncol*, 161: 211-21.

Kimstrand, P., N. Tilly, A. Ahnesjo, and E. Traneus. 2008. 'Experimental test of Monte Carlo proton transport at grazing incidence in GEANT4, FLUKA and MCNPX', *Phys Med Biol*, 53: 1115-29.

Koch, C. J., and S. M. Evans. 2015. 'Optimizing hypoxia detection and treatment strategies', *Semin Nucl Med*, 45: 163-76.

Kooy, H. M., and C. Grassberger. 2015. 'Intensity modulated proton therapy', *Br J Radiol*, 88: 20150195.

Langen, K., and M. Zhu. 2018. 'Concepts of PTV and Robustness in Passively Scattered and Pencil Beam Scanning Proton Therapy', *Semin Radiat Oncol*, 28: 248-55.

Lederman, Manuel. 1981. 'The early history of radiotherapy: 1895–1939', *International Journal of Radiation Oncology*Biology*Physics*, 7: 639-48.

Li, X., X. Ding, W. Zheng, G. Liu, G. Janssens, K. Souris, A. M. Barragan-Montero, D. Yan, C. Stevens, and P. Kabolizadeh. 2021. 'Linear Energy Transfer Incorporated Spot-Scanning Proton Arc Therapy Optimization: A Feasibility Study', *Front Oncol*, 11: 698537.

Li, X., P. Kabolizadeh, D. Yan, A. Qin, J. Zhou, Y. Hong, T. Guerrero, I. Grills, C. Stevens, and X. Ding. 2018. 'Improve dosimetric outcome in stage III non-small-cell lung cancer treatment using spot-scanning proton arc (SPArc) therapy', *Radiat Oncol*, 13: 35.

Li, X., G. Liu, G. Janssens, O. De Wilde, V. Bossier, X. Lerot, A. Pouppez, D. Yan, C. Stevens, P. Kabolizadeh, and X. Ding. 2019. 'The first prototype of spot-scanning proton arc treatment delivery', *Radiother Oncol*, 137: 130-36.

Liu, G., X. Li, A. Qin, W. Zheng, D. Yan, S. Zhang, C. Stevens, P. Kabolizadeh, and X. Ding. 2020a. 'Improve the dosimetric outcome in bilateral head and neck cancer (HNC) treatment using spot-scanning proton arc (SPArc) therapy: a feasibility study', *Radiat Oncol*, 15: 21.

Liu, G., X. Li, A. Qin, J. Zhou, W. Zheng, L. Zhao, J. Han, S. Zhang, D. Yan, C. Stevens, I. Grills, and X. Ding. 2021a. 'Is proton beam therapy ready for single fraction spine SBRS? - a feasibility study to use spot-scanning proton arc (SPArc) therapy to improve the robustness and dosimetric plan quality', *Acta Oncol*, 60: 653-57.

Liu, G., X. Li, L. Zhao, W. Zheng, A. Qin, S. Zhang, C. Stevens, D. Yan, P. Kabolizadeh, and X. Ding. 2020b. 'A novel energy sequence optimization algorithm for efficient spot-scanning proton arc (SPArc) treatment delivery', *Acta Oncol*: 1-8.

Liu, G., L. Zhao, A. Qin, I. Grills, R. Deraniyagala, C. Stevens, S. Zhang, D. Yan, X. Li, and X. Ding. 2021b. 'Lung Stereotactic Body Radiotherapy (SBRT) Using Spot-Scanning Proton Arc (SPArc) Therapy: A Feasibility Study', *Front Oncol*, 11: 664455.

Liu, Q., P. Ghosh, N. Magpayo, M. Testa, S. Tang, L. Gheorghiu, P. Biggs, H. Paganetti, J. A. Efstathiou, H. M. Lu, K. D. Held, and H. Willers. 2015. 'Lung cancer cell line screen links fanconi anemia/BRCA pathway defects to increased relative biological effectiveness of proton radiation', *Int J Radiat Oncol Biol Phys*, 91: 1081-9.

Lomax, Antony. 2016. 'SFUD, IMPT, and Plan Robustness.' in, *Particle Radiotherapy*.

Mairani, A., T. T. Bohlen, A. Schiavi, T. Tessonnier, S. Molinelli, S. Brons, G. Battistoni, K. Parodi, and V. Patera. 2013. 'A Monte Carlo-based treatment planning tool for proton therapy', *Phys Med Biol*, 58: 2471-90.

Mairani, A., I. Dokic, G. Magro, T. Tessonnier, J. Bauer, T. T. Bohlen, M. Ciocca, A. Ferrari, P. R. Sala, O. Jakel, J. Debus, T. Haberer, A. Abdollahi, and K. Parodi. 2017. 'A phenomenological relative biological effectiveness approach for proton therapy based on an improved description of the mixed radiation field', *Phys Med Biol*, 62: 1378-95.

Malinen, E., and A. Sovik. 2015. 'Dose or 'LET' painting--What is optimal in particle therapy of hypoxic tumors?', *Acta Oncol*, 54: 1614-22.

Mara, E., M. Clausen, S. Khachonkham, S. Deycmar, C. Pessy, W. Dorr, P. Kuess, D. Georg, and S. Gruber. 2020. 'Investigating the impact of alpha/beta and LETd on relative biological effectiveness in scanned proton beams: An in vitro study based on human cell lines', *Med Phys*, 47: 3691-702.

McKeown, S. R. 2014. 'Defining normoxia, physoxia and hypoxia in tumours-implications for treatment response', *Br J Radiol*, 87: 20130676.

McMahon, S. J. 2018. 'The linear quadratic model: usage, interpretation and challenges', *Phys Med Biol*, 64: 01TR01.

McMahon, S. J., H. Paganetti, and K. M. Prise. 2018. 'LET-weighted doses effectively reduce biological variability in proton radiotherapy planning', *Phys Med Biol*, 63: 225009.

McMahon, S. J., and K. M. Prise. 2019. 'Mechanistic Modelling of Radiation Responses', *Cancers (Basel)*, 11.

McNamara, A. L., J. Schuemann, and H. Paganetti. 2015. 'A phenomenological relative biological effectiveness (RBE) model for proton therapy based on all published in vitro cell survival data', *Phys Med Biol*, 60: 8399-416.

MD Anderson Cancer Center. 2018a. 'LET-IMPT and Standard Chemotherapy in Treating Patients With Newly Diagnosed Stage I-III Anal Canal Squamous Cell Cancer'. https://ClinicalTrials.gov/show/NCT03690921.

———. 2018b. 'LET Optimized IMPT in Treating Pediatric Patients With Ependymoma'. https://ClinicalTrials.gov/show/NCT03750513.

Meeks, Sanford L., John M. Buatti, Kelly D. Foote, William A. Friedman, and Francis J. Bova. 2000. 'Calculation of cranial nerve complication probability for acoustic neuroma radiosurgery', *International Journal of Radiation Oncology*Biology*Physics*, 47: 597-602.

Mein, S., B. Kopp, A. Vela, P. Dutheil, P. Lesueur, D. Stefan, J. Debus, T. Haberer, A. Abdollahi, A. Mairani, and T. Tessonnier. 2022. 'How can we consider variable RBE and LETd prediction during clinical practice? A pediatric case report at the Normandy Proton Therapy Centre using an independent dose engine', *Radiat Oncol*, 17: 23.

Mein, S., T. Tessonnier, B. Kopp, S. Harrabi, A. Abdollahi, J. Debus, T. Haberer, and A. Mairani. 2021. 'Spot-Scanning Hadron Arc (SHArc) Therapy: A Study With Light and Heavy Ions', *Adv Radiat Oncol*, 6: 100661.

Mendonca, Marc, and Robert D. Timmerman. 2002. 'In regard to Donaldson et al: results from the IRS-IV randomized trial of hyperfractionated radiotherapy in children with rhabdomyosarcoma—a report from the IRSG. IJROBP 2001;51:718–728', *International Journal of Radiation Oncology*Biology*Physics*, 54: 1579-80.

Mohan, R., and D. Grosshans. 2017. 'Proton therapy - Present and future', *Adv Drug Deliv Rev*, 109: 26-44.

Mortensen, L. S., J. Johansen, J. Kallehauge, H. Primdahl, M. Busk, P. Lassen, J. Alsner, B. S. Sorensen, K. Toustrup, S. Jakobsen, J. Petersen, H. Petersen, J. Theil, M. Nordsmark, and J. Overgaard. 2012. 'FAZA PET/CT hypoxia imaging in patients with squamous cell carcinoma of the head and neck treated with radiotherapy: results from the DAHANCA 24 trial', *Radiother Oncol*, 105: 14-20.

Nesteruk, K. P., A. Bolsi, A. J. Lomax, D. Meer, S. van de Water, and J. M. Schippers. 2021. 'A static beam delivery device for fast scanning proton arc-therapy', *Phys Med Biol*, 66: 055018.

Newhauser, W. D., and R. Zhang. 2015. 'The physics of proton therapy', *Phys Med Biol*, 60: R155-209.

Oden, J., I. Toma-Dasu, P. Witt Nystrom, E. Traneus, and A. Dasu. 2020. 'Spatial correlation of linear energy transfer and relative biological effectiveness with suspected treatment-related toxicities following proton therapy for intracranial tumors', *Med Phys*, 47: 342-51.

Paganetti, H. 2022. 'Mechanisms and Review of Clinical Evidence of Variations in Relative Biological Effectiveness in Proton Therapy', *Int J Radiat Oncol Biol Phys*, 112: 222-36.

Paganetti, H., E. Blakely, A. Carabe-Fernandez, D. J. Carlson, I. J. Das, L. Dong, D. Grosshans, K. D. Held, R. Mohan, V. Moiseenko, A. Niemierko, R. D. Stewart, and H. Willers. 2019. 'Report of the AAPM TG-256 on the relative biological effectiveness of proton beams in radiation therapy', *Med Phys*, 46: e53-e78.

Paganetti, Harald. 2016. *Proton Therapy Physics*.

Paganetti, Harald, Andrzej Niemierko, Marek Ancukiewicz, Leo E. Gerweck, Michael Goitein, Jay S. Loeffler, and Herman D. Suit. 2002. 'Relative biological effectiveness (RBE) values for proton beam therapy', *International Journal of Radiation Oncology*Biology*Physics*, 53: 407-21.

Papiez, L., and J. J. Battista. 1994. 'Radiance and particle fluence', *Phys Med Biol*, 39: 1053-62.

Parodi, K., A. Mairani, S. Brons, B. G. Hasch, F. Sommerer, J. Naumann, O. Jakel, T. Haberer, and J. Debus. 2012. 'Monte Carlo simulations to support start-up and treatment planning of scanned proton and carbon ion therapy at a synchrotron-based facility', *Phys Med Biol*, 57: 3759-84.

Pedicini, P., R. Caivano, A. Fiorentino, and L. Strigari. 2015. 'Clinical radiobiology of head and neck cancer: the hypothesis of stem cell activation', *Clin Transl Oncol*, 17: 469-76.

Peeler, C. R., D. Mirkovic, U. Titt, P. Blanchard, J. R. Gunther, A. Mahajan, R. Mohan, and D. R. Grosshans. 2016. 'Clinical evidence of variable proton biological effectiveness in pediatric patients treated for ependymoma', *Radiother Oncol*, 121: 395-401.

Powathil, G., M. Kohandel, M. Milosevic, and S. Sivaloganathan. 2012. 'Modeling the spatial distribution of chronic tumor hypoxia: implications for experimental and clinical studies', *Comput Math Methods Med*, 2012: 410602.

PTCOG, Particle Therapy Co-Operative Group. 2022. 'Particle therapy facilities in clinical operation', Accessed 24.01. https://www.ptcog.ch/index.php/facilities-in-operation.

Rah, Jeong-Eun, Gwe-Ya Kim, Do Hoon Oh, Tae Hyun Kim, Jong Won Kim, Dae Yong Kim, Sung Yong Park, and Dongho Shin. 2016. 'A treatment planning study of proton arc therapy for para-aortic lymph node tumors: dosimetric evaluation of conventional proton therapy, proton arc therapy, and intensity modulated radiotherapy', *Radiation Oncology*, 11.

Röntgen, W. C. 1896. 'On a New Kind of Rays', *Science*, 3: 227-31.

Rørvik, E., L. F. Fjæra, T. J. Dahle, J. E. Dale, G. M. Engeseth, C. H. Stokkevag, S. Thornqvist, and K. S. Ytre-Hauge. 2018. 'Exploration and application of phenomenological RBE models for proton therapy', *Phys Med Biol*, 63: 185013.

Rørvik, E., S. Thornqvist, C. H. Stokkevag, T. J. Dahle, L. F. Fjæra, and K. S. Ytre-Hauge. 2017. 'A phenomenological biological dose model for proton therapy based on linear energy transfer spectra', *Med Phys*, 44: 2586-94.

Rørvik, Eivind. 2017. 'A phenomenological biological dose model for proton therapy based on linear energy transfer spectra', *Med. Phys.*, 44.

Saini, J., E. Traneus, D. Maes, R. Regmi, S. R. Bowen, C. Bloch, and T. Wong. 2018. 'Advanced Proton Beam Dosimetry Part I: review and performance evaluation of dose calculation algorithms', *Transl Lung Cancer Res*, 7: 171-79.

Sanchez-Parcerisa, D., M. Kirk, M. Fager, B. Burgdorf, M. Stowe, T. Solberg, and A. Carabe. 2016. 'Range optimization for mono- and bi-energetic proton modulated arc therapy with pencil beam scanning', *Phys Med Biol*, 61: N565-N74.

Sanchez-Parcerisa, D., M. Lopez-Aguirre, A. Dolcet Llerena, and J. M. Udias. 2019. 'MultiRBE: Treatment planning for protons with selective radiobiological effectiveness', *Med Phys*, 46: 4276-84.

Sandison, G. A., E. Papiez, C. Bloch, and J. Morphis. 1997. 'Phantom assessment of lung dose from proton arc therapy', *International Journal of Radiation Oncology*Biology*Physics*, 38: 891-97.

Schaffner, B., E. Pedroni, and A. Lomax. 1999. 'Dose calculation models for proton treatment planning using a dynamic beam delivery system: an attempt to include density heterogeneity effects in the analytical dose calculation', *Phys Med Biol*, 44: 27-41.

Schardt, Dieter, Thilo Elsässer, and Daniela Schulz-Ertner. 2010. 'Heavy-ion tumor therapy: Physical and radiobiological benefits', *Reviews of Modern Physics*, 82: 383-425.

Scholz, M. 2003. 'Effects of Ion Radiation on Cells and Tissues.' in, *Radiation Effects on Polymers for Biological Use*.

Schreuder, A. N., D. S. Bridges, L. Rigsby, M. Blakey, M. Janson, S. G. Hedrick, and J. B. Wilkinson. 2019a. 'Validation of the RayStation Monte Carlo dose calculation algorithm using a realistic lung phantom', *J Appl Clin Med Phys*, 20: 127-37.

———. 2019b. 'Validation of the RayStation Monte Carlo dose calculation algorithm using realistic animal tissue phantoms', *J Appl Clin Med Phys*, 20: 160-71.

Sethi, R. V., D. Giantsoudi, M. Raiford, I. Malhi, A. Niemierko, O. Rapalino, P. Caruso, T. I. Yock, N. J. Tarbell, H. Paganetti, and S. M. MacDonald. 2014. 'Patterns of failure after proton therapy in medulloblastoma; linear energy transfer distributions and relative biological effectiveness associations for relapses', *Int J Radiat Oncol Biol Phys*, 88: 655-63.

Silvoniemi, A., S. Suilamo, T. Laitinen, S. Forsback, E. Loyttyniemi, S. Vaittinen, V. Saunavaara, O. Solin, T. J. Gronroos, and H. Minn. 2018. 'Repeatability of tumour hypoxia imaging using [(18)F]EF5 PET/CT in head and neck cancer', *Eur J Nucl Med Mol Imaging*, 45: 161-69.

Sorensen, B. S., N. Bassler, S. Nielsen, M. R. Horsman, L. Grzanka, H. Spejlborg, J. Swakon, P. Olko, and J. Overgaard. 2017. 'Relative biological effectiveness (RBE) and distal edge effects of proton radiation on early damage in vivo', *Acta Oncol*, 56: 1387-91.

Sorensen, B. S., J. Pawelke, J. Bauer, N. G. Burnet, A. Dasu, M. Hoyer, C. P. Karger, M. Krause, M. Schwarz, T. S. A. Underwood, D. Wagenaar, G. A. Whitfield,

and A. Luhr. 2021. 'Does the uncertainty in relative biological effectiveness affect patient treatment in proton therapy?', *Radiother Oncol*, 163: 177-84.

Strigari, L., F. Torriani, L. Manganaro, T. Inaniwa, F. Dalmasso, R. Cirio, and A. Attili. 2018. 'Tumour control in ion beam radiotherapy with different ions in the presence of hypoxia: an oxygen enhancement ratio model based on the microdosimetric kinetic model', *Phys Med Biol*, 63: 065012.

Suckert, T., E. Beyreuther, J. Muller, B. Azadegan, M. Meinhardt, F. Raschke, E. Bodenstein, C. von Neubeck, A. Luhr, M. Krause, and A. Dietrich. 2020. 'Late Side Effects in Normal Mouse Brain Tissue After Proton Irradiation', *Front Oncol*, 10: 598360.

Sung, H., J. Ferlay, R. L. Siegel, M. Laversanne, I. Soerjomataram, A. Jemal, and F. Bray. 2021. 'Global Cancer Statistics 2020: GLOBOCAN Estimates of Incidence and Mortality Worldwide for 36 Cancers in 185 Countries', *CA Cancer J Clin*, 71: 209-49.

Saager, M., P. Peschke, S. Brons, J. Debus, and C. P. Karger. 2018. 'Determination of the proton RBE in the rat spinal cord: Is there an increase towards the end of the spread-out Bragg peak?', *Radiother Oncol*, 128: 115-20.

Terry, N. H. A., and J. Denekamp. 1984. 'RBE values and repair characteristics for colo-rectal injury after caesium 137 gamma-ray and neutron irradiation. II. Fractionation up to ten doses', *The British Journal of Radiology*, 57: 617-29.

Tessonnier, T., A. Mairani, F. Cappucci, A. Mirandola, G. Vilches Freixas, S. Molinelli, M. Donetti, and M. Ciocca. 2014. 'Development and application of tools for Monte Carlo based simulations in a particle beam radiotherapy facility', *Appl Radiat Isot*, 83 Pt B: 155-8.

Thomas, D. J. 2012. 'ICRU report 85: fundamental quantities and units for ionizing radiation', *Radiation Protection Dosimetry*, 150: 550-52.

Tilly, N., J. Johansson, U. Isacsson, J. Medin, E. Blomqvist, E. Grusell, and B. Glimelius. 2005. 'The influence of RBE variations in a clinical proton treatment plan for a hypopharynx cancer', *Phys Med Biol*, 50: 2765-77.

Tinganelli, W., M. Durante, R. Hirayama, M. Kramer, A. Maier, W. Kraft-Weyrather, Y. Furusawa, T. Friedrich, and E. Scifoni. 2015. 'Kill-painting of hypoxic tumours in charged particle therapy', *Sci Rep*, 5: 17016.

Toussaint, L., D. J. Indelicato, K. S. Holgersen, J. B. B. Petersen, C. H. Stokkevag, Y. Lassen-Ramshad, O. Casares-Magaz, A. Vestergaard, and L. P. Muren. 2019. 'Towards proton arc therapy: physical and biologically equivalent doses with increasing number of beams in pediatric brain irradiation', *Acta Oncol*, 58: 1451-56.

Toustrup, K., B. S. Sorensen, P. Lassen, C. Wiuf, J. Alsner, J. Overgaard, Head Danish, and Group Neck Cancer. 2012. 'Gene expression classifier predicts for hypoxic modification of radiotherapy with nimorazole in squamous cell carcinomas of the head and neck', *Radiother Oncol*, 102: 122-9.

Underwood, T. S. A., C. Grassberger, R. Bass, S. M. MacDonald, N. M. Meyersohn, B. Y. Yeap, R. B. Jimenez, and H. Paganetti. 2018. 'Asymptomatic Late-phase

Radiographic Changes Among Chest-Wall Patients Are Associated With a Proton RBE Exceeding 1.1', *Int J Radiat Oncol Biol Phys*, 101: 809-19.

Unkelbach, J., P. Botas, D. Giantsoudi, B. L. Gorissen, and H. Paganetti. 2016. 'Reoptimization of Intensity Modulated Proton Therapy Plans Based on Linear Energy Transfer', *Int J Radiat Oncol Biol Phys*, 96: 1097-106.

Unkelbach, J., and H. Paganetti. 2018. 'Robust Proton Treatment Planning: Physical and Biological Optimization', *Semin Radiat Oncol*, 28: 88-96.

van Leeuwen, C. M., A. L. Oei, J. Crezee, A. Bel, N. A. P. Franken, L. J. A. Stalpers, and H. P. Kok. 2018. 'The alfa and beta of tumours: a review of parameters of the linear-quadratic model, derived from clinical radiotherapy studies', *Radiat Oncol*, 13: 96.

Vaupel, P., and A. Mayer. 2007. 'Hypoxia in cancer: significance and impact on clinical outcome', *Cancer Metastasis Rev*, 26: 225-39.

Wan Chan Tseung, H. S., J. Ma, C. R. Kreofsky, D. J. Ma, and C. Beltran. 2016. 'Clinically Applicable Monte Carlo-based Biological Dose Optimization for the Treatment of Head and Neck Cancers With Spot-Scanning Proton Therapy', *Int J Radiat Oncol Biol Phys*, 95: 1535-43.

Wang, C. C., A. L. McNamara, J. Shin, J. Schuemann, C. Grassberger, A. G. Taghian, R. B. Jimenez, S. M. MacDonald, and H. Paganetti. 2020. 'End-of-Range Radiobiological Effect on Rib Fractures in Patients Receiving Proton Therapy for Breast Cancer', *Int J Radiat Oncol Biol Phys*.

Wedenberg, M., B. K. Lind, and B. Hardemark. 2013. 'A model for the relative biological effectiveness of protons: the tissue specific parameter alpha/beta of photons is a predictor for the sensitivity to LET changes', *Acta Oncol*, 52: 580-8.

Welz, S., D. Monnich, C. Pfannenberg, K. Nikolaou, M. Reimold, C. La Fougere, G. Reischl, P. S. Mauz, F. Paulsen, M. Alber, C. Belka, D. Zips, and D. Thorwarth. 2017. 'Prognostic value of dynamic hypoxia PET in head and neck cancer: Results from a planned interim analysis of a randomized phase II hypoxia-image guided dose escalation trial', *Radiother Oncol*, 124: 526-32.

Wenzl, T., and J. J. Wilkens. 2011. 'Modelling of the oxygen enhancement ratio for ion beam radiation therapy', *Phys Med Biol*, 56: 3251-68.

Wilkens, J. J., and U. Oelfke. 2004. 'A phenomenological model for the relative biological effectiveness in therapeutic proton beams', *Phys Med Biol*, 49: 2811-25.

Wright, P., M. R. Arnesen, P. I. Lonne, S. Suilamo, A. Silvoniemi, E. Dale, H. Minn, and E. Malinen. 2021. 'Repeatability of hypoxia dose painting by numbers based on EF5-PET in head and neck cancer', *Acta Oncol*: 1-6.

Zhou, Q., M. E. Howard, X. Tu, Q. Zhu, J. M. Denbeigh, N. B. Remmes, M. G. Herman, C. J. Beltran, J. Yuan, P. T. Greipp, J. C. Boughey, L. Wang, N. Johnson, M. P. Goetz, J. N. Sarkaria, Z. Lou, and R. W. Mutter. 2021. 'Inhibition of ATM Induces Hypersensitivity to Proton Irradiation by Upregulating Toxic End Joining', *Cancer Res*, 81: 3333-46.

Publications

Scientific Article

The Organ Sparing Potential of Different Biological Optimization Strategies in Proton Therapy

Helge Henjum, MSc,[a],* Tordis J. Dahle, PhD,[a,b] Lars Fredrik Fjæra, MSc,[a]
Eivind Rørvik, MSc,[a] Sara Pilskog, PhD,[a,b] Camilla H. Stokkevåg, PhD,[a,b]
Andrea Mairani, PhD,[c,d] and Kristian S. Ytre-Hauge, PhD[a]

[a]*Department of Physics and Technology, University of Bergen, Bergen, Norway;* [b]*Department of Oncology and Medical
Physics, Haukeland University Hospital, Bergen, Norway;* [c]*Centro Nazionale di Adroterapia Oncologica (CNAO
Foundation), Pavia, Italy;* [d]*Heidelberg Ion Beam Therapy Center, Heidelberg, Germany*

Abstract

Purpose: Variable relative biological effectiveness (RBE) models allow for differences in linear energy transfer (LET), physical dose, and tissue type to be accounted for when quantifying and optimizing the biological damage of protons. These models are complex and fraught with uncertainties, and therefore, simpler RBE optimization strategies have also been suggested. Our aim was to compare several biological optimization strategies for proton therapy by evaluating their performance in different clinical cases.

Methods and Materials: Two different optimization strategies were compared: full variable RBE optimization and differential RBE optimization, which involve applying fixed RBE for the planning target volume (PTV) and variable RBE in organs at risk (OARs). The optimization strategies were coupled to 2 variable RBE models and 1 LET-weighted dose model, with performance demonstrated on 3 different clinical cases: brain, head and neck, and prostate tumors.

Results: In cases with low $(\alpha/\beta)_x$ in the tumor, the full RBE optimization strategies had a large effect, with up to 10% reduction in RBE-weighted dose to the PTV and OARs compared with the reference plan, whereas smaller variations (<5%) were obtained with differential optimization. For tumors with high $(\alpha/\beta)_x$, the differential RBE optimization strategy showed a greater reduction in RBE-weighted dose to the OARs compared with the reference plan and the full RBE optimization strategy.

Conclusions: Differences between the optimization strategies varied across the studied cases, influenced by both biological and physical parameters. Whereas full RBE optimization showed greater OAR sparing, awareness of underdosage to the target must be carefully considered.

Introduction

Currently, a constant relative biological effectiveness (RBE) of 1.1 (RBE$_{1.1}$) is applied in clinical proton therapy (PT), as recommended by the International Commission on Radiation Units and Measurements.[1,2] However, based on the broad range of in vitro data showing variability in the RBE, as well as recent in vivo data[3] and clinical results,[4-8] there is a growing concern that the

constant RBE approach may lead to suboptimal treatment. This has given rise to both phenomenologic and mechanistic RBE models, which can be applied to estimate the variation in RBE in PT treatment plans.[9-15] Most models show the same general dependencies, such as increasing RBE with decreasing dose, increasing linear energy transfer (LET), and decreasing α/β of the reference radiation (photon-based $(\alpha/\beta)_x$).[16] Owing to these observations, there is a growing consensus that incorporation of LET- or RBE-based parameters in the optimization of PT treatment plans is a natural step to improve the precision and quality of the treatment.[17,18] In a recent comprehensive report,[19] the PT community emphasized the risk of unexpected toxicities from ignoring RBE variation, underlining the importance to address RBE uncertainties and to provide clinical solutions for LET- or RBE-based optimization in PT.[6]

Full biological optimization, where variable RBE is used for both the planning target volume (PTV) and the organ at risk (OAR), is a strategy to reduce the suspected elevated RBE-weighted doses in both the target and healthy tissue. However, a significant uncertainty in RBE models lies in the cell-line dependency derived from in vitro data with considerable deviations in response.[20] This uncertainty is circumvented by instead using LET-weighted dose (LWD) models. McMahon et al[21] found that an LET-dependent dose is almost as effective as variable RBE models when it comes to reducing biological variability. The main reservations of full biological optimization have been a risk of underdosage to the target, a possible consequence if the RBE is overestimated. As a solution, a combination of multiple RBE models in the optimization was recently suggested in which the traditional RBE of 1.1 was applied to the target, whereas a variable RBE was allowed for OARs (differential biological optimization).[22] However, although different approaches to RBE-weighted dose optimization have been proposed,[23-27] a coherent comparison between different techniques has not yet been done. Hence, our aim was to compare full and differential biological optimization strategies using different RBE models, to quantify how the physical and RBE-weighted dose is affected in different clinical scenarios. For this purpose, we developed a flexible framework for biological optimization based on the FLUKA Monte Carlo (MC) code[28-30] and a prototype optimization algorithm.[31,32] Two recent proton RBE models and an LWD model were implemented into the biological optimization software and applied for 3 different clinical cases.

Materials and Methods

We used MC-based treatment plan optimization, enabling scoring of dose, LET, and secondary particles and biological parameters, thus allowing optimization with respect to the RBE-weighted dose. The FLUKA-based treatment plan reoptimization method consists of 3 steps: a FLUKA MC simulation of a treatment plan from a commercial treatment planning system using the FLUKA development version, reoptimization of the pencil beam weightings with respect to the variable RBE-based strategies using the dose estimates for each pencil beam from the initial simulation, and a second FLUKA MC simulation of the new plan for verification. The scored values (the proton radiosensitivity parameters along with the physical dose (αD and $\sqrt{\beta}D$), along with spatial information about the planning target volume and OARs and their respective $(\alpha/\beta)_x$, are used as input to the optimization algorithm. To achieve a homogeneous RBE-weighted dose to the PTV while minimizing the dose to the OARs according to the selected objectives, the optimizer adjusts the weightings of the pencil beams without adding or removing pencil beams from the original plan to achieve a homogeneous RBE-weighted dose to the PTV while minimizing the dose to the OARs according to the selected objectives.

Optimization strategies

We implemented full and differential RBE optimization strategies by applying RBE-weighted dose objectives. During the RBE optimization, the RBE-models by Rørvik et al (ROR)[15] and McNamara et al (MCN)[13] were incorporated. These models include LET, dose, and $(\alpha/\beta)_x$ as input parameters. The MCN model assumes a linear relationship between LET and RBE and can therefore make use of the dose-weighted LET (LET$_d$) as an input parameter, whereas the ROR model is based on a nonlinear LET-RBE relationship and requires the full LET spectrum to estimate the RBE. We also applied the LWD approach, which combines only the physical dose and LET$_d$.[23,27] This approach does not account for tissue dependence and uses a normalization factor to maintain the mean RBE of 1.1 to the clinical target volume, as described by Fjaera et al[33] (details are provided in Appendix E1 in the Supplement). Identical target prescription for the RBE-weighted dose was applied for all the different strategies; that is, all optimization strategies aimed to give the same prescribed dose accounting for their respective RBE variations, primarily enabling comparison of the optimization strategies and the resulting physical parameters of absorbed dose and LET resulting from the different optimization processes. In addition, all patient cases were also optimized using a global RBE of 1.1 for reference. The RBE$_{1.1}$ optimized plans were also recalculated using the different RBE models for comparison in terms of variable-RBE weighted doses.

The following optimization strategies were thereby explored:

1. Full RBE optimization (FO): Optimizing the dose to both the PTV and the OARs with respect to each of

the models—MCN (FO_{MCN}), ROR (FO_{ROR}), and LWD (FO_{LWD})—using organ-specific tissue parameters in RBE modeling for the MCN and ROR models.

2. Differential RBE optimization (DO): Optimizing the dose to the PTV using $RBE_{1.1}$ to avoid potential underdosage while applying the MCN (DO_{MCN}), ROR (DO_{ROR}), and LWD (DO_{LWD}) models when optimizing the RBE-weighted dose to the OARs.

In the results, the RBE-weighted doses are denoted D_Y^X, X is the model used for plan optimization, and Y is the model applied to calculate the reported dose (eg, $D_{MCN}^{RBE_{1.1}}$ is the RBE-weighted dose from a plan optimized with $RBE_{1.1}$ and recalculated with the MCN model).

The generated dose distributions were compared in terms of dose-volume histograms and dose metrics for the PTVs and OARs. The RBE-weighted dose difference between the strategies and the reference $RBE_{1.1}$ were also quantified, where the $RBE_{1.1}$-optimized dose was recalculated to the respective RBE models of the different strategies to provide a comparison of the variable RBE-weighted dose. The evaluated values for the PTV were mean dose, volumes receiving 95% and 107% dose ($V_{95\%}$ and $V_{107\%}$), and for OARs, the mean dose and dose to 95% and 2% of the volume ($D_{95\%}$ and $D_{2\%}$).

Treatment plans

Intensity modulated proton therapy (IMPT) treatment plans were generated in the Eclipse treatment planning system (Varian Medical Systems, Palo Alto, California) applying an RBE of 1.1. For verification of the biological optimization software, simple treatment plans were created for a water phantom. An RBE-weighted dose of 2 Gy (RBE) was prescribed to a spread-out Bragg peak 4 cm wide.

The 3 patient cases included a brain tumor (pituitary adenoma), a prostate cancer case, and a head and neck cancer case (rhabdomyosarcoma). Multifield optimization was used for all 3 cases. The $(\alpha/\beta)_x$ for the different regions of interest were found in the literature[13,34-38] and are given in Appendix E2 together with treatment specifications. In many cases, depending on the $(\alpha/\beta)_x$ value, the MCN and ROR models' RBE estimates will differ significantly from the LWD estimates (no $(\alpha/\beta)_x$ dependency). Owing to the large differences between models in RBE and RBE-weighted dose in the OARs, the use of the identical OAR dose constraint across different models likely would not give optimal OAR sparing for all strategies. To achieve the best possible OAR sparing with the different strategies, the planning and optimization process was done in 2 steps. First, a pure PTV-based optimization (no constraints on the OAR dose) was performed with respect to RBE-weighted dose. Then, the OAR dose constraint levels were set below the maximum values

from the previous step to penalize the OAR dose equally for all strategies (values are provided in Table EB.1). The highest priority during optimization was the mean dose to the PTV. We defined a homogeneity criterion specifying that 100% of the PTV should be receiving 95% and 107% of the dose after step 2.

The optimizer

The framework for biological optimization was based on a prototype optimizer for particle therapy developed by Mairani et al.[31,32] The optimizer uses the information about pencil beams, physical dose, biological variables from the linear-quadratic model (αD and $\sqrt{\beta}D$), and voxel information to achieve an optimized treatment plan with respect to either physical or RBE-weighted dose.

The optimization algorithm is described in Appendix E2 and the calculation of RBE-weighted dose in Appendix E3. In short, for the MCN and ROR models, the dose is calculated as a combination of the linear quadratic model and the definition of RBE, which makes the RBE dependent on α and β for both reference radiation and the physical dose. For the LWD, the RBE is defined as a linear function of the LET, normalized to provide a mean RBE of 1.1 to the clinical target volume. For differential RBE optimization, the variable RBE-weighted dose in the PTV-term is replaced with a constant $RBE_{1.1}$-weighted dose, whereas a variable RBE-weighted dose is used in the OAR term. This allowed us to apply different biological and physical objectives to different segmented volumes during the same optimization. For regions where the PTV and OARs overlapped, the cost for each volume was calculated independently using their respective $(\alpha/\beta)_x$ values, with no additional priority of the PTV.

Results

All optimization strategies resulted in a homogeneous RBE-weighted dose within the spread-out Bragg peak for the water phantom (Appendix E4), verifying the implementation of the optimization software. RBE values were consistent with previous results from the respective RBE models, and as expected, a lower $(\alpha/\beta)_x$ reduced the physical dose to the PTV (Fig E4.1).

Prostate cancer case

Full optimization with $(\alpha/\beta)_x$-dependent models gave alterations of the dose to the PTV and lower RBE-weighted doses to the rectum and bladder compared with the differential strategies and the $RBE_{1.1}$ reference plan. The FO_{MCN} model provided a mean PTV RBE-weighted dose reduction of 10% compared with the reference plan, whereas the
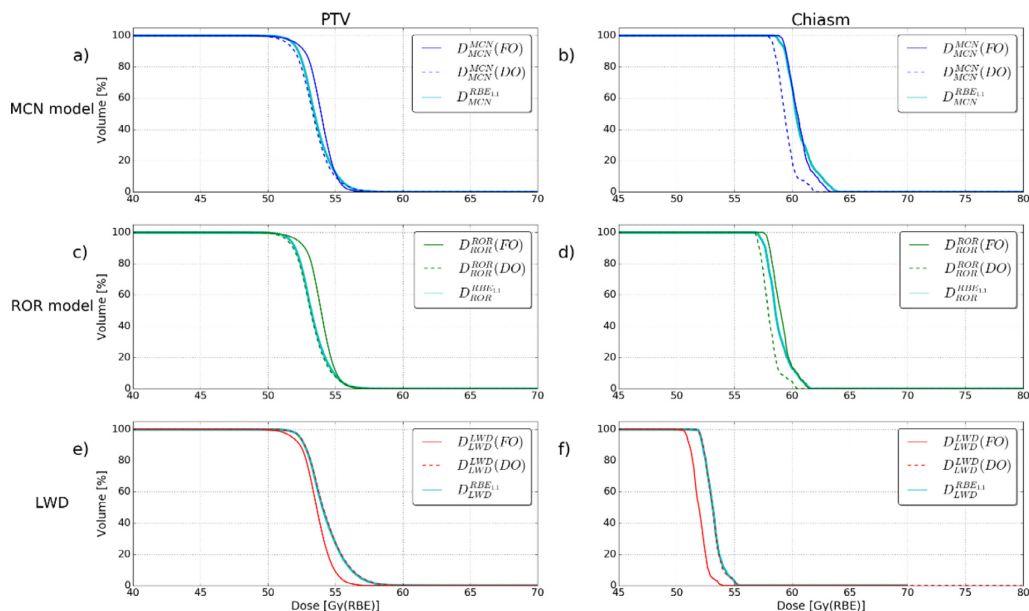
Figure 1   The RBE-weighted dose difference between the reference RBE$_{1.1}$ plan and the variable RBE models in the different strategies. The blue, red and green areas represent the PTV for the respective cases. In the brain tumor case, the OARs are brain stem (yellow), left optic nerve (turquoise), and chiasm (yellow). For the prostate case, the OARs are bladder (blue) and rectum (pink). For the head and neck case, the OARs are the right pterygoid (orange) and left parotid gland (light green). *Abbreviations:* OAR = organ at risk; PTV = planning target volume; RBE = relative biological effectiveness.

FO$_{ROR}$ model gave a mean dose reduction of 5% (Fig 1A and 1C). For the OARs, the FO$_{MCN}$ model reduced the maximum dose (D$_{2\%}$) by 10% for the rectum. The corresponding value for the FO$_{ROR}$ model was 5% (Fig 1B and 1D).

The high RBE in the target volume, owed to a low $(\alpha/\beta)_x$, provided large differences between the reference plan and the variable RBE plans from the FO strategies with the MCN and ROR models. This is shown in Figure 2B for both the mean and maximum RBE$_{1.1}$-weighted dose to the PTV and OARs, respectively; the full RBE strategies provided significantly lower doses compared with the other strategies. Both LWD-based strategies and the differential MCN and ROR strategies provided only negligible differences compared with the RBE$_{1.1}$ reference plan.

Brain tumor case

The results from the optimization strategies for the brain-tumor case showed less variation compared with the results for the prostate case. However, the differential MCN and ROR optimization as well as the FO$_{LWD}$ strategy achieved some OAR sparing in terms of both the RBE$_{1.1}$ dose (Fig 2A) and the RBE-weighted dose (Fig 3B and 3D). The DO$_{MCN}$ strategy reduced the RBE-weighted maximum dose by 3% to 5% for the OARs

compared with the RBE$_{1.1}$ plan, and the DO$_{ROR}$ strategy showed a reduction of 2% to 3%, whereas for the DO$_{LWD}$ strategy, the dose difference was negligible (Fig 3F). The reduction in the maximum OAR dose compared with the reference plan for FO$_{MCN}$ and FO$_{ROR}$ was small (<1%), whereas for FO$_{LWD}$, the reduction varied from 2% to 3% (Fig 3B, D, and F).

The largest reductions in dose were observed at the distal part of the beams where the chiasm and left optic nerve are located (first column in Fig 4). For the tissue-dependent models, the DO strategy gave the largest reduction in OAR dose (Fig 3B and 3D), whereas FO gave the largest reduction when applying the LWD model (Fig 3F). We observed only minor changes in the median LET$_d$ between the different strategies (Fig 2D), which indicates that the difference between the strategies are mainly based on the physical dose and the $(\alpha/\beta)_x$.

Patient with head and neck cancer

In the case of head and neck cancer, the full RBE optimization strategies provided a larger reduction in OAR dose compared with the differential strategies, whereas the MCN strategies provided the greatest OAR dose reduction and the LWD strategies provided the lowest compared with the RBE$_{1.1}$ reference plan (Fig 2C). Full
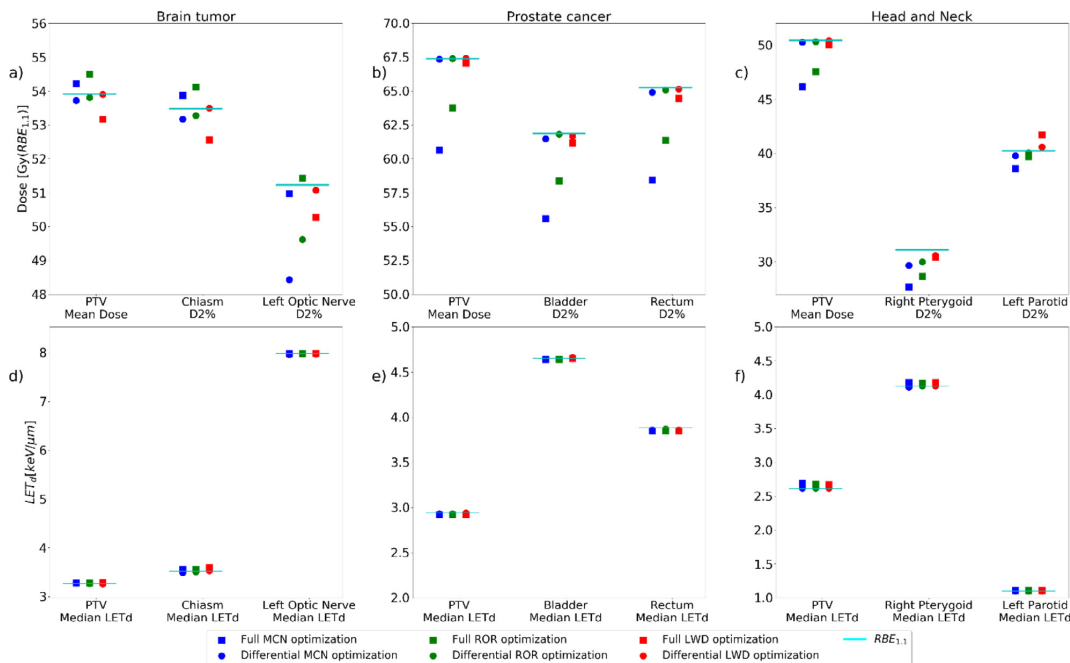
Figure 2 Overview of $RBE_{1.1}$-weighted dose (top row) and LET_d (bottom row) resulting from the different optimization strategies. The colors indicate the respective RBE and LWD models and the cyan line represents the reference plan ($RBE_{1.1}$ optimization). The square markers represent the full strategy and the circle markers represent the differential strategies. *Abbreviations:* LET = linear energy transfer; LWD = LET-weighted dose; RBE = relative biological effectiveness.

optimization with $(\alpha/\beta)_x$-dependent models provided a lower RBE-weighted dose overall compared with the RBE-weighted dose recalculated from the reference plan (Fig 4P and 4Q). Here, the greatest change relative to the reference plan was seen for the FO_{MCN} model, in which the maximum dose to the right pterygoid was reduced by 10% (Fig 5B). The FO_{ROR} model provided similar results, with a reduction in maximum dose of 7% (Fig 5D). For FO_{LWD}, the corresponding dose was reduced by 2% (Fig 5F). The observed variations between strategies were likely owed to the low $(\alpha/\beta)_x$ values for the target volume and the OARs, leading to a high RBE in both the target organ and OARs for the $(\alpha/\beta)_x$-dependent models. Not allowing a variable RBE in the target from the differential RBE strategies, the DO_{MCN} strategy provided a 4% reduction in the maximum dose to the right pterygoid, whereas the DO_{LWD} strategy provided a reduction of 1%. The DO_{ROR} model provided a similar but slightly smaller reduction in the OAR dose compared with DO_{MCN}. There was no significant change in the median LET_d between the strategies in this case (Fig 2F). The trends from the differential optimizations are similar to those observed in the brain tumor case, suggesting lower case variability for the differential strategies.

The head and neck case provided plans outside the homogeneity criterion, but a comparison between the original treatment plan and the RBE-optimized plans from our optimizer (Fig E7.3 in Appendix E7) showed only small differences between the original treatment plan and the optimized plans in terms of dose coverage to the PTV.

Discussion

Motivated by the concern for unanticipated toxicity from LET and RBE effects when using $RBE_{1.1}$ in treatment planning[7,19,39] and the need to assess the impact of different biological optimization strategies, variable RBE models, and an LWD model were implemented and applied for dose calculation in 2 optimization strategies. Overall, the full RBE optimization was found to give the greatest reduction in the RBE-weighted dose to both the PTV and the OARs compared with the reference plan. However, in the brain tumor case, where the high target $(\alpha/\beta)_x$ resulted in low RBE values, differential RBE optimization gave the greatest reduction in the RBE-weighted dose to the OARs. We also observed that LWD strategies reduced the RBE-weighted dose to the OARs,
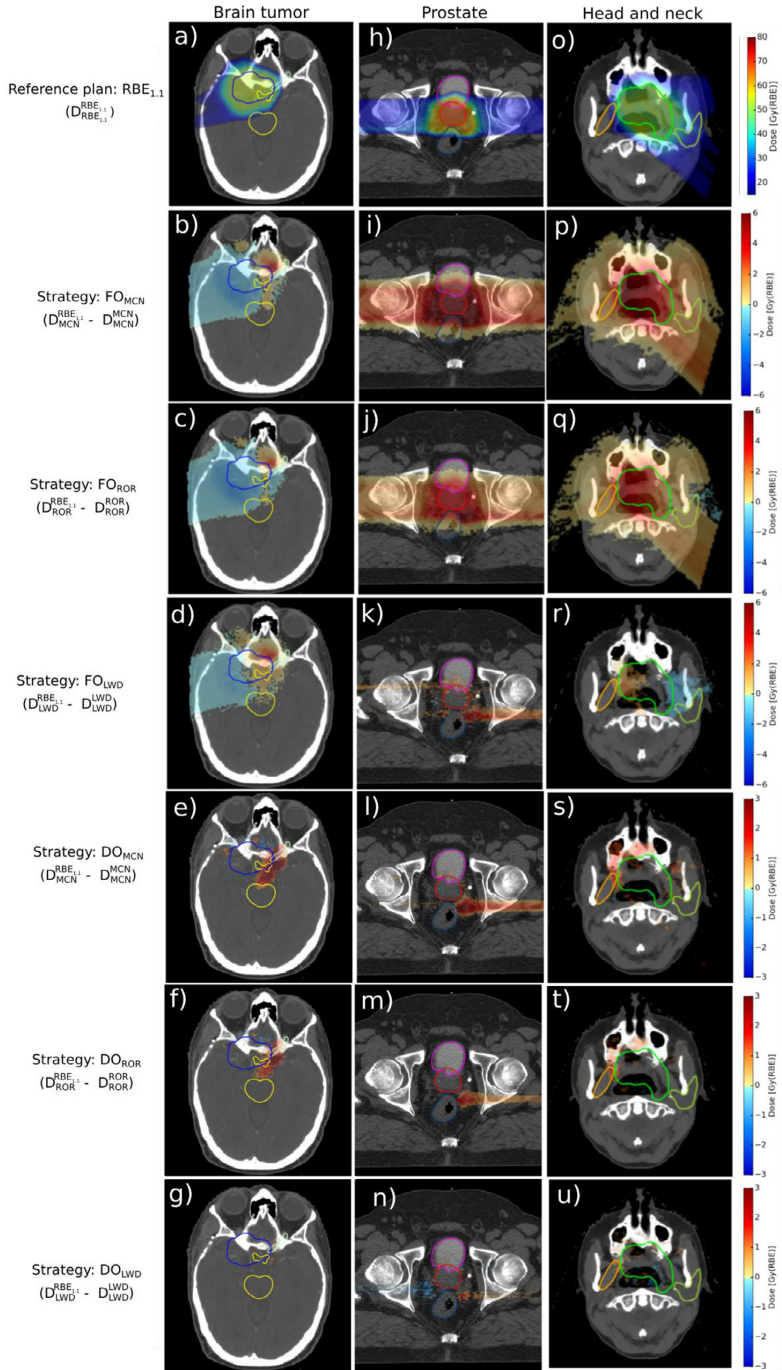
Figure 3 Dose-volume histograms for all strategies in the prostate case. The solid line represents the RBE-weighted dose for the full RBE optimization strategies and the dashed line represents the RBE-weighted dose for the differential RBE optimization strategies. The teal color represents the respective model recalculated from the $RBE_{1.1}$ reference plan. The dose on the axis is the RBE-weighted dose for the given model. *Abbreviation:* RBE = relative biological effectiveness.
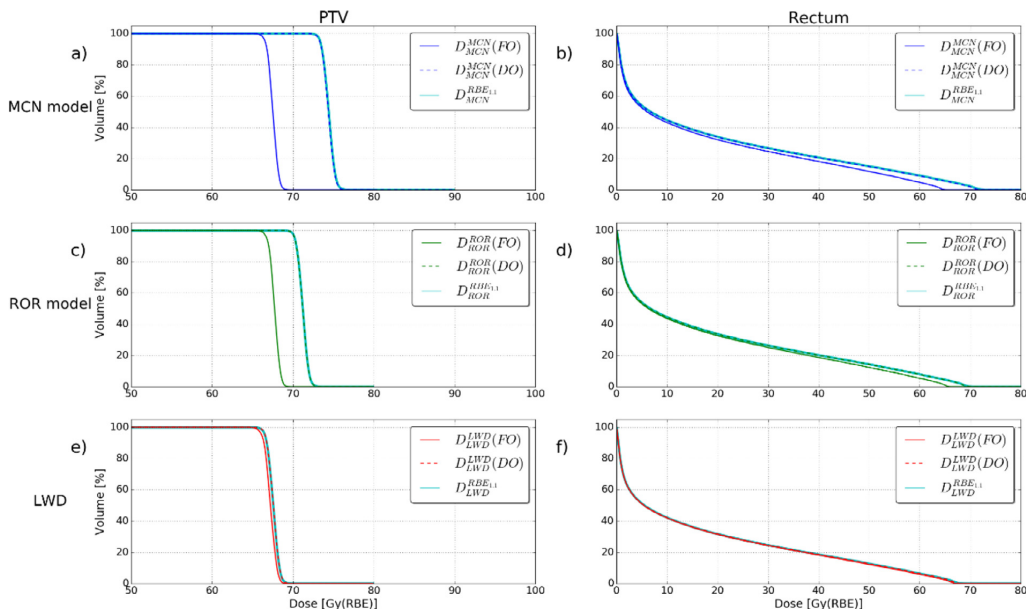
Figure 4 Dose-volume histograms for all strategies in the brain tumor case. The solid line represents the RBE-weighted dose for the full RBE optimization strategies (FO) and the dashed line represents the RBE-weighted dose for the differential RBE optimization strategies (DO). The teal color represents the respective model recalculated from the $RBE_{1.1}$ reference plan. The dose on the axis is the RBE-weighted dose for the given model. *Abbreviation:* RBE = relative biological effectiveness.
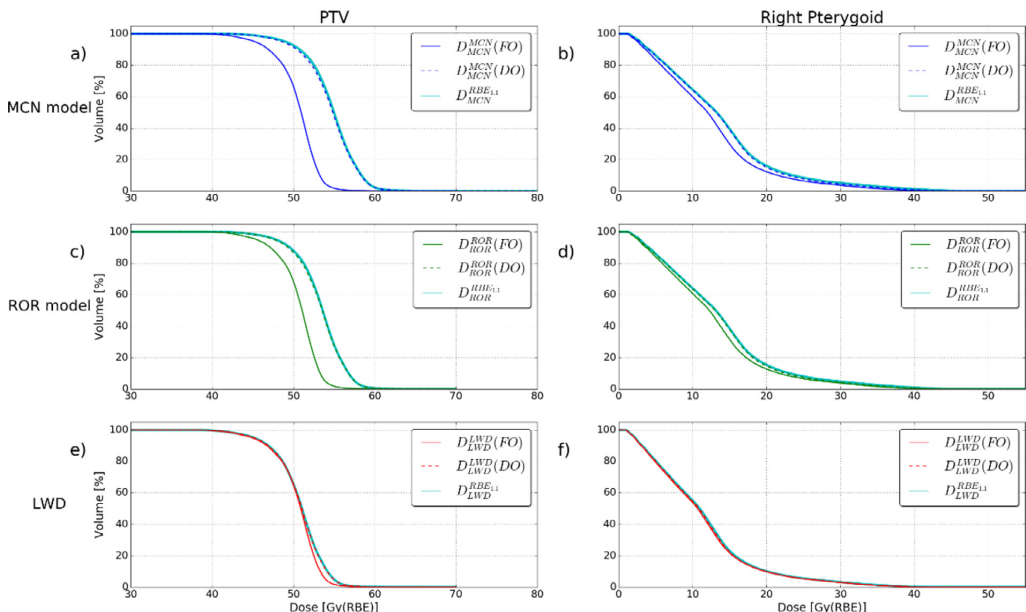

Figure 5 Dose-volume histograms for all strategies in the head and neck cancer case. The solid line represents the RBE-weighted dose for the full RBE optimization strategies and the dashed line represents the RBE-weighted dose for the differential RBE optimization strategies. The teal color represents the respective model recalculated from the $RBE_{1.1}$ reference plan. The dose on the axis is the RBE-weighted dose for the given model. *Abbreviation:* RBE = relative biological effectiveness.

but generally to a lesser degree than the MCN and ROR models.

The FO_{MCN} and FO_{ROR} strategies showed similar RBE-weighted dose distributions for all cases, although the MCN-based optimization provided a greater RBE-weighted dose reduction compared with the reference plan ($RBE_{1.1}$). This implies that introducing the MCN model clinically will be a greater step away from an RBE of 1.1 compared with applying the ROR model. For the brain tumor case, with high $(\alpha/\beta)_x$ to the PTV and low $(\alpha/\beta)_x$ elsewhere, the optimizer was not able to significantly reduce the RBE-weighted dose to the OARs through full RBE optimization (Fig 3B and 3D). Therefore, the full LWD optimization strategy gave the largest differences in RBE-weighted dose compared with the reference plan in this case, because it was not affected by the large difference in $(\alpha/\beta)_x$ between the OARs and the PTV. This suggests that for high $(\alpha/\beta)_x$ tumors, full RBE optimization may overestimate the need for physical dose deposition in the PTV. Also, to our knowledge, observation of underdosage in proton therapy from using an RBE of 1.1 has not been an issue raised, with the exception of medulloblastoma cases with high $(\alpha/\beta)_x$.[40]

For the case of full RBE optimization of the prostate, the mean physical dose reduction to the reference plan for the PTV was 10% and for the MCN and ROR models, 5%, showing both a larger difference to the reference plan and a difference between the RBE models as compared with the brain tumor case. This is a reflection of the low PTV $(\alpha/\beta)_x$ value for the prostate, giving opportunities for OAR dose reduction at the cost of reduced physical dose delivered to the target. The relatively homogeneous LET distribution, owed to the opposing fields, resulted in a small effect for both the full and differential LWD-optimization strategies, with marginal differences compared with the reference plan. This was also the case for all the differential RBE optimization results, indicating that this strategy is indeed more effective in reducing dose to OARs when having notable high LET values. Overall, these results suggest that applying a differential strategy or an LWD-based strategy for a prostate case, or similar cases with opposing fields, would have little potential to reduce OAR doses. On the other hand, for such cases with a low target $(\alpha/\beta)_x$ value, full MCN and ROR could be a good option if OAR sparing is of high priority. This should only be done after a careful consideration of potential underdosage of the tumor because this strategy will significantly reduce the physical dose (up to 10% in this case) in the high-LET regions in the target.

In the head and neck case, the 3 fields, combined with an identical $(\alpha/\beta)_x$ value for both the PTV and the OARs, resulted in a clear reduction in maximum dose for all the full RBE strategies, because the higher degree of freedom allowed reduction of the RBE-weighted dose at the distal beam ends. Because the largest differences in this case were found in the distal part of the beams, as in the brain tumor case (Fig 4, columns 1 and

3), it is clear that the effect of a certain optimization strategy in general will depend on the field configuration. Further investigation of this could be relevant (eg, for proton arc therapy).

The $(\alpha/\beta)_x$ parameter has uncertainties and is thereby a current intrinsic limitation of the variable RBE models. They are, however, commonly accepted in clinics, and we therefore found it relevant to use them in this study. Other limitations of the study include the parameter $D_{2\%}$, which was applied to assess the maximum dose levels to the OARs. In this study, we used the parameter for case comparisons, although an alternative approach would be to compare dose levels directly associated with reported toxicity. The cases in this study were selected to show and compare the optimization strategies relative to each other, and therefore, 3 common cases for proton therapy were chosen. Another factor that could be included would be to keep the same OAR constraint for all models and then see how the different strategies would differ from the results in this study. Because the dose constraint to the OARs varied between the cases, a common physical dose constraint could be applied to compare the strategies' abilities.

The largest differences between the optimization strategies were observed at the distal part of the beams. This could relate to clinical LET effects; possible evidence of this was found by Eulitz et al, Peeler et al, Underwood et al, Bahn et al, and Engeseth et al,[4-7,39] who observed treatment-related change, mostly at the distal end of the PTV, in magnetic resonance imaging and computed tomography follow-up in patients who received proton therapy. The treatment plans from these studies were optimized using an RBE of 1.1, which might indicate that there is some overdosage at the distal end of the beam, and this may have negative consequences both inside and outside the target. Although more clinical evidence is warranted, the emerging clinical observations support the introduction of OAR dose reduction through full RBE or LWD optimization by reducing the dose within OARs. A combination between this study's strategies and robust optimization could provide a good continuation from this work. With robust optimizaton, for example, biological range uncertainties would be taken into account. Robust optimization of set-up errors could also reveal potential LET and RBE hotspots in the patient. The disadvantage is that with MC-based treatment-planning tools, robust optimization would be time consuming.

The results in this study could be generalized for cases with similar properties in terms of field positioning. The prostate case, especially, could be generalized becuase it is a very standard case in terms of field positioning. For the other cases, the field configuration created high LET values in the distal end, which will likely be similar for many brain tumor and head and neck cases.

Conclusion

This study shows that RBE- and LET-based optimization has great potential for OAR dose reduction, but the risk of target underdosage must be carefully considered. The varying effects of the optimization strategies depending on case-specific parameters illustrate that applicability of a certain model and optimization strategy requires solid understanding of the models, input variables, and potential dosimetric pitfalls. For tumors with high $(\alpha/\beta)_x$, better OAR sparing may in some cases be achieved with differential RBE optimization or LWD optimization strategies compared with full RBE optimization. However, applying a differential strategy or an LWD-based strategy for a prostate case, or similar cases with opposing fields and low target $(\alpha/\beta)_x$, would have little potential for lowering OAR doses.

Supplementary materials

Supplementary material associated with this article can be found in the online version at https://doi.org/10.1016/j.adro.2021.100776.

References

1. Paganetti H, Niemierko A, Ancukiewicz M, et al. Relative biological effectiveness (RBE) values for proton beam therapy. *Int J Radiat Oncol Biol Phys*. 2002;53:407–421.
2. Wayne Newhauser. *International Commission on Radiation Units and Measurements Report 78: Prescribing, Recording and Reporting Proton-beam Therapy, Radiation Protection Dosimetry*. 2009;133:60–62.
3. Saager M, Peschke P, Brons S, Debus J, Karger CP. Determination of the proton RBE in the rat spinal cord: Is there an increase towards the end of the spread-out Bragg peak? *Radiother Oncol*. 2018;128:115–120.
4. Peeler CR, Mirkovic D, Titt U, et al. Clinical evidence of variable proton biological effectiveness in pediatric patients treated for ependymoma. *Radiother Oncol*. 2016;121(3):395–401.
5. Underwood TSA, Grassberger C, Bass R, et al. Asymptomatic late-phase radiographic changes among chest-wall patients are associated with a proton RBE exceeding 1.1. *Int J Radiat Oncol Biol Phys*. 2018;101(4):809–819.
6. Eulitz J, Troost EGC, Raschke F, et al. Predicting late magnetic resonance image changes in glioma patients after proton therapy. *Acta Oncol*. 2019;58(10):1536–1539.
7. Bahn E, Bauer J, Harrabi S, et al. Late contrast enhancing brain lesions in proton-treated patients with low-grade glioma: Clinical Evidence for increased periventricular sensitivity and variable RBE. *Int J Radiat Oncol Biol Phys*. 2020;107(3):571–578.
8. Wang CC, McNamara AL, Shin J, et al. End-of-range radiobiological effect on rib fractures in patients receiving proton therapy for breast cancer. *Int J Radiat Oncol Biol Phys*. 2020;107(3):449–454.
9. Chen Y, Ahmad S. Empirical model estimation of relative biological effectiveness for proton beam therapy. *Radiat Prot Dosimetry*. 2012;149(2):116–123.
10. Carabe A, Moteabbed M, Depauw N, et al. Range uncertainty in proton therapy due to variable biological effectiveness. *Phys Med Biol*. 2012;57(5):1159–1172.
11. Wedenberg M, Lind BK, Hardemark B. A model for the relative biological effectiveness of protons: The tissue specific parameter alpha/beta of photons is a predictor for the sensitivity to LET changes. *Acta Oncol*. 2013;52(3):580–588.
12. Jones B. A simpler energy transfer efficiency model to predict relative biological effect for protons and heavier ions. *Front Oncol*. 2015;5:184.
13. McNamara AL, Schuemann J, Paganetti H. A phenomenological relative biological effectiveness (RBE) model for proton therapy based on all published in vitro cell survival data. *Phys Med Biol*. 2015;60(21):8399–8416.
14. Mairani A, Dokic I, Magro G, et al. A phenomenological relative biological effectiveness approach for proton therapy based on an improved description of the mixed radiation field. *Phys Med Biol*. 2017;62(4):1378–1395.
15. Rorvik E, Thörnqvist S, Stokkevåg CH, et al. A phenomenological biological dose model for proton therapy based on linear energy transfer spectra. *Med Phys*. 2017;44(6):2586–2594.
16. Rorvik E, Fjæra LF, Dahle TJ, et al. Exploration and application of phenomenological RBE models for proton therapy. *Phys Med Biol*. 2018;63(18) 185013.
17. Mohan R, Peeler CR, Guan F, et al. Radiobiological issues in proton therapy. *Acta Oncol*. 2017;56(11):1367–1373.
18. Willers H, Allen A, Grosshans D, et al. Toward a variable RBE for proton beam therapy. *Radiother Oncol*. 2018;128(1):68–75.
19. Paganetti H, Blakely E, Carabe-Fernandez A, et al. Report of the AAPM TG-256 on the relative biological effectiveness of proton beams in radiation therapy. *Med Phys*. 2019;46(3):e53–e78.
20. McMahon SJ. Proton RBE models: Commonalities and differences. *Phys Med Biol*. 2021;66(4):04NT02.
21. McMahon SJ, Paganetti H, Prise KM. LET-weighted doses effectively reduce biological variability in proton radiotherapy planning. *Phys Med Biol*. 2018;63(22):225009.
22. Sanchez-Parcerisa D, López-Aguirre M, Llerena AD, Udías JM. MultiRBE: Treatment planning for protons with selective radiobiological effectiveness. *Med Phys*. 2019;46(9):4276–4284.
23. Unkelbach J, Botas P, Giantsoudi D, Gorissen BL, Paganetti H. Reoptimization of intensity modulated proton therapy plans based on linear energy transfer. *Int J Radiat Oncol Biol Phys*. 2016;96(5):1097–1106.
24. Guan F, Geng C, Ma D, et al. RBE Model-Based Biological Dose Optimization for Proton Radiobiology Studies. *Int J Part Ther*. 2018;5:160–171.
25. Giantsoudi D, Grassberger C, Craft D, et al. Linear energy transfer-guided optimization in intensity modulated proton therapy: Feasibility study and clinical potential. *Int J Radiat Oncol Biol Phys*. 2013;87:216–222.
26. Fager M, Toma-Dasu I, Kirk M, et al. Linear energy transfer painting with proton therapy: A means of reducing radiation doses with equivalent clinical effectiveness. *Int J Radiat Oncol Biol Phys*. 2015;91:1057–1064.
27. Wan Chan Tseung HS, Ma J, Kreofsky CR, Ma DJ, Beltran C. Clinically applicable Monte Carlo-based biological dose optimization for the treatment of head and neck cancers with spot-scanning proton therapy. *Int J Radiat Oncol Biol Phys*. 2016;95:1535–1543.
28. Ferrari A, Sala PR, Fassó A, Ranft J. FLUKA: A multi-particle transport code, in CERN-2005-10 (2005), INFN/TC_05/11, SLAC-R-773. 2005.
29. Bohlen TT, Cerutti F, Chin MPW, et al. The FLUKA Code: Developments and Challenges for High Energy and Medical Applications. *Nuclear Data Sheets*. 2014;120:211–214.
30. Battistoni G, Bauer J, Boehlen TT, et al. The FLUKA Code: An Accurate Simulation Tool for Particle Therapy. *Front Oncol*. 2016;6:116.

31. Mairani A, Böhlen TT, Schiavi A, et al. A Monte Carlo-based treatment planning tool for proton therapy. *Phys Med Biol*. 2013;58:2471–2490.

32. Bohlen TT, Bauer J, Dosanjh M, Ferrari A, et al. A Monte Carlo-based treatment-planning tool for ion beam therapy. *J Radiat Res*. 2013;54(Suppl 1):i77–i81.

33. Fjaera LF, Li Z, Ytre-Hauge KS, et al. Linear energy transfer distributions in the brainstem depending on tumour location in intensity-modulated proton therapy of paediatric cancer. *Acta Oncol*. 2017;56:763–768.

34. Pedicini P, Caivano R, Fiorentino A, Strigari L. Clinical radiobiology of head and neck cancer: The hypothesis of stem cell activation. *Clin Transl Oncol*. 2015;17:469–476.

35. Brenner DJ, Hall EJ. Fractionation and protraction for radiotherapy of prostate carcinoma. *Int J Radiat Oncol Biol Phys*. 1999;43:1095–1101.

36. Mendonca M, Timmerman RD. In regard to Donaldson et al: Results from the IRS-IV randomized trial of hyperfractionated radiotherapy in children with rhabdomyosarcoma—A report from the IRSG. IJROBP 2001;51:718-728. *Int J Radiat Oncol Biol Phys*. 2002;54:1579–1580.

37. Terry NHA, Denekamp J. RBE values and repair characteristics for colo-rectal injury after caesium 137 gamma-ray and neutron irradiation. II. Fractionation up to ten doses. *Br J Radiol*. 1984;57:617–629.

38. Meeks SL, Buatti JM, Foote KD, Friedman WA, Bova FJ. Calculation of cranial nerve complication probability for acoustic neuroma radiosurgery. *Int J Radiat Oncol Biol Phys*. 2000;47:597–602.

39. Engeseth GM, Stieb S, Mohamed ASR, et al. Outcomes and patterns of radiation associated brain image changes after proton therapy for head and neck skull base cancers. *Radiother Oncol*. 2020;151:119–125.

40. Jones B, Wilson P, Nagano A, Fenwick J, McKenna G. Dilemmas concerning dose distribution and the influence of relative biological effect in proton beam therapy of medulloblastoma. *Br J Radiol*. 2012;85:e912–e918.

41. Bauer J, Sommerer F, Mairani A, et al. Integration and evaluation of automated Monte Carlo simulations in the clinical practice of scanned proton and carbon ion beam therapy. *Phys Med Biol*. 2014;59:4635–4659.

42. Grassberger C, Paganetti H. Elevated LET components in clinical proton beams. *Phys Med Biol*. 2011;56:6677–6691.

43. Suckert T, Müller J, Beyreuther E, et al. High-precision image-guided proton irradiation of mouse brain sub-volumes. *Radiother Oncol*. 2020;146:205–212.

44. Lomax A. Intensity modulation methods for proton radiotherapy. *Phys Med Biol*. 1999;44:185–205.

45. Paganetti H. Relative biological effectiveness (RBE) values for proton beam therapy. Variations as a function of biological endpoint, dose, and linear energy transfer. *Phys Med Biol*. 2014;59: R419–R472.

Supplementary materials

This is the supplementary material, where the first paragraph explains the RBE models, and the background for choosing them in our project. The second paragraph contains details about the treatment plans and the optimization algorithm. Appendix E3 describes how the RBE is derived and used in our study, while Appendix E4 contains the results for the water phantom case. The next paragraphs consist of additional results in terms of physical dose to the different cases, and DVHs.

Appendix E1   RBE models

MCN model

The MCN model is based on a regression fit to 287 experimental data points. It is based on all published *in vitro* cell survival data [13]. The RBE_{max} and RBE_{min} are defined as follows:

$$RBE_{max} = 0.99064 + \frac{0.35605\ Gy}{\left(\frac{\alpha}{\beta}\right)_x} LET_d$$

$$RBE_{min} = 1.1012 - 0.0038703 Gy^{-\frac{1}{2}}(keV\ \mu m)^{-1} \sqrt{\left(\frac{\alpha}{\beta}\right)_x} LET_d$$

ROR model

ROR is based on a non-linear dependency between the RBE and LET. The $RBE_{min} = 1$, while the RBE_{max} is based on a biological weighting function (BWF) which is derived from *in vitro* cell experiments. The BWF $(r_{max}(L))$ weights the LET spectrum $(d(L))$. The RBE_{max} and RBE_{min} are defined as follows:

$$RBE_{max}(d(L)) = \int_0^\infty r_{max}(L)d(L)dL,$$

$$r_{max}(L) = 1 + \frac{1\text{ Gy}}{(\alpha/\beta)_x}\left(0.578\left(\tfrac{\text{keV}}{\mu\text{m}}\right)^{-1}L - 0.0808\left(\tfrac{\text{keV}}{\mu\text{m}}\right)^{-2}L^2 + 0.00564\left(\tfrac{\text{keV}}{\mu\text{m}}\right)^{-3}L^3\right.$$

$$\left. - 9.92\times10^{-5}\left(\tfrac{\text{keV}}{\mu\text{m}}\right)^{-4}L^4\right), \qquad L < 37.0\,\frac{\text{keV}}{\mu\text{m}}$$

$$r_{max}(L) = 1 + 10.5\frac{Gy}{(\alpha/\beta)_x}, \qquad\qquad L \geq 37.0\,\frac{\text{keV}}{\mu\text{m}}$$

$$RBE_{min} = 1$$

LWD model

LWD is not an explicit RBE-model, but a model made for LET-optimization. The principle is that the LET has a linear dependency to the RBE, and the median RBE should be 1.1 to the CTV. The RBE can therefore be written as:

$$RBE = 1 + c \times LET_d$$

To create an RBE model after our formalism, we put $RBE = RBE_{max} = RBE_{min}$ which gives us

$$RBE_{max}(LET_d) = 1 + c \times (keV\ \mu m)^{-1}LET_d$$

$$RBE_{min}(LET_d) = 1 + c \times (keV\ \mu m)^{-1}LET_d$$

where the c is calculated from the median LET to the CTV, so that the RBE is 1.1 :

$$c = \frac{RBE_{median} - 1}{LET_{d-median}} = \frac{0.1}{LET_{d-median}}$$

The $LET_{d-median}$ used in this study, and their respective c-values are given in Table E1.1. The c-value for the water phantom case comes from Unkelbach et al. [23].

Table E1.1 Mean median dose to the CTV, and the calculated c-value for each case

	Water Phantom	Brain Tumor	Prostate	Head and neck
LET$_{d\text{-median}}$(CTV) [$keV/\mu m$]	N/A	3.16	2.87	2.57
c-value	0.040	0.0316	0.0348	0.0389

The LET$_d$ for each voxel, *v* is calculated by the equation (E1.1)[41]:

$$LET_{d,v} = \frac{\sum_i \int \frac{\Phi_v(E)}{\rho_w} \big(LET_v(E)\big)^2 dE}{\sum_i \int \frac{\Phi_v(E)}{\rho_w} \big(LET_v(E)\big) dE} \qquad \text{E1.1}$$

where $\Phi_{i,v}(E)$ is the fluence of the proton with kinetic energy E in voxel v, $LET_v(E)$ is the unrestricted LET for the same kinetic energy and voxel, and ρ_w is the density of water (1 g/cm³). Here, only the LET from primary and secondary protons was considered as described by Grassberger and Paganetti [42].

Background of model selection

The MCN model is based on the largest collection of cell-line data of all published models and fitted linearly to the LET, and this model was therefore natural to consider in this study. Other RBE models which are based on linear fit to the LET, generally have similar linear RBE vs. LET relationship as the MCN model [16]. The ROR model is also based on a large cell-line library and on the LET but applies a non-linear relationship between RBE and LET relationship. Therefore, only monoenergetic *in vitro* experiments are included in the database and the model also uses the LET spectrum as parameter for the radiation quality, in contrast to most models which applies the LET$_d$. It was important to have two RBE models which was depended on the $(\alpha/\beta)_x$ so the differences between the models were

3

illuminated, and thus we could compare the differences and quantify the uncertainties in the strategies. A comparison to more recent and emerging RBE data from *in vivo* [3, 43] and clinical studies [6, 7] may be useful to adapt RBE models to application for OARs, as more knowledge of the RBE in especially OARs is still needed. Therefore, using the LWD model could be a wise step in the right direction until the uncertainties in these libraries are lower. The LWD model is purely dependent on the LET without any use of cell-line data, and was made to prevent high LET values in critical structures, as shown by Unkelbach et al. [23]. Here, a c-value scales the value of the RBE, so that the mean RBE to the CTV was 1.1. This value was varied in this study, depending on the median LET_d in the computed target volume (CTV). The LWD model is not technically classified as an RBE model because of its neglection of the quadratic term in the LQ-model, which should be taken into consideration as it represents the fractionation effects [23].

Appendix E2   Treatment plans

Details of the treatment plans are given below in Table E2.1, while the details of the optimization algorithm are given in the following paragraph.

Table E2.1 Properties and parameters for the different cases used in this study, with the angles given as Gantry Angle (GA)

and Patient Support Angle (PSA)

	Water phantom	Brain tumor	Prostate	Head and neck
Number of fields and field angles	1	GA 257°, PSA 0° GA 291°, PSA 60°	2 opposing fields	GA 55°, PSA 0° GA 85°, PSA 0° GA 135°, PSA 0°
Prescribed dose to PTV [Gy(RBE)]	2	54	67.5	50.4
OARs included in the optimization	N/A	Brainstem Left optic nerve	Rectum Bladder	Left pterygoid Right parotid gland
Upper dose limit to OAR [Gy(RBE)] (FO$_{MCN}$ and FO$_{ROR}$)	N/A	55	58	40
Upper dose limit to OAR [Gy(RBE)] (FO$_{LWD}$)	N/A	50	64	45
Upper dose limit OAR [Gy(RBE)] (DO$_{MCN}$ and DO$_{ROR}$)	N/A	55	67.5	45
Upper dose limit OAR [Gy(RBE)] (DO$_{LWD}$)	N/A	45	67.5	40
Fractions	1	30	25	28
$(\alpha/\beta)_x$ **PTV [Gy]**	2 and 10	10.6 [34]	1.5 [35]	2.8 [36]
$(\alpha/\beta)_x$ **OAR [Gy]**	N/A	2.1 [38]	3.5 [37]	2.8 [36]

Treatment planning

This optimizer is part of a multi-step procedure to optimize a given number of particles (N_x) for a given pencil beam (P_x), from $P_1(N_1)$ to an MC optimized solution $P_2(N_2)$.

Based on the pre-optimized spot list, we define the physical dose to a voxel j as:

$$D_j(\boldsymbol{N}) = \sum_{i \in PB} d_{i,j} \cdot N_i, \tag{E2.1}$$

where $\boldsymbol{N}$ is the vector of beam particle numbers for each pencil beam i and $d_{i,j}$ is the dose contribution from pencil beam i to the dose in voxel D_j.

For the optimization problem, we defined the cost function to be minimized as:

$$\chi^2(\boldsymbol{N}) = \sum_{j \in PTV} \frac{w_j(\widehat{\boldsymbol{D}}_j - \boldsymbol{D}_j)^2}{\widehat{\boldsymbol{D}}_j^2} + \sum_{j \in OAR} \frac{w_j(\widehat{\boldsymbol{D}}_j - \boldsymbol{D}_j)^2}{\widehat{\boldsymbol{D}}_j^2} \Theta(\widehat{\boldsymbol{D}}_j - \boldsymbol{D}_j), \tag{E2.2}$$

where $\widehat{\boldsymbol{D}}_j$ is the prescribed dose in voxel j, $\boldsymbol{D}_j \equiv D_j(\boldsymbol{N})$, as given in equation (E2.1) and w_j is the weighting factor for the different PTV and OARs. Θ is the Heaviside function, with contribution only if the dose in the voxel is higher than the prescribed dose.

In the optimizer, the dose difference algorithm is used, introduced by Lomax [44]. It states that for the $(k + 1)$th iteration step, the particle numbers $\boldsymbol{N}_{i+k}$ for pencil beam i are calculated as:

$$\boldsymbol{N}_{i,k+1} = \boldsymbol{N}_{i,k} \cdot \left[1 + F_{DDO} \left(\frac{\sum_{j \in PTV} w_j d_{j,k}^2 \frac{\widehat{\boldsymbol{D}}_j}{\boldsymbol{D}_{j,k}} + \sum_{j \in OAR} w_j d_{j,k}^2 \frac{\widehat{\boldsymbol{D}}_j}{\boldsymbol{D}_{j,k}} \Theta(\widehat{\boldsymbol{D}}_j - \boldsymbol{D}_j)}{\sum_{j \in PTV} w_j d_{j,k}^2 + \sum_{j \in OAR} w_j d_{j,k}^2 \Theta(\widehat{\boldsymbol{D}}_j - \boldsymbol{D}_j)} - 1 \right) \right], \tag{E2.3}$$

where F_{DDO} is a damping factor. There is no monitor unit constraint for the optimizer, i.e., there were no lower boundary for particles per pencil beam.

For biological optimization, we replace the dose in equation (E2.1) with the RBE-weighted dose.

Appendix E3   Definition of variable RBE and LET$_d$-weighted dose (LWD)

The variable RBE models for RBE are based on the definition of RBE and the LQ-model, where the RBE can be written as:

$$RBE\left(D_p, \left(\frac{\alpha_x}{\beta_x}\right), RBE_{max}, RBE_{min}\right) = \frac{1}{2D_p}\left(\sqrt{\left(\frac{\alpha_x}{\beta_x}\right)^2 + 4D_p\left(\frac{\alpha_x}{\beta_x}\right)RBE_{max} + 4D_p^2 RBE_{min}^2} - \left(\frac{\alpha_x}{\beta_x}\right)\right).$$

Here, D_p is the physical proton dose, α_x and β_x are the LQ-model parameters for the reference radiation [45], and RBE_{max} and RBE_{min} are the parameters which are varied for each individual model. RBE_{max} and RBE_{min} are defined as

$$\lim_{D_p \to 0} RBE = RBE_{max} = \frac{\alpha}{\alpha_x}$$

$$\lim_{D_p \to \infty} RBE = RBE_{min} = \sqrt{\frac{\beta}{\beta_x}}.$$

The LWD approach is a tissue-independent alternative which may reduce the risk of RBE-weighted dose hotspots in OARs without explicit modelling of the RBE and the associated uncertainties. It assumes an RBE surrogate, given as

$$RBE_{LWD} = 1 + (c \times LET)$$

where c is a constant that scales the LET and is normalized so the mean RBE to the CTV is 1.1.

Appendix E4   Water phantom results

Implementation verification in water phantom

All optimization strategies resulted in a homogenous RBE-weighted dose within the SOBP for their respective RBE models, as seen in Figure E4.1 panels a and b, thus verifying the implementation. The shape of the physical dose distribution is similar for the different variable RBE optimizations, with the highest physical dose at the proximal part of the SOBP and decreasing dose towards the distal end as the optimization strategies compensates for the expected increase in RBE along the beam path. The LWD model is based on a mean RBE of 1.1 to the target, which we observe for this case where the mean physical dose (D_{phys}^{LWD}) was 1.78 Gy, close to the prescribed physical dose of 1.82 Gy (corresponding to a 2 Gy(RBE$_{1.1}$) dose). For low $(\alpha/\beta)_x$, a clear reduction in physical dose to the target for the tissue dependent models was, as expected, seen since both ROR and MCN have an inverse relationship with the $(\alpha/\beta)_x$. Therefore, the $(\alpha/\beta)_x$ dependent models provided a lower mean physical dose for $(\alpha/\beta)_x$ of 2 Gy, and higher for $(\alpha/\beta)_x$ of 10 Gy (panel a and b in Figure E4.1), showing the strong impact of the tissue parameters in the optimization process. The difference in physical dose between the 2 and 10 Gy $(\alpha/\beta)_x$ was greater near the distal end of the beam, compared to the entrance region, as seen in Figure E5.1 in Appendix E5.

The SOBP optimized with RBE$_{1.1}$ and recalculated with the variable RBE models can be seen in panels c and d in Figure E4.1, with corresponding DVHs for the water phantom plan are given in Appendix E7, Figure E7.1 and Figure E7.2. Here, the highest mean RBE-weighted dose comes from the MCN model for $(\alpha/\beta)_x$ of 2 Gy (($D_{MCN}^{RBE_{1.1}}$) of 2.22 Gy(RBE)), and the LWD gives the highest for $(\alpha/\beta)_x$ of 10 Gy (($D_{LWD}^{RBE_{1.1}}$) of 2.03 Gy(RBE)), also displayed by the color wash plots of the RBE-weighted dose differences in Figure E5.1 in Appendix E6. A shift up to several millimeters in the dose fall-off is also observed towards the distal part in the $(\alpha/\beta)_x$ = 2 Gy scenario, for all recalculations.
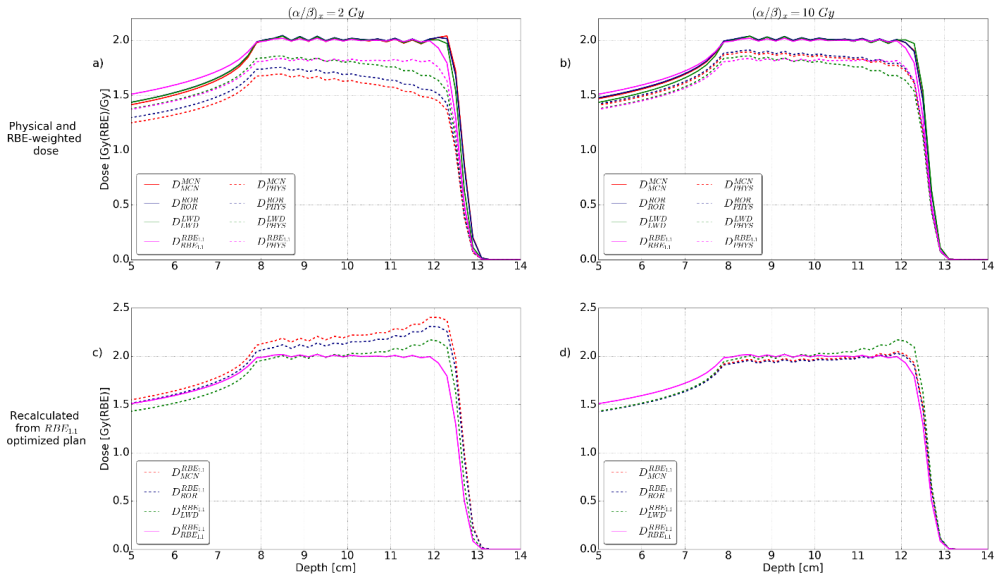
Figure E4.1 Depth dose distributions for the water phantom with $(\alpha/\beta)_x$ of 2 Gy to the left and $(\alpha/\beta)_x$ of 10 Gy to the right. The upper panels (a and b) show the RBE-weighted (solid) and physical (dashed) dose of the plans optimized with respect to the four different models. The lower panels (c and d) show the $RBE_{1.1}$-optimized plan (solid line), recalculated with the variable RBE-models (dashed lines).

Appendix E5   Physical dose comparison

In this appendix, the physical dose distribution for the different strategies are compared. Figure E5.1 shows the physical dose difference between the variable RBE and the reference $RBE_{1.1}$-plan, while Figure E5.2 shows the same difference for the three patient cases. The DVH for the physical dose difference for the patient cases are given in Figure E5.3 and FigureE5.4

9
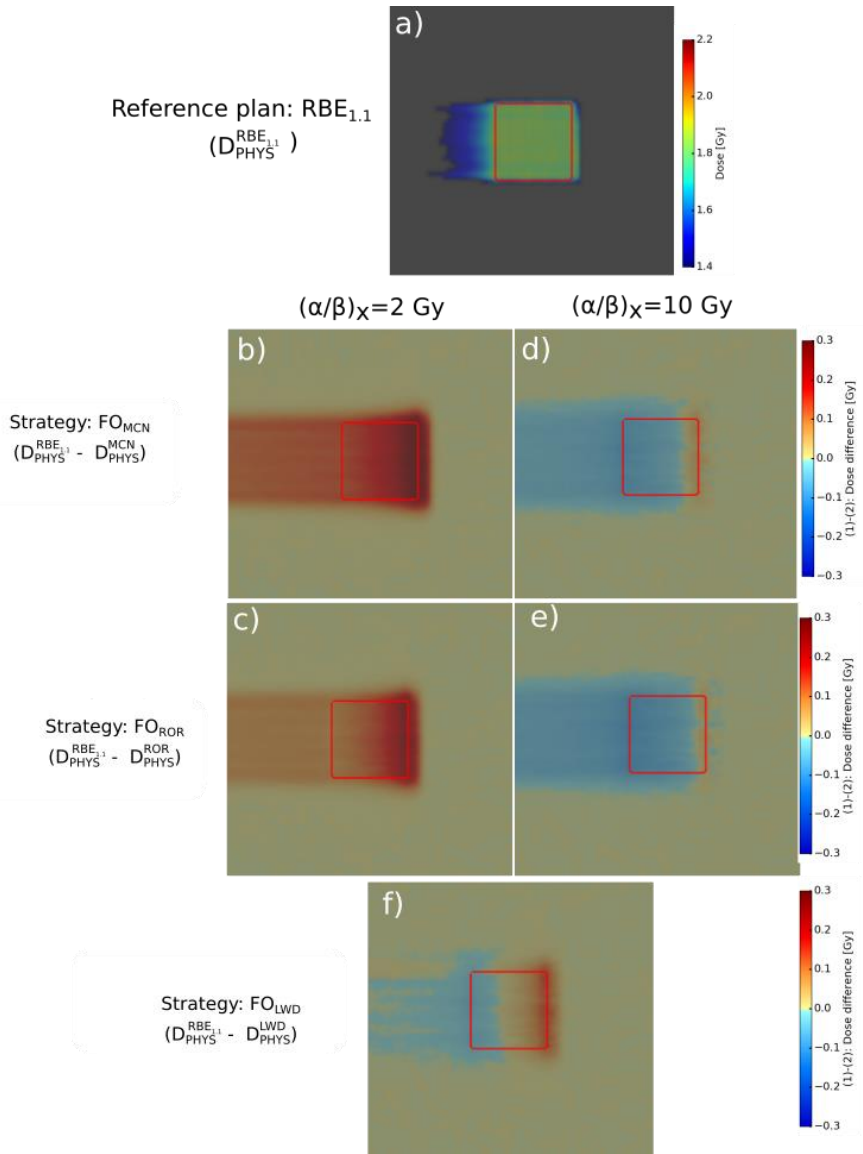
Figure E5.1 Physical dose difference for the different variable models and the RBE$_{1.1}$ reference plan, for the water phantom case.
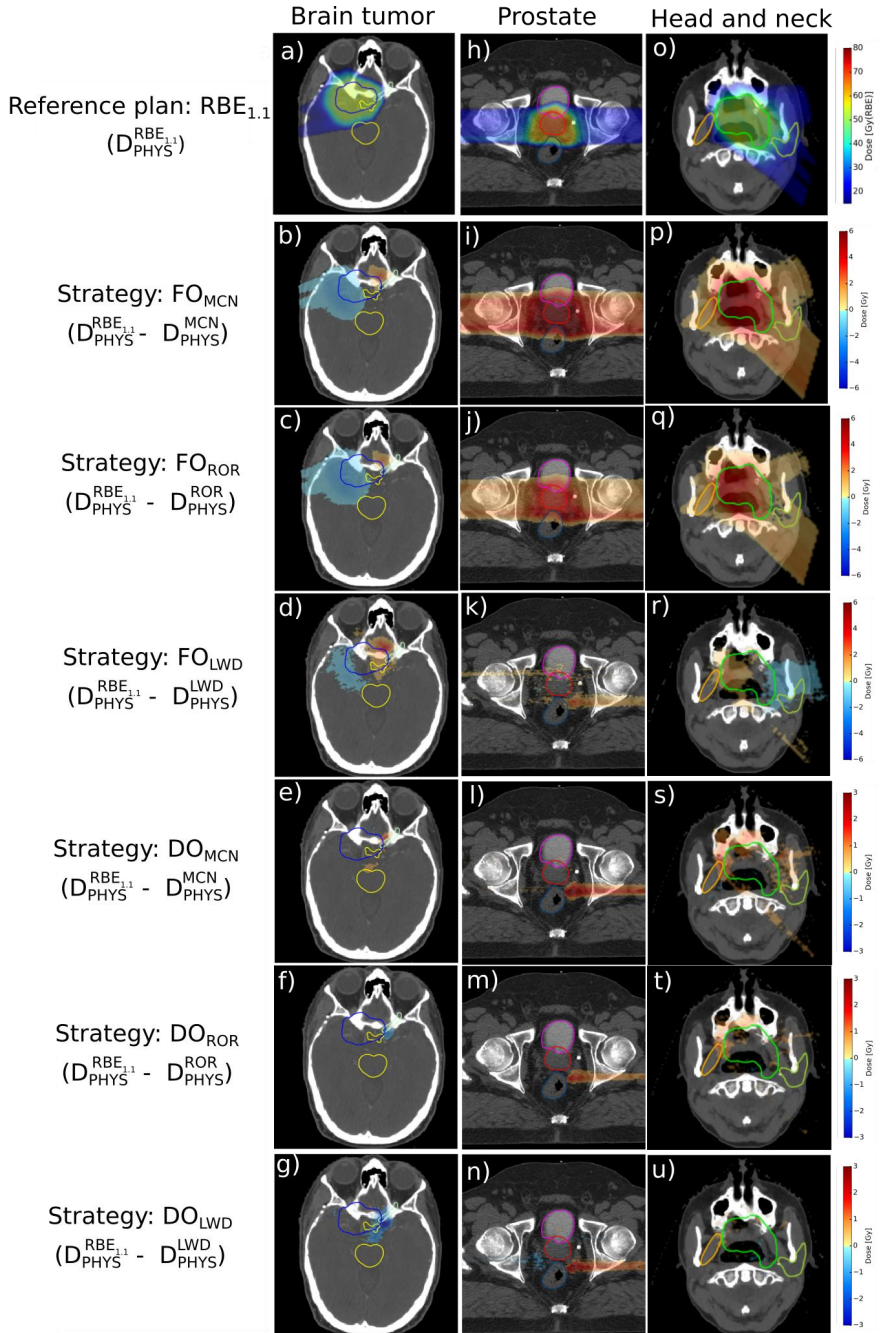
Figure E5.2 Physical dose difference for the different variable models and the RBE$_{1.1}$ reference plan, for the different patient cases.
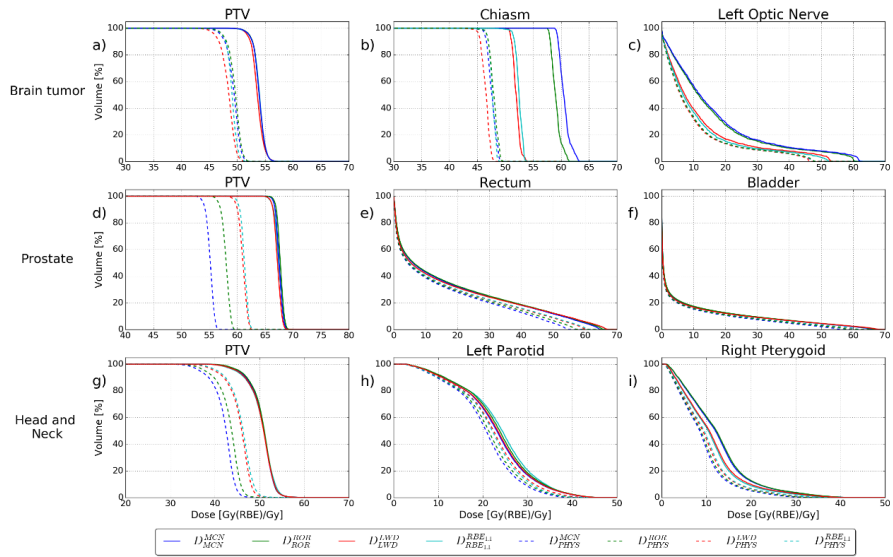
Figure E5.3 DVH for the physical dose (dashed lines) and the RBE₁.₁ reference plan for the full RBE optimization strategies
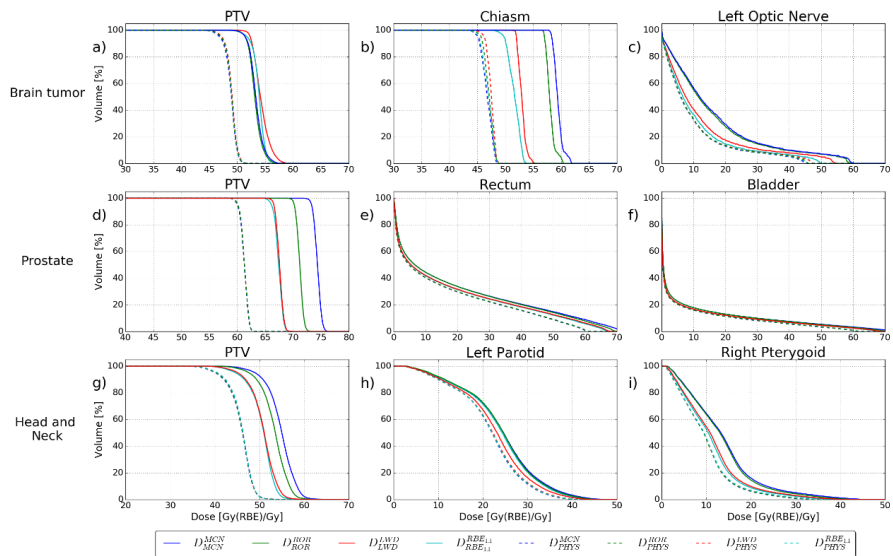
(solid lines).

Figure E5.4 DVH for the physical dose for the different variable models and the RBE$_{1.1}$ reference plan for the differential RBE

optimization strategies.

Appendix E6   Additional colorwash plots

Water Phantom

The RBE-weighted dose differences between the RBE$_{1.1}$ and the variable RBE models for the water

phantom are seen in Figure E6.1.
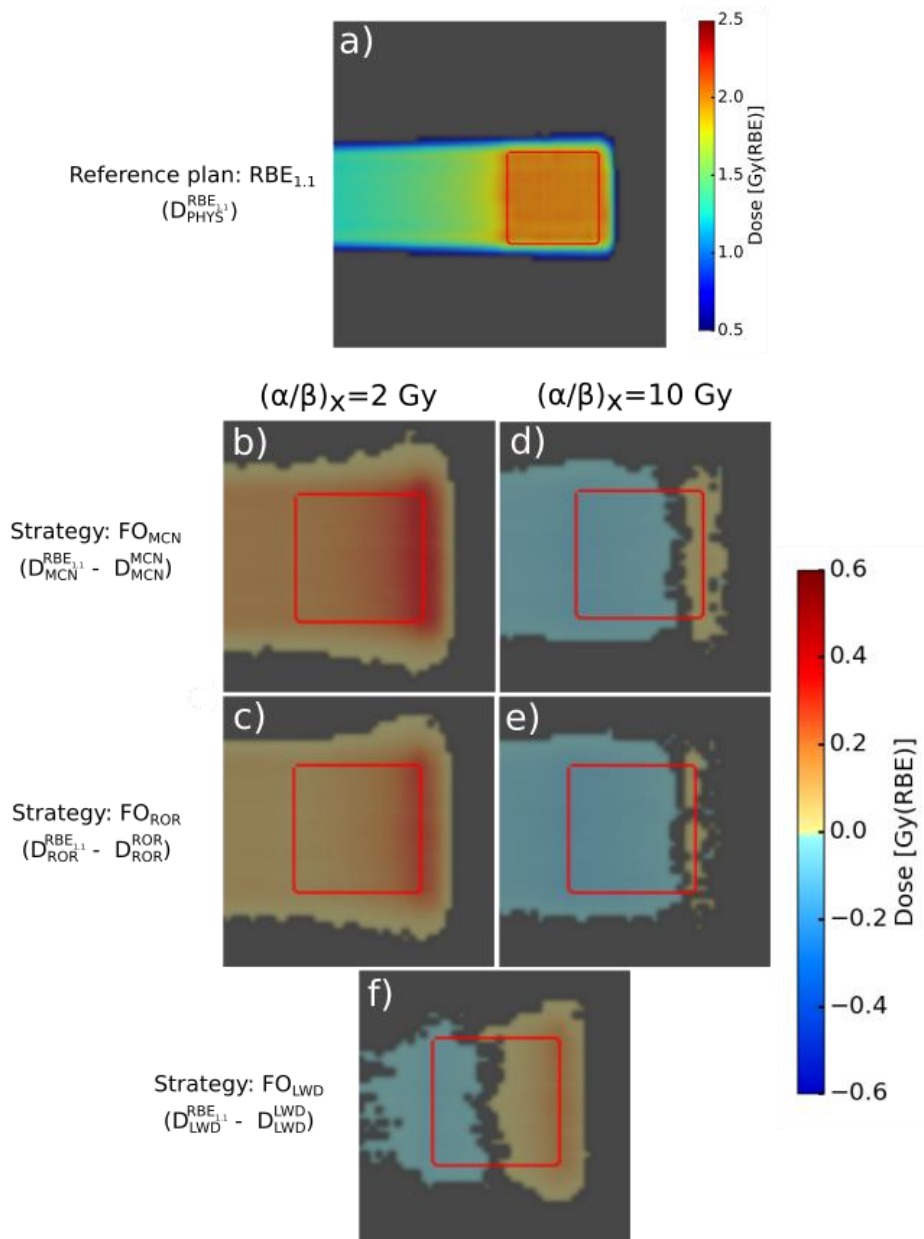
Figure E6.1 RBE-weighted dose differences between the variable RBE models and the variable RBE recalculated from the

RBE₁.₁-plan.

Patient cases

Figure E6.2 shows the RBE-weighted dose for the different strategies for the three cases respectively.
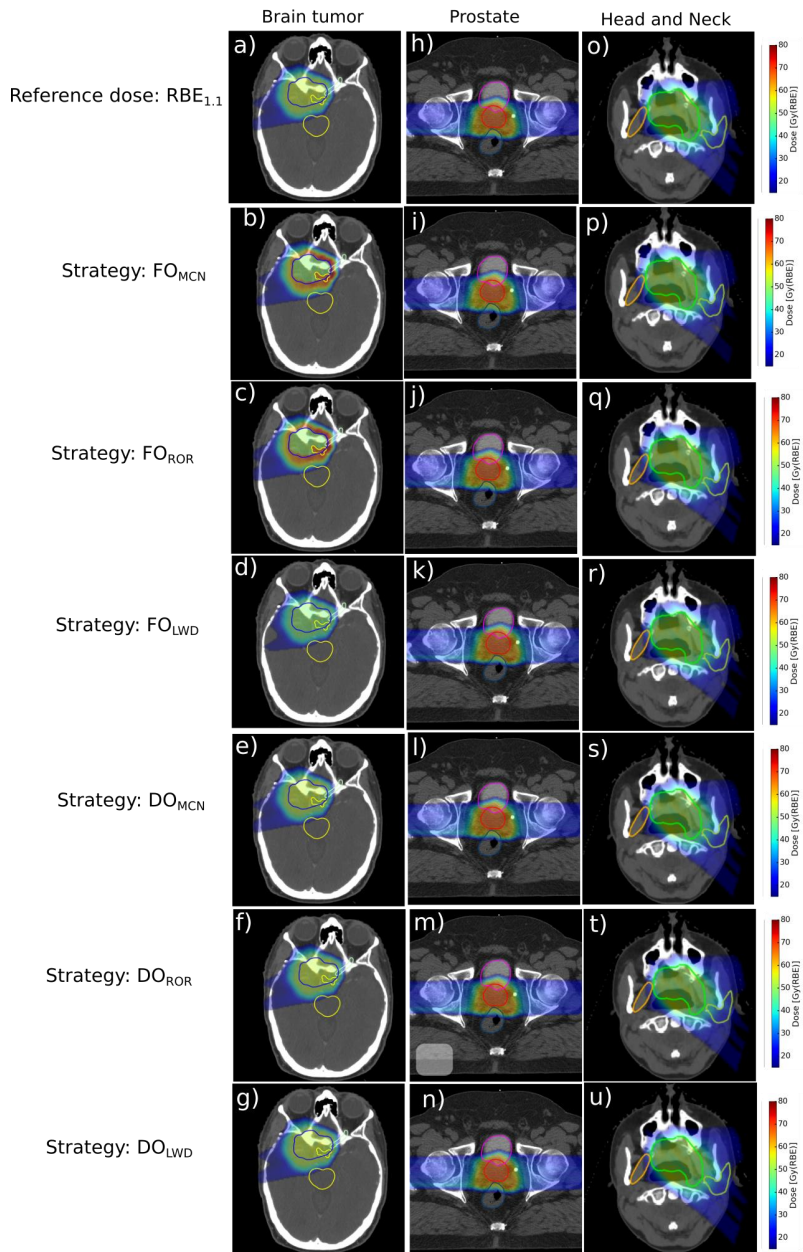
Appendix E7   Additional Dose Volume Histograms

Water phantom

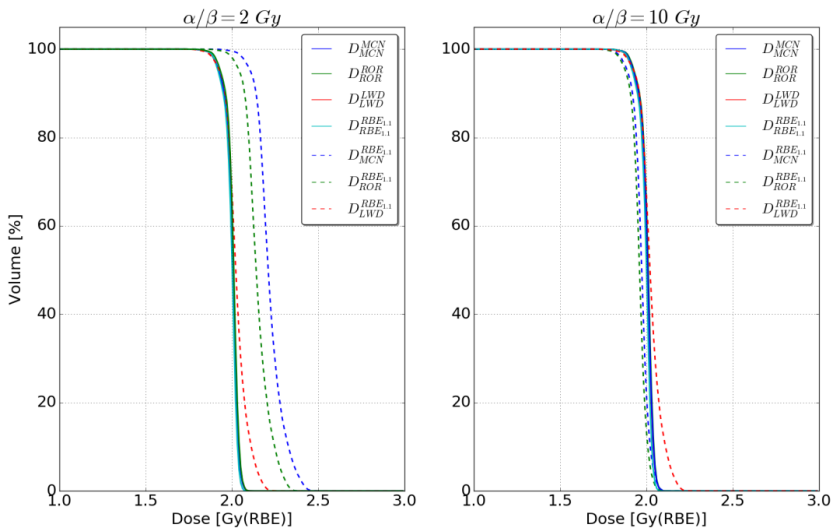The DVH for the water phantom strategies are given below in Figure E7.1 (RBE$_{1.1}$-comparison) and Figure E7.2 (MCN-comparison).

Figure E7.1 DVH for the water phantom. The solid lines represent the RBE-weighted dose from the different strategies, while the dashed lines represent the RBE-weighted dose from the respective models, recalculated from the RBE$_{1.1}$-plan.
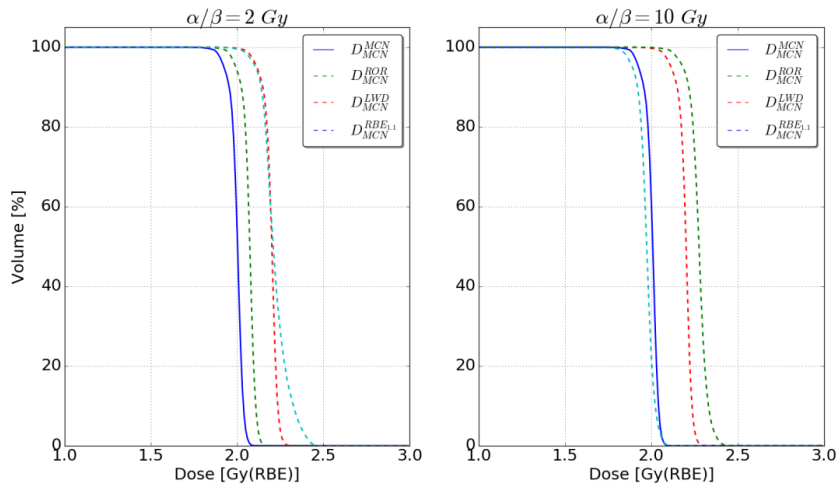
Figure E7.2 DVH for the water phantom. The dashed lines represent the RBE-weighted dose from the respective plans calculated with the MCN-model.

Patient cases:

Figure E7.3 shows the RBE-weighted dose to the PTV for the different strategies in the head and neck case, as well as the RBE-weighted dose to the PTV from the original Eclipse plan.
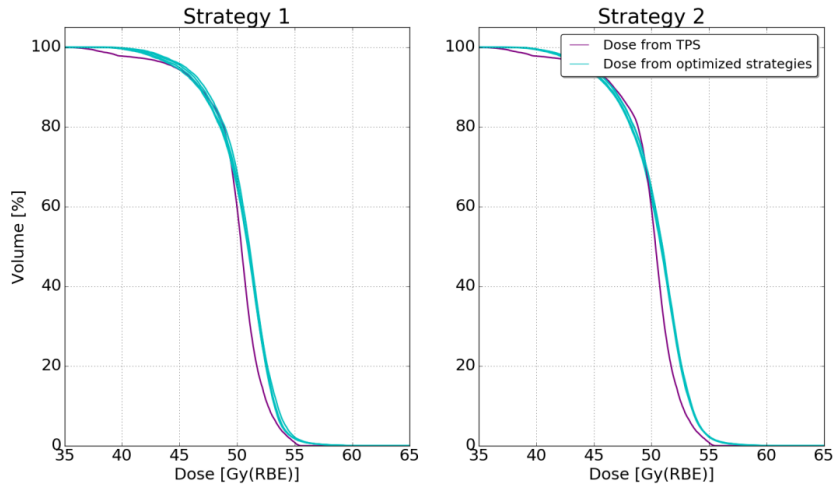
Figure E7.3 Comparison of the RBE-weighted dose to the PTV in the head and neck case. The TPS-plans are given in purple,

and the optimized RBE-weighted dose for the different strategies are given in their respective colors.

uib.no